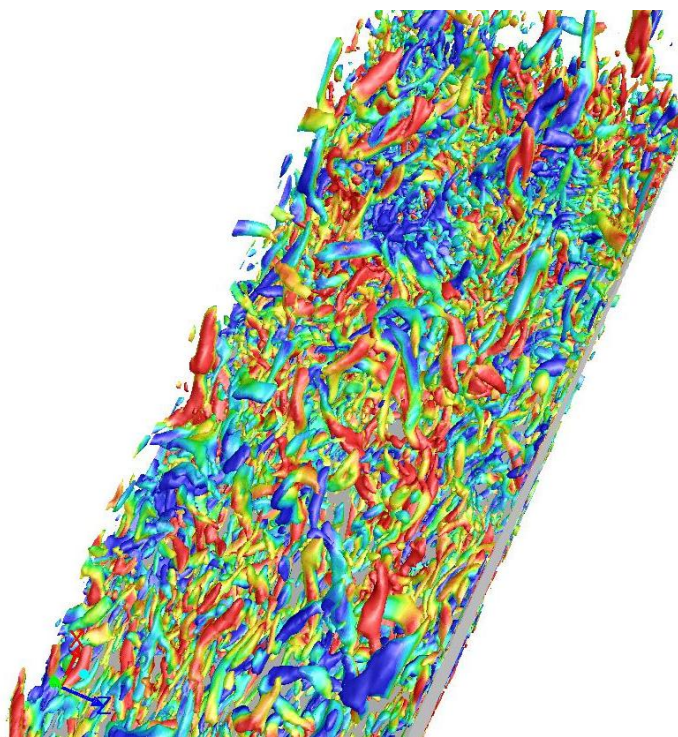


# **Best Practice: Scale-Resolving Simulations in ANSYS CFD**

**Version 1.0**

---

F.R. Menter  
ANSYS Germany GmbH



---

**April 2012**

# Table of Contents

1.	Introduction .....	4
2.	General Aspects.....	5
2.1.	Limitations of Large Eddy Simulation (LES) .....	5
3.	Scale-Resolving Simulation (SRS) Models – Basic Formulations .....	13
3.1.	Scale-Adaptive Simulation (SAS).....	13
3.2.	Detached Eddy Simulation (DES).....	15
3.3.	Large Eddy Simulation (LES) .....	16
3.4.	Wall Modeled Large Eddy Simulation (WMLES).....	17
3.5.	Embedded/Zonal LES (ELES, ZLES).....	19
3.6.	Unsteady Inlet/Interface Turbulence .....	19
4.	Generic Flow Types and Basic Model Selection .....	20
4.1.	Globally Unstable Flows .....	20
4.1.1.	Flow Physics.....	20
4.1.2.	Modeling .....	21
4.1.3.	Mesning Requirements .....	22
4.1.4.	Numerical Settings .....	22
4.1.5.	Examples .....	23
4.2.	Locally Unstable Flows.....	28
4.2.1.	Flow Physics.....	28
4.2.2.	Modeling .....	29
4.2.3.	Mesning Requirements .....	31
4.2.4.	Numerical Settings .....	32
4.2.5.	Examples .....	32
4.3.	Stable Flows and Wall Boundary Layers .....	35
4.3.1.	Flow Physics.....	35
4.3.2.	Modeling .....	36
4.3.3.	Mesning Requirements .....	36
4.3.4.	Numerical Settings .....	38
4.3.5.	Examples .....	38
5.	Numerical Settings for SRS .....	54
5.1.	Spatial Discretization .....	54
5.1.1.	Momentum .....	54
5.1.2.	Turbulence Equations.....	55
5.1.3.	Gradients (ANSYS Fluent) .....	56
5.1.4.	Pressure (ANSYS Fluent) .....	56
5.2.	Time Discretization .....	56
5.2.1.	Time Integration .....	56
5.2.2.	Time Advancement and Under-Relaxation (ANSYS Fluent) .....	56
6.	Initial and Boundary Conditions .....	57

6.1.	Initialization of SRS .....	57
6.2.	Boundary conditions for SRS.....	57
6.2.1.	Inlet Conditions .....	57
6.2.2.	Outlet Conditions .....	57
6.2.3.	Wall Conditions.....	58
6.2.4.	Symmetry vs. Periodicity .....	58
7.	Post-Processing and Averaging.....	58
7.1.	Visual Inspection.....	58
7.2.	Averaging .....	60
8.	Summary .....	61
	Acknowledgment.....	61
	References .....	61
	Appendix 1: Summary of Numerics Settings with ANSYS Fluent .....	64
	Appendix 2: Summary of Numerics Settings With ANSYS CFX .....	65
	Appendix 3: Models .....	66
	Appendix 4: Generic Flow Types and Modeling .....	68

© 2011 ANSYS, Inc. All Rights Reserved.

ANSYS and any and all ANSYS, Inc. brand, product, service and feature names, logos and slogans are registered trademarks or trademarks of ANSYS, Inc. or its subsidiaries in the United States or other countries. All other brand, product, service and features names or trademarks are the property of their respective owners.

ANSYS, Inc.  
[www.ansys.com](http://www.ansys.com)  
[ansysinfo@ansys.com](mailto:ansysinfo@ansys.com)  
[866.267.9724](tel:866.267.9724)

# 1. Introduction

While today's CFD simulations are mainly based on Reynolds-Averaged Navier-Stokes (RANS) turbulence models, it is becoming increasingly clear that certain classes of flows are better covered by models in which all or a part of the turbulence spectrum is resolved in at least a portion of the numerical domain. Such methods are termed Scale-Resolving Simulation (SRS) models in this paper.

There are two main motivations for using SRS models in favor of RANS formulations. The first reason for using SRS models is the need for additional information that cannot be obtained from the RANS simulation. Examples are acoustics simulations where the turbulence generates noise sources, which cannot be extracted with accuracy from RANS simulations. Other examples are unsteady heat loading in unsteady mixing zones of flow streams at different temperatures, which can lead to material failure, or multi-physics effects like vortex cavitation, where the unsteady turbulence pressure field is the cause of cavitation. In such situations, the need for SRS can exist even in cases where the RANS model would in principle be capable of computing the correct time-averaged flow field.

The second reason for using SRS models is related to accuracy. It is known that RANS models have their limitations in accuracy in certain flow situations. RANS models have shown their strength essentially for wall-bounded flows, where the calibration according to the law-of-the-wall provides a sound foundation for further refinement. For free shear flows, the performance of RANS models is much less uniform. There is a wide variety of such flows, ranging from simple self-similar flows such as jets, mixing layers, and wakes to impinging flows, flows with strong swirl, massively separated flows, and many more. Considering that RANS models typically already have limitations covering the most basic self-similar free shear flows with one set of constants, there is little hope that even the most advanced Reynolds Stress Models (RSM) will eventually be able to provide a reliable foundation for all such flows. (For an overview of RANS modeling, see Durbin, Pettersson and Reif, 2003; Wilcox, 2006; or Hanjalic and Launder, 2011.)

For free shear flows, it is typically much easier to resolve the largest turbulence scales, as they are of the order of the shear layer thickness. In contrast, in wall boundary layers the turbulence length scale near the wall becomes very small relative to the boundary layer thickness (increasingly so at higher  $Re$  numbers). This poses severe limitations for Large Eddy Simulation (LES) as the computational effort required is still far from the computing power available to industry (Spalart, 1997). (For an overview of LES modeling, see Guerts, 2004, and Wagner et al., 2007.) For this reason, hybrid models are under development where large eddies are resolved only away from walls and the wall boundary layers are covered by a RANS model. Examples of such global hybrid models are Detached Eddy Simulation – DES (Spalart, 2000) or Scale-Adaptive Simulation – SAS (Menter and Egorov 2011). A further step is to apply a RANS model only in the innermost part of the wall boundary layer and then to switch to a LES model for the main part of the boundary layer. Such models are termed Wall-Modelled LES (WMLES) (e.g. Shur et al., 2008). Finally, for large domains, it is frequently necessary to cover only a small portion with SRS models, while the majority of the flow can be computed in RANS mode. In such situations, zonal or embedded LES methods are attractive as they allow the user to specify ahead of time the region where LES is required. Such methods are typically not new models in the strict sense, but allow the combination of existing models/technologies in a flexible way in different portions of the flowfield. Important elements of zonal models are interface conditions, which convert turbulence from RANS mode to resolved mode at pre-defined locations. In most cases, this is achieved by introducing synthetic turbulence based on the length and time scales from the RANS model.

There are many hybrid RANS-LES models, often with somewhat confusing naming conventions, that vary in the range of turbulence eddies they can resolve. On close inspection, many of these models are only slight variations of the Detached Eddy Simulation (DES) concept of Spalart (2000) and have very similar performance. For a general overview of SRS modeling concepts, see Fröhlich and von Terzi (2008), Sagaut et al. (2006).

SRS models are very challenging in their proper application to industrial flows. The models typically require special attention to various details such as:

- Model selection
- Grid generation
- Numerical settings
- Solution interpretation
- Post-processing
- Quality assurance

Unfortunately, there is no unique model covering all industrial flows, and each individual model poses its own set of challenges. In general, the user of a CFD code must understand the intricacies of the SRS model formulation in order to be able to select the optimal model and to use it efficiently. This report is intended to support the user in the basic understanding of such models and to provide best practice guidelines for their usage. The discussion is focused on the models available in the ANSYS CFD software.

This report is intended as an addition to the code-specific Theory and User Documentation available for both ANSYS Fluent™ and ANSYS CFX™. That documentation describes in detail how to select and activate these models, so that information is not repeated here. The current document is intended to provide you with a general understanding of the underlying principles and the associated limitations of each of the described modeling concepts. It also covers the types of flows for which the models are suitable as well as flows where they will likely not work well. Finally, the impact of numerical settings on model performance is discussed.

In accordance with the intention of providing you with recommendations for your day-to-day work, several Appendices can be found at the end of the document for quick reference of the most important points.

## 2. General Aspects

### 2.1. Limitations of Large Eddy Simulation (LES)

In order to understand the motivation for hybrid models, one has to discuss the limitations of Large Eddy Simulation (LES). LES has been the most widely used SRS model over the last decades. It is based on the concept of resolving only the large scales of turbulence and to model the small scales. The classical motivation for LES is that the large scales are problem-dependent and difficult to model, whereas the smaller scales become more and more universal and isotropic and can be modeled more easily.

LES is based on filtering the Navier-Stokes equations over a finite spatial region (typically the grid volume) and aimed at only resolving the portions of turbulence larger than the filter width. Turbulence structures smaller than the filter are then modeled – typically by a simple Eddy Viscosity model.

The filtering operation is defined as:

$$\bar{\Phi} = \int_{-\infty}^{\infty} \Phi(\vec{x}') G(\vec{x} - \vec{x}') d\vec{x}' \quad \int_{-\infty}^{\infty} G(\vec{x} - \vec{x}') d\vec{x}' = 1$$

where  $G$  is the spatial filter. Filtering the Navier-Stokes equations results in the following form (density fluctuations neglected):

$$\frac{\partial \rho \bar{U}_i}{\partial t} + \frac{\partial \rho \bar{U}_j \bar{U}_i}{\partial x_j} = -\frac{\partial P}{\partial x_i} + \frac{\partial}{\partial x_j} (\bar{\tau}_{ij} + \tau_{ij}^{LES})$$

The equations feature an additional stress term due to the filtering operation:

$$\tau_{ij}^{LES} = \rho \bar{U}_i \bar{U}_j - \rho \bar{U}_i \bar{U}_j$$

Despite the difference in derivation, the additional sub-grid stress tensor is typically modelled as in RANS using an eddy viscosity model:

$$\tau_{ij}^{LES} = \mu_t \left( \frac{\partial \bar{U}_i}{\partial x_j} + \frac{\partial \bar{U}_j}{\partial x_i} \right)$$

The important practical implication from this modeling approach is that the modeled momentum equations for RANS and LES are identical if an eddy-viscosity model is used in both cases. In other words, the modeled Navier-Stokes equations have no knowledge of their derivation. The only information they obtain from the turbulence model is the size of the eddy viscosity. Depending on that, the equations will operate in RANS or LES mode (or in some intermediate mode). The formal identity of the filtered Navier-Stokes and the RANS equations is the basis of hybrid RANS-LES turbulence models, which can obviously be introduced into the same set of momentum equations. Only the model (and the numerics) have to be switched.

Classical LES models are of the form of the Smagorinsky (1963) model:

$$\mu_t = \rho (C_s \Delta)^2 S$$

where  $\Delta$  is a measure of the grid spacing of the numerical mesh,  $S$  is the strain rate scalar and  $C_s$  is a constant. This is obviously a rather simple formulation, indicating that LES models will not provide a highly accurate representation of the smallest scales. From a practical standpoint, a very detailed modeling might not be required. A more appropriate goal for LES is not to model the impact of the unresolved scales onto the resolved ones, but to model the *dissipation* of the smallest resolved scales. This can be seen from Figure 1 showing the turbulence energy spectrum of a Decaying Isotropic Turbulence – DIT test case, i.e. initially stirred turbulence in a box, decaying over time (Comte-Bellot and Corrsin, 1971).  $E(\kappa)$  is the turbulence energy as a function of wave number  $\kappa$ . Small  $\kappa$  values represent large eddies and large  $\kappa$  values represent small eddies. Turbulence is moving down the turbulence spectrum from the small wave number to the high wave numbers. In a fully resolved simulation (Direct Numerical Simulation – DNS), the turbulence is dissipated into heat at the smallest scales ( $k \sim 100$  in Figure 1), by viscosity. The dissipation is achieved by:

$$\varepsilon_{DNS} = \nu \frac{\partial U_i}{\partial x_j} \frac{\partial U_i}{\partial x_j}$$

where  $\nu$  is typically a very small kinematic molecular viscosity. The dissipation  $\varepsilon_{DNS}$  is still of finite value as the velocity gradients of the smallest scales are very large.

However, LES computations are usually performed on numerical grids that are too coarse to resolve the smallest scales. In the current example, the cut-off limit of LES (resolution limit) is at around  $\kappa=10$ . The velocity gradients of the smallest resolved scales in LES are therefore much smaller than those at the DNS limit. The molecular viscosity is then not sufficient to provide the correct level of dissipation. In this case, the proper amount of dissipation can be achieved by increasing the viscosity, using an eddy-viscosity:

$$\varepsilon_{LES} = \nu_t \frac{\partial \bar{U}_i}{\partial x_j} \frac{\partial \bar{U}_i}{\partial x_j}$$

The eddy viscosity is calibrated to provide the correct amount of dissipation at the LES grid limit. The effect can be seen in Figure 1, where a LES of the DIT case is performed without a LES model and with different LES models. When the LES models are activated, the energy is dissipated and the models provide a sensible spectrum for all resolved scales. In other words, LES is not modeling the influence of unresolved small scale turbulence onto the larger, resolved scales, but the dissipation of turbulence into heat (the dissipated energy is typically very small relative to the thermal energy of the fluid and does not have to be accounted for, except for high Mach number flows).

DIT-t, grid 64×64×64, energy spectra at t=2.0

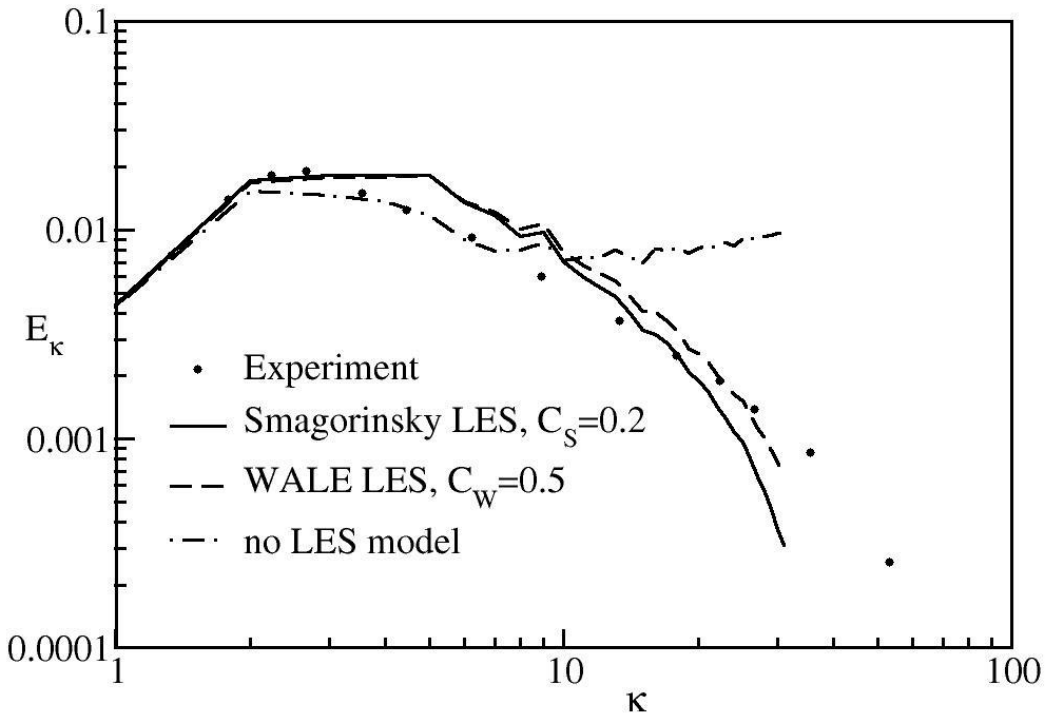


**Figure 1: Turbulence spectrum for DIT test case after t=2. Comparison of results without Sub-Grid Scale model ('no LES') with WALE and Smagorinsky LES model simulations.**

This discussion shows that LES is a fairly simple technology, which does not provide a reliable backbone of modeling. This is also true for more complex LES models like dynamic models. Dynamic eddy viscosity LES models (see e.g. Guerts 2004) are designed to estimate the required level of dissipation at the grid limit from flow conditions at larger scales (typically twice the filter width), thereby reducing the need for model calibration. However, again, such models also only

provide a suitable eddy viscosity level for energy dissipation. Within the LES framework, all features and effects of the flow that are of interest and relevance to engineers have to be resolved in space and time. This makes LES in principle a very CPU-expensive technology.

Even more demanding is the application of LES to wall-bounded flows – which is the typical situation in engineering flows. The turbulent length scale,  $L$ , of the large eddies can be expressed as:

$$L = \kappa y$$

where  $y$  is the wall distance and  $\kappa$  a constant. In other words, even the (locally) largest scales become very small near the wall and require a high resolution in all three space dimensions and in time.

The linear dependence of  $L$  on  $y$  indicates that the turbulence length scales approach zero near the wall, which would require an infinitely fine grid to resolve them. This is not the case in reality, as the molecular viscosity prevents scales smaller than the Kolmogorov limit. This is manifested by the viscous or laminar sublayer, a region very close to the wall, where turbulence is damped and does not need to be resolved. However, the viscous sublayer thickness is a function of the Reynolds number,  $Re$ , of the flow. At higher  $Re$  numbers, the viscous sublayer becomes increasingly thinner and thereby allows the survival of smaller and smaller eddies, which need to be resolved. This is depicted in Figure 2 showing a sketch of turbulence structures in the vicinity of the wall (e.g. channel flow with flow direction normal to observer). The upper part of the picture represents a low  $Re$  number and the lower part a higher  $Re$  number. The grey box indicates the viscous sublayer for the two  $Re$  numbers. The structures inside the viscous sublayer (circles inside the grey box) are depicted but not present in reality due to viscous damping. Only the structures outside of the viscous sublayer (i.e., above the grey box) exist and need to be resolved. Due to the reduced thickness of the viscous sublayer in the high  $Re$  case, substantially more resolution is required to resolve all active scales. Wall-resolved LES is therefore prohibitively expensive for moderate to high Reynolds numbers. This is the main reason why LES is not suitable for most engineering flows.

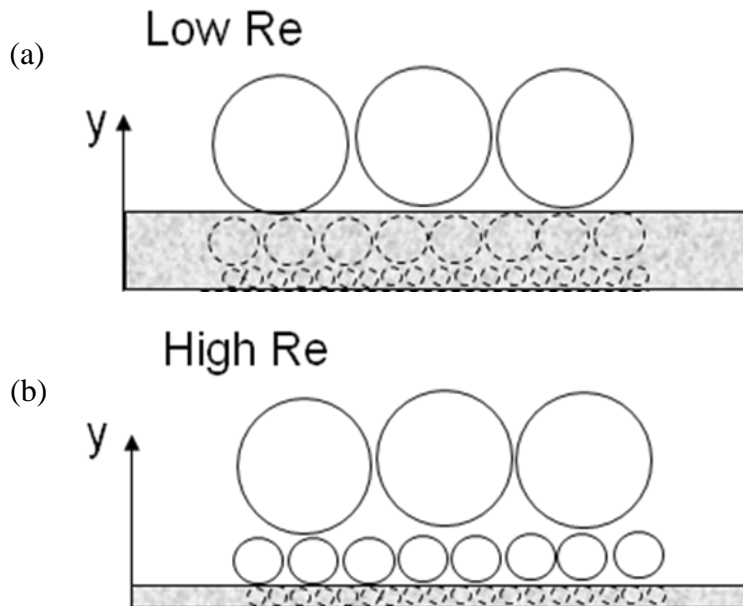


**Figure 2: Sketch of turbulence structures for wall-bounded channel flow with viscous sublayer (a) Low Re number (b) High Re number (Grey area: viscous sublayer)**

The Reynolds number dependence of wall-resolved LES can be estimated for a simple periodic channel flow as shown in Figure 3 ( $x$ -streamwise,  $y$ -wall-normal,  $z$ -spanwise,  $H$  is the channel height).

$$L_x = 4H, \quad L_y = H = 2h, \quad L_z = 1.5H$$

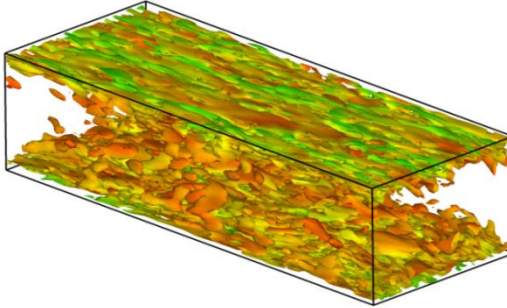


**Figure 3: Turbulence structures in a channel flow**

The typical resolution requirements for LES are:

$$\Delta x^+ = 40, \quad \Delta z^+ = 20, \quad N_y = 60 - 80$$

where  $\Delta x^+$  is the non-dimensional grid spacing in the streamwise direction,  $\Delta z^+$  in the spanwise and  $N_y$  the number of cells across half of the channel height. With the definitions:

$$\Delta x^+ = \frac{u_\tau \Delta x}{\nu}, \quad \Delta z^+ = \frac{u_\tau \Delta z}{\nu}$$

one can find the number,  $N_t = N_x N_y N_z$  of cells required as a function of  $Re_\tau$  for resolving this limited domain of simple flow (see Table 1):

$$N_x = \frac{8h}{\Delta x} = \frac{8 Re_\tau}{\Delta x^+}, \quad N_z = \frac{3h}{\Delta z} = \frac{3 Re_\tau}{\Delta z^+} \quad \text{with} \quad Re_\tau = \frac{u_\tau h}{\nu}$$

$Re_\tau$	500	$10^3$	$10^4$	$10^5$
$N_t$	$5 \times 10^5$	$2 \times 10^6$	$2 \times 10^8$	$2 \times 10^{10}$

**Table 1: Number of cells,  $N_t$ , vs Reynolds number for channel flow**

(For the practitioner: the Reynolds,  $Re$ , number based on the bulk velocity is around a factor of ten larger than the Reynolds number,  $Re_\tau$ , based on friction velocity. Note that  $Re_\tau$  is based on  $h=H/2$ ). The number of cells increases strongly with  $Re$  number, demanding high computing resources even for very simple flows. The CPU power scales even less favorably, as the time step also needs to be reduced to maintain a constant CFL number ( $CFL = (U \Delta t) / \Delta x$ ).

The  $Re$  number scaling for channel flows could be reduced by the application of wall functions with ever increasing  $y^+$  values for higher  $Re$  numbers. However, wall functions are a strong source

of modeling uncertainty and can undermine the overall accuracy of simulations. Furthermore, the experience with RANS models shows that the generation of high quality wall-function grids for complex geometries is a very challenging task. This is even more so for LES applications, where the user would have to control the resolution in all three space dimensions to conform to the LES requirements (e.g.  $\Delta x^+$  and  $\Delta z^+$  then depend on  $\Delta y^+$ ).

For external flows, there is an additional  $Re$  number effect resulting from the relative thickness of the boundary layer (e.g. boundary layer thickness relative to chord length of an airfoil). At high  $Re$  numbers, the boundary layer becomes very thin relative to the body's dimensions. Assuming a constant resolution per boundary layer volume, Spalart et al. (1997, 2000) provided estimates of computing power requirements for high Reynolds number aerodynamic flows under the most favorable assumptions. Even then, the computing resources are excessive and will not be met even by optimistic estimates of computing power increases for several decades.

While the computing requirements for high  $Re$  number flows are dominated by the relatively thin boundary layers, the situation for low  $Re$  number technical flows is often equally unfavorable, as effects such as laminar-turbulent transition dominate and need to be resolved. Based on reduced geometry simulations of turbomachinery blades (e.g. Michelassi, 2003), an estimate for a single turbine blade with end-walls is given in Table 2:

Method	Cells	Time steps	Inner loops per time step	Ratio to RANS
RANS	$\sim 10^6$	$\sim 10^2$	1	1
LES	$\sim 10^8\text{-}10^9$	$\sim 10^4\text{-}10^5$	10	$10^5\text{-}10^7$

**Table 2: Computing power estimate for a single turbomachinery blade with end-walls**

Considering that the goal of turbomachinery companies is the simulation of entire machines (or parts of them), it is unrealistic to assume that LES will become a major element of industrial CFD simulations even for such low  $Re$  number ( $Re\sim 10^5$ ) applications. However, LES can play a role in the detailed analysis of elements of such flows like cooling holes or active flow control.

All the above does not mean that LES of wall-bounded flows is not feasible at all, but just that the costs of such simulations are high. Figure 4 shows the grid used for a LES around a NACA 0012 airfoil using the WALE model. The computational domain is limited in the spanwise direction to 5% of the airfoil chord length using periodic boundary conditions in that direction. At a Reynolds number of  $Re=1.1\times 10^6$  a spanwise extent of 5% has been estimated as the minimum domain size that allows turbulence structures to develop without being synchronized across the span by the periodic boundary conditions. The estimate was based on the boundary layer thickness at the trailing edge as obtained from a precursor RANS computation. This boundary layer thickness is about 2% chord length. The grid had 80 cells in the spanwise direction and overall  $11\times 10^6$  cells. The simulation was carried out at an angle of attack of  $\alpha=7.3^\circ$ , using ANSYS Fluent in incompressible mode. The chord length was set to  $c=0.23$  [m], the freestream velocity,  $U=71.3$  [m/s] and the fluid is air at standard conditions. The time step was set to  $\Delta t=1.5\times 10^{-6}$  [s] giving a Courant number of  $CFL\sim 0.8$  inside the boundary layer. Figure 5 shows turbulence structures near the leading edge (a) and the trailing edge (b). Near the leading edge, the laminar-turbulent transition can clearly be seen. It is triggered by a laminar separation bubble. Near the trailing edge, the turbulence structures are already relatively large, but still appear unsynchronized in the spanwise direction (no large scale 2d structures with axis orientation in the spanwise direction). The simulation was run for  $\sim 10^4$  time steps before the averaging procedure was started. The time averaging was conducted for  $\sim 1\times 10^4$  time steps. Figure 6 (a) shows a comparison of the wall pressure coefficient  $C_p$  and Figure 6 (b) of the wall shear stress coefficient  $C_f$  on the suction side of the airfoil in comparison to a RANS computation using the SST model (Menter, 1994). No detailed discussion of the simulation is intended here, but the comparison of the wall shear stress with the well-calibrated RANS model indicates that the resolution of the grid

is still insufficient for capturing the near-wall details. For this reason, the wall shear stress is significantly underestimated by about 30% compared to the SST model in the leading edge area. As the trailing edge is approached, the comparison improves, mainly because the boundary layer thickness is increased whereas the wall shear stress is decreased, meaning that a higher relative resolution is achieved in the LES. Based on this simulation, it is estimated that a refinement by a factor of 2, in both streamwise and spanwise directions would be required in order to reproduce the correct wall shear stress. While such a resolution is not outside the realm of available computers, it is still far too high for day-to-day simulations.

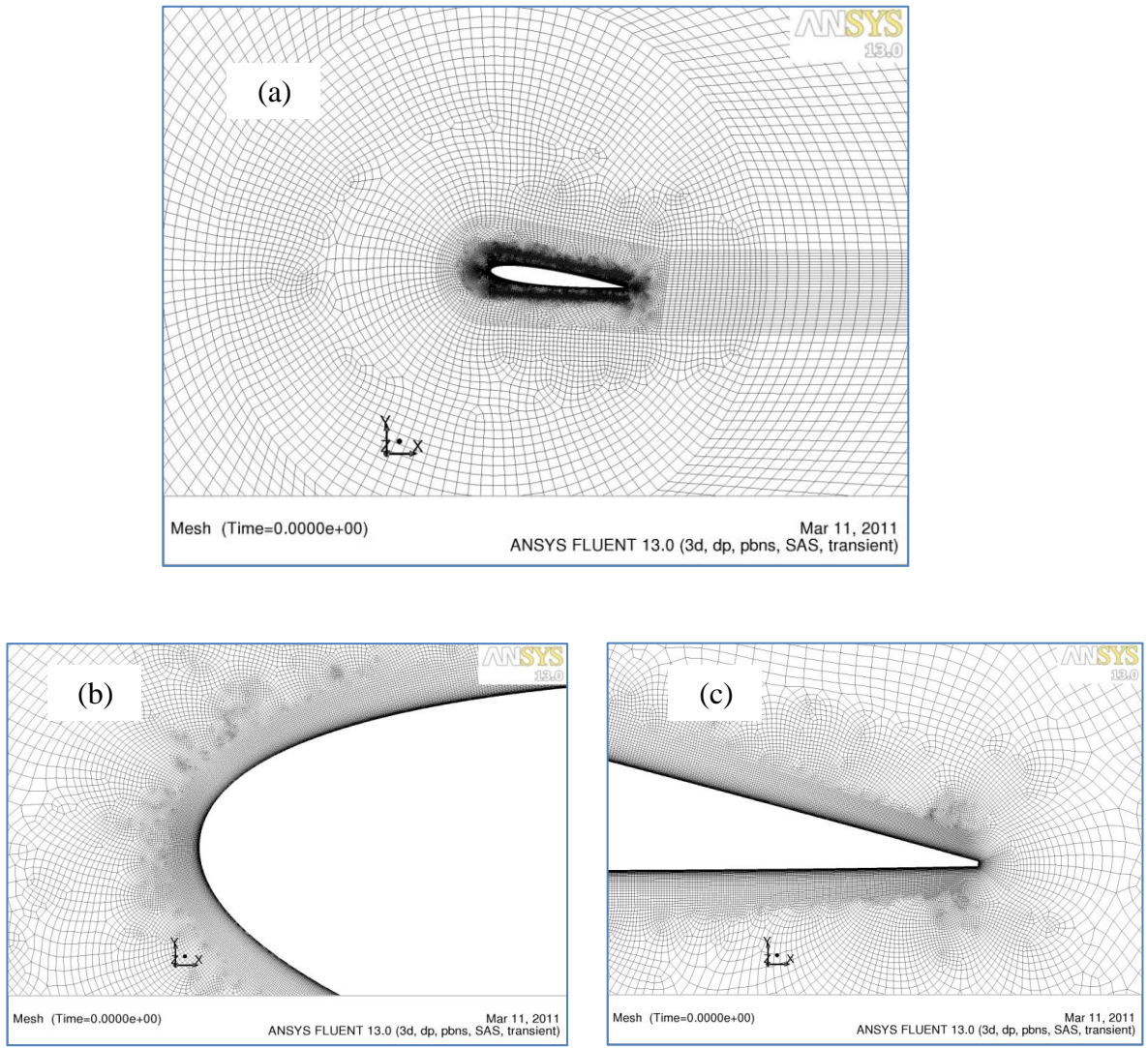


**Figure 4: Details of grid around a NACA 4412 airfoil (a) grid topology (b) Leading edge area (c) Trailing edge area**

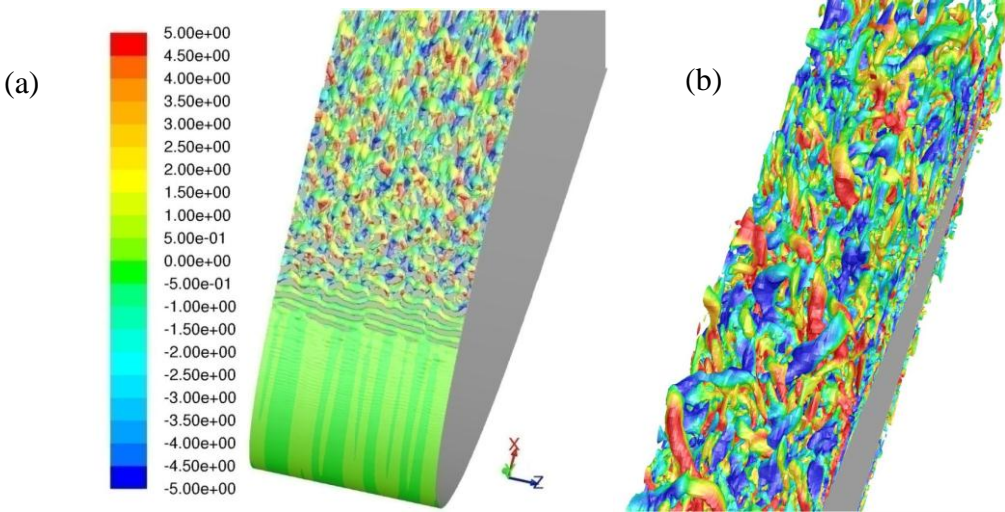


**Figure 5:** Turbulence structures of WALE LES computation around a NACA 4412 airfoil (a) Leading edge (b) Trailing edge (Q-criterion, color- spanwsie velocity component)

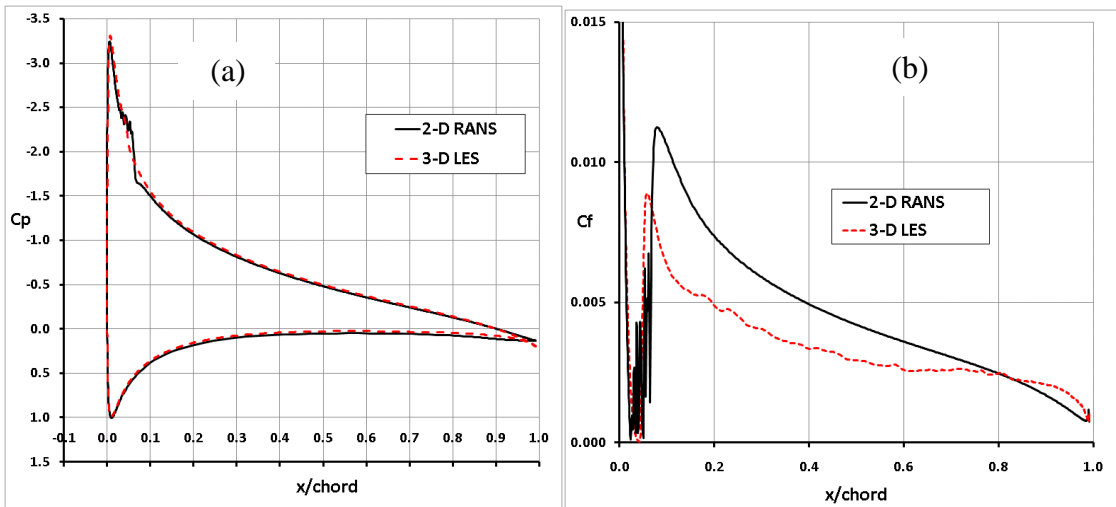


**Figure 6:** (a) Wall pressure coefficient  $C_p$  and (b) wall shear stress coefficient  $C_f$  on the suction side of a NACA 4412 airfoil. Comparison of RANS-SST and LES-WALE results.

Overall, LES for industrial flows will be restricted in the foreseeable future to flows not involving wall boundary layers, or wall-bounded flows in strongly reduced geometries, preferentially at low Re numbers.

The limitations of the conventional LES approach are the driving force behind the development of hybrid RANS-LES models that are described in the later parts of this report.

### 3. Scale-Resolving Simulation (SRS) Models – Basic Formulations

In the ANSYS CFD codes the following SRS models are available:

1. Scale-Adaptive Simulation (SAS) models
  - a. SAS-SST model (Fluent, CFX)
2. Detached Eddy Simulation (DES) Models
  - a. DES-SA (DDES) model (Fluent)
  - b. DES-SST (DDES) model (Fluent, CFX)
  - c. Realizable k- $\epsilon$ -DES model (Fluent)
3. Large Eddy Simulation (LES)
  - a. Smagorinsky-Lilly model (+dynamic) (Fluent, CFX)
  - b. WALE model (Fluent, CFX)
  - c. Kinetic energy subgrid model dynamic (Fluent)
  - d. Algebraic Wall Modeled LES (WMLES) (Fluent, CFX)
4. Embedded LES (ELES) model
  - a. Combination of all RANS models with all non-dynamic LES models (Fluent)
  - b. Zonal forcing model (CFX)
5. Synthetic turbulence generator
  - a. Vortex method (Fluent)
  - b. Harmonic Turbulence Generator (HTG) (CFX)

#### 3.1. Scale-Adaptive Simulation (SAS)

In principle, all RANS models can be solved in unsteady mode (URANS). Experience shows, however, that classical URANS models do not provide any spectral content, even if the grid and time step resolution would be sufficient for that purpose. It has long been argued that this behavior is a natural outcome of the RANS averaging procedure (typically time averaging), which eliminates *all* turbulence content from the velocity field. By that argument, it has been concluded that URANS can work only in situations of a ‘separation of scales’, e.g. resolve time variations that are of much lower frequency than turbulence. An example would be the flow over a slowly oscillating airfoil, where the turbulence is modeled entirely by the RANS model and only the slow super-imposed motion is resolved in time. A borderline case for this scenario is the flow over bluff bodies, like a cylinder in crossflow. For such flows, the URANS simulation provides unsteady solutions even without an independent external forcing. The frequency of the resulting vortex shedding is not necessarily much lower than the frequencies of the largest turbulent scales. This scenario is depicted in Figure 7. It shows that URANS models (in this case SST) produce a single mode vortex shedding even at a relatively high  $Re$  number of  $Re=10^6$ . The vortex stream extends far into the cylinder wake, maintaining a single frequency. This is in contradiction to experimental observations of a broadband turbulence spectrum.

However, as shown in a series of publications (e.g. Menter and Egorov 2010, Egorov et al., 2010), a class of RANS models can be derived based on a theoretical concept dating back to Rotta (see Rotta, 1972), which perform like standard RANS models in steady flows, but allow the formation of a broadband turbulence spectrum for certain types of unstable flows (for the types of flows, see Chapter 4). Such models are termed Scale-Adaptive Simulation (SAS) models. This scenario is illustrated by Figure 8 which shows the same simulation as in Figure 7 but with the

SAS-SST model. The behavior seen in Figure 7 is therefore not inherent to all RANS models, but only to those derived in a special fashion.

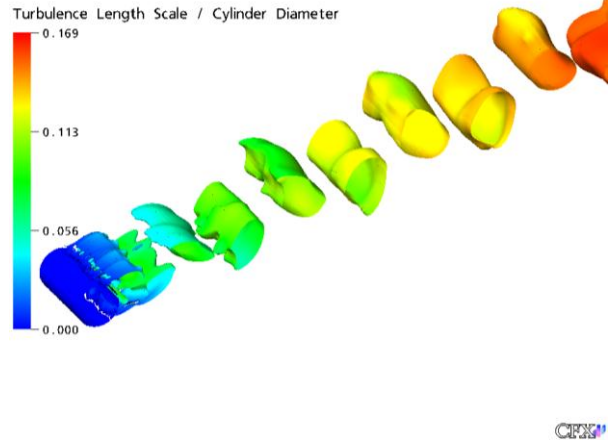


**Figure 7:** URANS computations of a flow past a circular cylinder (SST model)

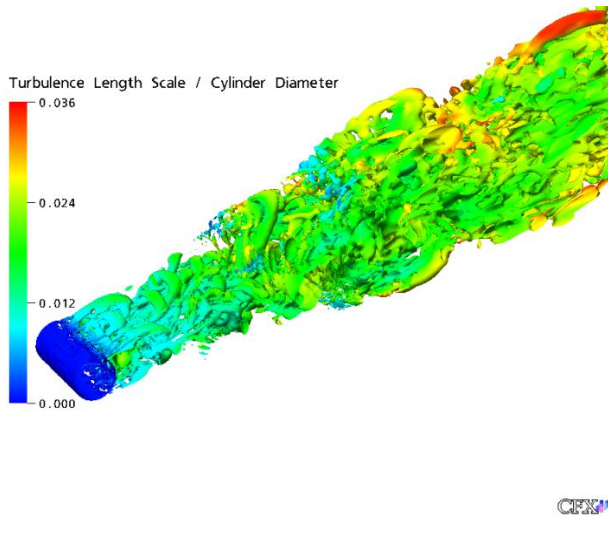


**Figure 8:** SAS simulation of flow past a circular cylinder (SAS-SST model)

The SAS concept is described in much detail in the cited references and will not be repeated here. However, the basic model formulation needs to be provided for a discussion of the model's characteristics. The difference between standard RANS and SAS models lies in the treatment of the scale-defining equation (typically  $\varepsilon$ -,  $\omega$ , or  $L_t$ -equation). In classic RANS models, the scale equation is modeled based on an analogy with the  $k$ -equation using simple dimensional arguments. The scale equation of SAS models is based on an exact transport equation for the turbulence length scale as proposed by Rotta. This method was re-visited by Menter and Egorov (2010) and avoids some limitations of the original Rotta model. As a result of this re-formulation, it was shown that the second derivative of the velocity field needs to be included in the source terms of the scale equation. The original SAS model (Menter and Egorov 2010) was formulated as a two-equation model, with the variable  $\Phi = \sqrt{k} L_t$  for the scale equation:

$$\frac{\partial(\rho k)}{\partial t} + \frac{\partial(\rho \bar{U}_j k)}{\partial x_j} = P_k - c_{\mu}^{3/4} \rho \frac{k}{\Phi^2} + \frac{\partial}{\partial x_j} \left( \frac{\mu_t}{\sigma_k} \frac{\partial k}{\partial x_j} \right)$$

$$\frac{\partial(\rho\Phi)}{\partial t} + \frac{\partial(\rho\bar{U}_j\Phi)}{\partial x_j} = \frac{\Phi}{k} P_k \left( \zeta_1 - \zeta_2 \left( \frac{L_t}{L_{vK}} \right)^2 \right) - \zeta_3 \rho k + \frac{\partial}{\partial x_j} \left( \frac{\mu_t}{\sigma_\Phi} \frac{\partial\Phi}{\partial x_j} \right)$$

$$\mu_t = c_\mu^{1/4} \rho \Phi$$

$$L_{vK} = \kappa \left| \frac{\bar{U}'}{\bar{U}''} \right|; \quad \bar{U}' = S = \sqrt{2S_{ij}S_{ij}}; \quad \bar{U}'' = \sqrt{\frac{\partial^2 \bar{U}_i}{\partial x_j \partial x_j} \frac{\partial^2 \bar{U}_i}{\partial x_k \partial x_k}}; \quad S_{ij} = \frac{1}{2} \left( \frac{\partial \bar{U}_i}{\partial x_j} + \frac{\partial \bar{U}_j}{\partial x_i} \right); \quad L_t = \frac{\Phi}{\sqrt{k}}$$

The main new term is the one including the von Karman length scale  $L_{vK}$ , which does not appear in any standard RANS model. The second velocity derivative allows the model to adjust its length scale to those structures already resolved in the flow. This functionality is not present in standard RANS models. This leads to the behavior shown in Figure 8, which agrees more closely with the experimental observations for such flows.

The  $L_{vK}$  term can be transformed and implemented into any other scale-defining equation resulting in SAS capabilities as in the case of the SAS-SST model. For the SAS-SST model, the additional term in the  $\omega$ -equation resulting from the transformation has been designed to have no effect on the SST model's RANS performance for wall boundary layers. It can have a moderate effect on free shear flows (Davidson, 2006).

The SAS model will remain in steady RANS mode for wall bounded flows, and can switch to SRS mode in flows with large and unstable separation zones (see Chapter 4).

### 3.2. Detached Eddy Simulation (DES)

Detached Eddy Simulation (DES) was introduced by Spalart and co-workers (Spalart et al., 1997, 2000, Travin et al., 2000, Strelets, 2001), to eliminate the main limitation of LES models by proposing a hybrid formulation that switches between RANS and LES based on the grid resolution provided. By this formulation, the wall boundary layers are entirely covered by the RANS model and the free shear flows away from walls are typically computed in LES mode. The formulation is mathematically relatively simple and can be built on top of any RANS turbulence model. DES has attained significant attention in the turbulence community as it was the first SRS model that allowed the inclusion of SRS capabilities into common engineering flow simulations.

Within DES models, the switch between RANS and LES is based on a criterion like:

$$\begin{aligned} C_{DES} \Delta_{max} > L_t &\rightarrow RANS; \quad \Delta_{max} = \max(\Delta_x, \Delta_y, \Delta_z) \\ C_{DES} \Delta_{max} \leq L_t &\rightarrow LES; \end{aligned}$$

where  $\Delta_{max}$  is the maximum edge length of the local computational cell. The actual formulation for a two-equation model is (e.g.,  $k$ -equation of the  $k$ - $\omega$  model):

$$\begin{aligned} \frac{\partial(\rho k)}{\partial t} + \frac{\partial(\rho \bar{U}_j k)}{\partial x_j} &= P_k - \rho \frac{k^{3/2}}{\min(L_t, C_{DES} \Delta_{max})} + \frac{\partial}{\partial x_j} \left( \left( \mu + \frac{\mu_t}{\sigma_k} \right) \frac{\partial k}{\partial x_j} \right) \\ L_t &= \frac{k^{3/2}}{\varepsilon} = \frac{\sqrt{k}}{\beta^* \omega} \end{aligned}$$

As the grid is refined below the limit  $\Delta_{max} \leq L_t$  the DES-limiter is activated and switches the model from RANS to LES mode. The intention of the model is to run in RANS mode for attached flow regions, and to switch to LES mode in detached regions away from walls. This suggests that

the original DES formulation, as well as its later versions, requires a grid and time step resolution to be of LES quality once they switch to the grid spacing as the defining length scale. Once the limiter is activated, the models lose their RANS calibration and all relevant turbulence information needs to be resolved. For this reason, e.g., in free shear flows, the DES approach offers no computational savings over a standard LES model. However, it allows the user to avoid the high computing costs of covering the wall boundary layers in LES mode.

It is also important to note that the DES limiter can already be activated by grid refinement inside attached boundary layers. This is undesirable as it affects the RANS model by reducing the eddy viscosity which, in turn, can lead to Grid-Induced Separation (GIS), as discussed by Menter and Kuntz (2002), where the boundary layers can separate at arbitrary locations depending on the grid spacing. In order to avoid this limitation, the DES concept has been extended to Delayed-DES (DDES) by Spalart et al. (2006), following the proposal of Menter and Kuntz (2003) of ‘shielding’ the boundary layer from the DES limiter. The DDES extension was also applied to the DES-SA formulation resulting in the DDES-SA model, as well as to the SST model giving the DDES-SST model.

For two-equation models, the dissipation term in the  $k$ -equation is thereby re-formulated as follows:

$$E_{DES} = \rho \frac{k^{3/2}}{\min(L_t, C_{DES}\Delta)} = \rho \frac{k^{3/2}}{L_t \min\left(L_t, C_{DES} \frac{\Delta}{L_t}\right)} = \rho \frac{k^{3/2}}{L_t} \max\left(1; \frac{L_t}{C_{DES}\Delta}\right)$$

$$E_{DDES} = \rho \frac{k^{3/2}}{L_t} \max\left(1; \frac{L_t}{C_{DES}\Delta} (1 - F_{DDES})\right)$$

The function  $F_{DDES}$  is designed in such a way as to give  $F_{DDES}=1$  inside the wall boundary layer and  $F_{DDES}=0$  away from the wall. The definition of this function is intricate as it involves a balance between proper shielding and not suppressing the formation of resolved turbulence as the flow separates from the wall.

There are a number of DDES models available in ANSYS CFD. They follow the same principal idea with respect to switching between RANS and LES mode. The models differ therefore mostly by their RANS capabilities and should be selected accordingly.

### 3.3. Large Eddy Simulation (LES)

The details of different LES models can be found in the User and Theory documentation of the corresponding solvers. As described in Section 2.1, the main purpose of LES models is to provide sufficient damping for the smallest (unresolved) scales. For this reason, it is not advisable to use complex formulations, but stay with simple algebraic models. The most widely used LES model is the Smagorinsky (1963) model:

$$\nu_t = (C_S \Delta)^2 S$$

The main deficiency of the Smagorinsky model is that its eddy-viscosity does not go to zero for laminar shear flows (only  $\partial U / \partial y \neq 0$ ). For this reason, this model also requires a near-wall damping function in the viscous sublayer. It is desirable to have a LES formulation that automatically provides zero eddy-viscosity for simple laminar shear flows. This is especially important when computing flows with laminar turbulent transition, where the Smagorinsky model would negatively affect the laminar flow. The simplest model to provide this functionality is the WALE (Wall-Adapting Local Eddy-viscosity) model of Nicoud and Ducros (1999). The same

effect is also achieved by dynamic LES models, but at the cost of a somewhat higher complexity. None of the classical LES models addresses the main industrial problem of excessive computing costs for wall-bounded flows at moderate to high Reynolds numbers.

However, there are numerous cases at very low Reynolds numbers where LES can be an industrial option. Under such conditions, the wall boundary layers are likely laminar and turbulence forms only in separated shear layers and detached flow regions. Such situations can be identified by analyzing RANS eddy viscosity solutions for a given flow. In case the ratio of turbulence to molecular viscosity  $R=(\mu_t/\mu)$  is smaller than  $R \sim 15$  inside the boundary layer, it can be assumed that the boundary layers are laminar and no resolution of near-wall turbulence is required. Such conditions are observed for flows around valves or other small-scale devices at low Reynolds numbers.

LES can also be applied to free shear flows, where resolution requirements are much reduced relative to wall-bounded flows.

### 3.4. Wall Modeled Large Eddy Simulation (WMLES)

Wall Modeled LES (WMLES) is an alternative to classical LES and reduces the stringent and  $Re$  number-dependent grid resolution requirements of classical wall-resolved LES (Section 2.1.) The principle idea is depicted in Figure 9. As described in Section 2.1, the near-wall turbulence length scales increase linearly with the wall distance, resulting in smaller and smaller eddies as the wall is approached. This effect is limited by molecular viscosity, which damps out eddies inside the viscous sublayer (VS). As the  $Re$  number increases, smaller and smaller eddies appear, since the viscous sublayer becomes thinner. In order to avoid the resolution of these small near-wall scales, RANS and LES models are combined such that the RANS model covers the very near-wall layer, and then switches over to the LES formulation once the grid spacing becomes sufficient to resolve the local scales. This is seen in Figure 9(b), where the RANS layer extends outside of the VS, thus avoiding the need to resolve the inner ‘second’ row of eddies depicted in the sketch.

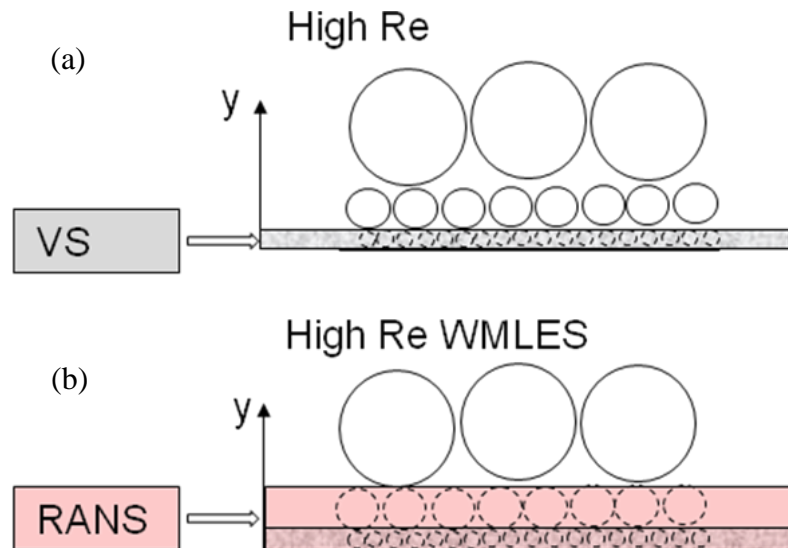


**Figure 9: Concept of WMLES for high Re number flows (a) Wall-resolved LES. (b) WMLES**

The WMLES formulation in ANSYS CFD is based on the formulation of Shur et al. (2008):

$$\nu_t = f_D \min \left\{ (\kappa y)^2, (C_{SMAG} \Delta)^2 \right\} S$$

where  $y$  is the wall distance,  $\kappa$  is the von Karman constant,  $S$  is the strain rate and  $f_D$  is a near-wall damping function. This formulation was adapted to suit the needs of the ANSYS general purpose

CFD codes. Near the wall, the min-function selects the Prandtl mixing length model whereas away from the wall it switches over to the Smagorinsky model. Meshing requirements for the WMLES approach are given in 4.3.3.

For wall boundary layer flows, the resolution requirements of WMLES depend on the details of the model formulation. In ANSYS Fluent and ANSYS CFX they are (assuming for this estimate that  $x$  is the streamwise,  $y$  the wall normal and  $z$  the spanwise direction as shown in Figure 10):

$$N_x \approx \frac{\delta}{\Delta x} \approx 10; \quad N_y \approx 30 - 40; \quad N_z \approx \frac{\delta}{\Delta z} \approx 20$$

where  $N_x$ ,  $N_y$ , and  $N_z$  are the numbers of cells in the streamwise, wall normal, and spanwise directions respectively per boundary layer thickness,  $\delta$ , (see Figure 10). In other words, one needs about 6000-8000 cells for covering one boundary layer volume  $\delta x \delta y \delta z$ . This is also the minimal resolution for classical LES models at low Reynolds numbers. Actually, for low Reynolds numbers, WMLES turns essentially into classical LES. The advantage of WMLES is that the resolution requirements relative to the boundary layer thickness remain independent of the Reynolds number.

While WMLES is largely Reynolds number-independent for channel and pipe flows (where the boundary layer thickness needs to be replaced by half of the channel height) there remains a Reynolds number sensitivity for aerodynamic boundary layer flows, where the ratio of the boundary layer thickness,  $\delta$ , to a characteristic body dimension,  $L$ , is decreasing with increasing Reynolds number, e.g. there are more boundary layer volumes to consider at increased Reynolds numbers. It should also be noted that despite the large cost savings of WMLES compared to wall-resolved LES, the cost increase relative to RANS models is still high. Typical RANS computations feature only one cell per boundary layer thickness in streamwise and spanwise directions ( $N_x \sim N_z \sim 1$ ). In addition, RANS steady state simulations can be converged in the order of  $\sim 10^2 - 10^3$  iterations, whereas unsteady simulations typically require  $\sim 10^4 - 10^5$ .

For wall normal resolution in WMLES, it is recommended to use grids with  $\Delta y^+ = \sim 1$  at the wall. If this cannot be achieved, the WMLES model is formulated to tolerate coarser  $\Delta y^+$  values ( $\Delta y^+$ -insensitive formulation) as well.

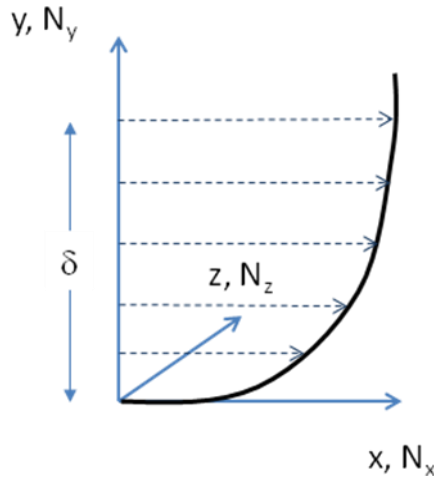


**Figure 10: Sketch of boundary layer profile with thickness  $\delta$ .  $x$ -streamwise,  $y$  normal and  $z$ -spanwise**

For channel and pipe flows, the above resolution requirements for the boundary layer should be applied, only replacing the boundary layer thickness,  $\delta$ , with half the channel height, or with the pipe radius in the grid estimation. This estimate would result in a minimum of  $\sim 120$  cells in the circumferential direction ( $360^\circ$ ) for a fully developed pipe flow.

It should be noted that reductions in grid resolution similar to WMLES can be achieved with classical LES models when using LES wall functions. However, the generation of suitable grids for LES wall functions is very challenging as the grid spacing normal to the wall and the wall-parallel grid resolution requirements are coupled and strongly dependent on  $Re$  number (unlike RANS where only the wall-normal resolution must be considered).

In ANSYS Fluent, the WMLES formulation can be selected as one of the LES options; in ANSYS CFX it is always activated inside the LES zone of the Zonal Forced LES (ZFLES) method.

### 3.5. Embedded/Zonal LES (ELES, ZLES)

The idea behind ELES is to predefine different zones with different treatments of turbulence in the pre-processing stage. The domain is split into a RANS and a LES portion ahead of the simulation. Between the different regions, the turbulence model is switched from RANS to LES/WMLES. In order to maintain consistency, synthetic turbulence is generally introduced at RANS-LES interfaces. ELES is actually not a new model, but an infrastructure that combines existing elements of technology in a zonal fashion. The recommendations for each zone are therefore the same as those applicable to the individual models.

In ANSYS Fluent, an Embedded LES formulation is available (Cokljat et al., 2009). It allows the combination of most RANS models with all non-dynamic LES models in the predefined RANS and LES regions respectively. The conversion from modeled turbulence to resolved turbulence is achieved at the RANS-LES interface using the Vortex Method (Mathey et al., 2003).

In CFX, a similar functionality is achieved using a method called Zonal Forced LES (ZFLES) (Menter et al., 2009). The simulation is based on a pre-selected RANS model. In a LES zone, specified via a CEL expression, forcing terms in the momentum and turbulence equations are activated. These terms push the RANS model into a WMLES formulation. In addition, synthetic turbulence is generated at the RANS-LES interface,

There is an additional option in ANSYS Fluent that involves using a global turbulence model (SAS or DDES), and activates the generation of synthetic turbulence at a pre-defined interface. The code takes care of balancing the resolved and modeled turbulence through the interface. This option can be used to force global hybrid models (like SAS or DDES) into unsteadiness for cases where the natural flow instability is not sufficient. Unlike ELES, where different models are used in different zones, the same turbulence model is used upstream and downstream of the interface. This is different from ELES, where different models are used in different zones on opposite sides of the interface.

Such forcing can also be achieved in ANSYS CFX by specifying a thin LES region and using the SAS or DDES model globally.

### 3.6. Unsteady Inlet/Interface Turbulence

Classical LES requires providing unsteady fluctuations at turbulent inlets/interfaces (RANS-LES interface) to the LES domain. This makes LES substantially more demanding than RANS, where profiles of the mean turbulence quantities ( $k$  and  $\varepsilon$ , or  $k$  and  $\omega$ ) are typically specified. An example is a fully turbulent channel (pipe) flow. The flow enters the domain in a fully turbulent state at the inlet. The user is therefore required to provide suitable resolved turbulence at such an inlet location through unsteady inlet velocity profiles. The inlet profiles have to be composed in such a way that their time average corresponds to the correct mean flow inlet profiles, as well as to all relevant turbulence characteristics (turbulence time and length scales, turbulence stresses, and so on). For fully turbulent channel and pipe flows, this requirement can be circumvented by the application of periodic boundary conditions in the flow direction. The flow is thereby driven by a source term in the momentum equation acting in the streamwise direction. By that ‘trick,’ the turbulence leaving the domain at the outlet enters the domain again at the inlet, thereby avoiding the explicit specification of unsteady turbulence profiles. This approach can obviously be employed for only very simple configurations. It requires a sufficient length of the domain (at

least  $\sim 8\text{-}10h$  (see Figure 3)) in the streamwise direction to allow the formation inside the domain of turbulence structures independent of the periodic boundaries.

In most practical cases, the geometry does not allow fully periodic simulations. It can however feature fully developed profiles at the inlet (again typically pipe/channel flows). In such cases, one can perform a periodic precursor simulation on a separate periodic domain and then insert the unsteady profiles obtained at any cross section of that simulation to the inlet of the complex CFD domain. This approach requires either a direct coupling of two separate CFD simulations or the storage of a sufficient number of unsteady profiles from the periodic simulation to be read in by the full simulation.

In a real situation, however, the inlet profiles might not be fully developed and no simple method exists for producing consistent inlet turbulence. In such cases, synthetic turbulence can be generated, based on given inlet profiles from RANS. These are typically obtained from a precursor RANS computation of the domain upstream of the LES inlet.

There are several methods for generating synthetic turbulence. In ANSYS Fluent, the most widely used method is the Vortex Method (VM) (Mathey et al., 2003), where a number of discrete vortices are generated at the inlet. Their distribution, strength, and size are modeled to provide the desirable characteristics of real turbulence. The input parameters to the VM are the two scales ( $k$  and  $\varepsilon$ , or  $k$  and  $\omega$ ) from the upstream RANS computation. CFX uses the generation of synthetic turbulence by using suitable harmonic functions as an alternative to the VM (e.g. Menter et al., 2009).

The characteristic of high-quality synthetic turbulence in wall-bounded flows is that it recovers the time-averaged turbulent stress tensor quickly downstream of the inlet. This can be checked by plotting sensitive quantities like the time-averaged wall shear stress or heat transfer coefficient and observing their variation downstream of the inlet. It is also advisable to investigate the turbulence structures visually by using, for example, an iso-surface of the  $Q$ -criterion,  $Q=1/2(\Omega^2-S^2)$  ( $S$  – Strain rate,  $\Omega$  – vorticity rate). This can be done even after a few hundred time steps into the simulation.

Because synthetic turbulence will never coincide in all aspects with true turbulence, avoid putting an inlet/interface at a location with strong non-equilibrium turbulence activity. In boundary layer flows, that means that the inlet or RANS-LES interface should be located several (at least  $\sim 3$ ) boundary layer thicknesses upstream of any strong non-equilibrium zone (e.g. separation). The boundary layers downstream of the inlet/interface need to be resolved with a sufficiently high spatial resolution (see Section 4.3.3).

## 4. Generic Flow Types and Basic Model Selection

As will be discussed, there is a wide range of complex industrial turbulent flows and there is no single SRS approach to cover all of them with high efficiency. The most difficult question for the user is therefore: how to select the optimal model combination for a given simulation? For this task, it is useful to categorize flows into different types. Although such a categorization is not always easy and by no means scientifically exact (there are many flows which do not exactly fall into any one of the proposed categories or fall into more than one) it might still help in the selection of the most appropriate SRS modeling approach.

### 4.1. Globally Unstable Flows

#### 4.1.1. Flow Physics

The classical example of a globally unstable flow is a flow past a bluff body. Even when computed with a classical URANS model, the simulation will typically provide an unsteady output. Figure 13 shows the flow around a triangular cylinder in crossflow as computed with both the SAS-SST and the DES-SST model. It is important to emphasize that the flow is computed with steady-state boundary conditions (as would be employed for a RANS simulation). Still, the

flow downstream of the obstacle turns quickly into unsteady (scale-resolving) mode, even though no unsteadiness is introduced by any boundary or interface condition.

From a physical standpoint, such flows are characterized by the formation of ‘new’ turbulence downstream of the body. This turbulence is independent from, and effectively overrides, the turbulence coming from the thin, attached boundary layers around the body. In other words, the turbulence in the attached boundary layers has very little effect on the turbulence in the separated zone. The attached boundary layers can, however, define the separation point/line on a smoothly curved body and thereby affect the size of the downstream separation zone. This effect can be tackled by a suitable underlying RANS model.

Typical members of this family of flows are given in the list below. Such flows are very common in engineering applications and are also the type of flows where RANS models can exhibit a significant deterioration of their predictive accuracy.

Examples of globally unstable flows include:

- Flows past bluff bodies
  - Flow past buildings
  - Landing gears of airplanes
  - Baffles in mixers etc.
  - Side mirrors of cars
  - Stalled wings/sails
  - Re-entry vehicles
  - Trains/trucks/cars in crossflow
  - Tip gap of turbomachinery blades
  - Flows past orifices, sharp nozzles etc.
  - Cavities
  - Flows with large separation zones (relative to attached boundary layer thickness)
- Flows with strong swirl instabilities include:
  - Flow in combustion chambers of gas turbines etc.
  - Flows past vortex generators
  - Some tip vortex flows in adverse pressure gradients
- Flows with strong flow interaction include:
  - Impinging/colliding jets
  - Jets in crossflow

The color scheme of the preceding points above identifies flows that are clearly within the definition of globally unstable flows (black) and those where the type of the flow depends on details of its regime/geometry (grey). Such flows fall in-between globally and locally unstable flows (see section 4.2).

#### 4.1.2. Modeling

Of all flows where SRS modeling is required, globally unstable flows are conceptually the easiest to handle. They can be typically be captured by a global RANS-LES model such as SAS or DDES. Such models cover the attached and mildly separated boundary layers in RANS mode, thereby avoiding the high costs of resolving wall turbulence. Due to the strong flow instability past the separation line, there is no need for specifying unsteady inlet turbulence nor to define specific LES zones. Globally unstable flows are also the most beneficial for SRS, as experience shows that RANS models can fail with significant margins of error for such flows. A large number of industrial flows fall into this category.

The safest SRS model for such flows is the SAS approach. It offers the advantage that the RANS model is not affected by the grid spacing and thereby avoids the potential negative effects of (D)DES (grey zones or grid induced separation). The SAS concept reverts back to (U)RANS in case the mesh/time step is not sufficient for LES and thereby preserves a ‘backbone’ of modeling that is independent of space and time resolution, albeit at the increased cost that is associated with any transient SRS calculation. SAS also avoids the need for shielding, which for internal flows with multiple walls can suppress turbulence formation in DDES models.

The alternative to SAS is DDES. If proper care is taken to ensure LES mesh quality in the detached flow regions, the model will be operating in the environment for which it was designed, typically providing high-quality solutions. DDES has shown advantages for flows at the limit of globally unstable flows (see Figure 42) where the SAS model can produce URANS-like solutions. In cases like these, DDES still provides SRS in the separated regions.

For globally unstable flows, the behavior of SAS and DDES is often very similar and they should both be tried.

#### 4.1.3. Meshing Requirements

The part of the domain where the turbulence model acts in RANS mode has to be covered by a suitable RANS grid. It is especially important that all relevant boundary layers are covered with sufficient resolution (typically a minimum of 10-15 structured cells across the boundary layer). It is assumed that the user is familiar with grid requirements for RANS simulations.

The estimate for the lowest possible mesh resolution in the detached SRS region is based on the assumption that the largest relevant scales are similar in size to the width of the instability zone. For a bluff body, this would be the diameter  $D$  of the body; for a combustor, the diameter of the core vortex; for a jet in crossflow, the diameter of the jet; and so on. Experience shows that the minimum resolution for such flows is of the order:

$$\Delta_{\max} \leq 0.05D$$

e.g. more than 20 cells per characteristic diameter,  $D$  (in some applications with very strong instabilities, even 10 cells across the layer may be sufficient). As is generally the case for SRS, it is best to provide isotropic (cubic) cells, or at least to avoid large aspect ratios (aspect ratios smaller than <5 would be optimal, but cannot always be achieved in complex geometries).

With the above estimate for  $\Delta_{\max}$ , there is a good chance of resolving the main flow instability and the resulting strong turbulent mixing processes associated with the global flow instability (an effect often missed by RANS models). For acoustics simulations, it might also be important to resolve the turbulence generated in the (often thin) shear layer that is separating from the body. This poses a much more stringent demand on grid resolution on the simulation as this shear layer scales with the boundary layer thickness at separation and can be much smaller than the body dimension. This situation is covered in Section 4.2.

#### 4.1.4. Numerical Settings

The general numerical settings are described in Section 5. Globally unstable flows are relatively forgiving with respect to numerics, at least as far as the mean flow characteristics are concerned. The recommended choice for the advection terms is the Bounded Central Difference (BCD) scheme, especially for complex geometries and flows. For such flows, the classical Central Difference (CD) scheme can be unstable or produce unphysical wiggles in the solution (see Figure 50). The BCD scheme is slightly more dissipative, but is substantially more robust and is therefore frequently the optimal choice. If a visual inspection of the flow (see Section 7.1) shows that turbulence structures are not produced in agreement with the expectations for the flow, one can switch to CD. If this switch is made, it is advisable to closely monitor the solution (visually and numerically through residuals) to ensure that wiggles are not dominating the simulation. With

SAS the ‘Least Square Cell Based’ gradient method is essential in ANSYS Fluent, as it allows a better representation of the second derivative of the velocity field that is required for the model formulation (von Karman length scale).

In ANSYS CFX, the default hybrid numerical option switches explicitly between the High Resolution Scheme (in the RANS region) and the CD scheme (in the LES region). However, for most applications, it appears that the use of the BCD scheme should also be favored in ANSYS CFX (see also section 5.1.1)

#### 4.1.5. Examples

**Flow Around a Fighter Aircraft** Figure 11 shows a highly complex, globally unstable flow field, around a generic fighter aircraft geometry at high angle of attack as computed with the SAS-SST model. The grid consists of  $10^8$  hybrid cells. This simulation is currently in progress within the EU project ATAAC and no detailed discussion of this flow is intended. This image demonstrates the complex regional appearance of resolved turbulence around the aircraft. It is obvious that the application of global models like SAS or DDES greatly simplifies the setup for such flows compared to using ELES/ZLES, where the user would have to define the ‘LES’ regions and suitable interfaces between the RANS and LES regions in a pre-processing step. In contracts, when using global models, the simulation is first carried out in standard RANS mode. Starting from that RANS solution, the model is then simply switched to the SAS or DDES variant of the RANS model, the solver is set to unsteady mode, and the numeric is adjusted according to 4.1.4. No further adjustment is required in order to produce the solutions shown in Figure 11.

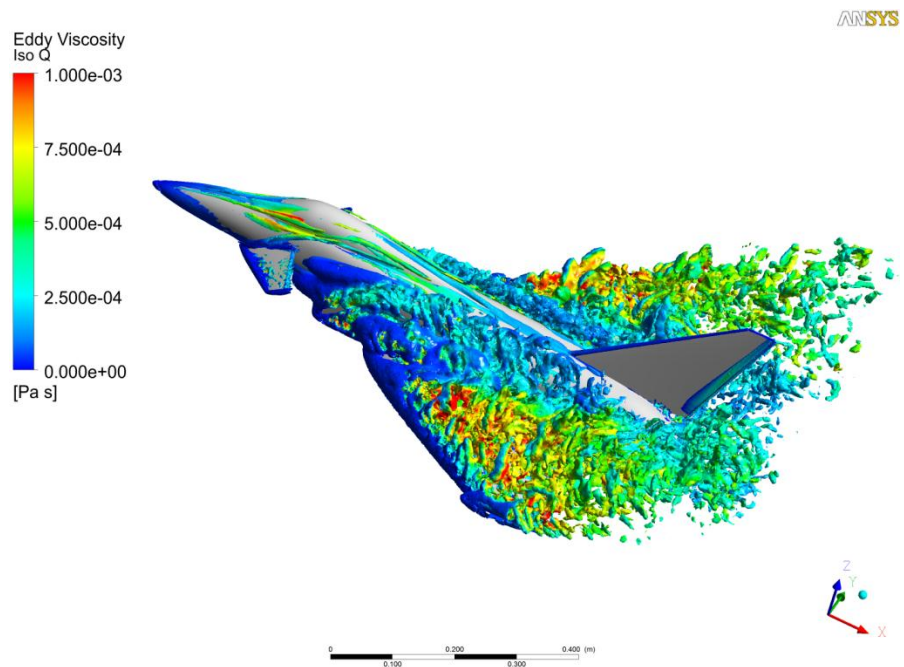


**Figure 11:** Turbulence structures for flow around a generic fighter aircraft (Q-criterion) as computed by SAS-SST model

#### Flow Around a Triangular Cylinder

Figure 12 shows the grid around a triangular cylinder in crossflow. The Reynolds number based on the freestream velocity (17.3 m/s) and the edge length is 45,500. Periodic boundary conditions have been applied in the spanwise direction. The simulations have been run with ANSYS Fluent using the BCD (bounded central difference) and CD (Central Difference)

advection schemes and a time step of  $\Delta t = 10^{-5}$  s (CFL~1 behind cylinder). The grid features 26 cells across its base. It is extended in the spanwise direction to cover 6 times the edge length of the triangle with 81 cells in that direction. Due to the strong global instability of this flow, such resolution was sufficient and has produced highly accurate solutions for mean flow and turbulence quantities (Figure 13).

It should be noted that not all flows produce such strong instability as the triangular cylinder, and a higher grid resolution might be required for flows with less instability. Figure 13 shows that the grid does not provide resolution of the boundary layer on the walls of the triangular body. This is not a problem in the current case because the wall boundary layer has no influence on the global flow, as it separates at the corners of the triangle. In real flows, this might not always be the case and the boundary layer should be resolved with a RANS-type mesh i.e. a finer mesh in the near-wall region with higher aspect ratios being acceptable.

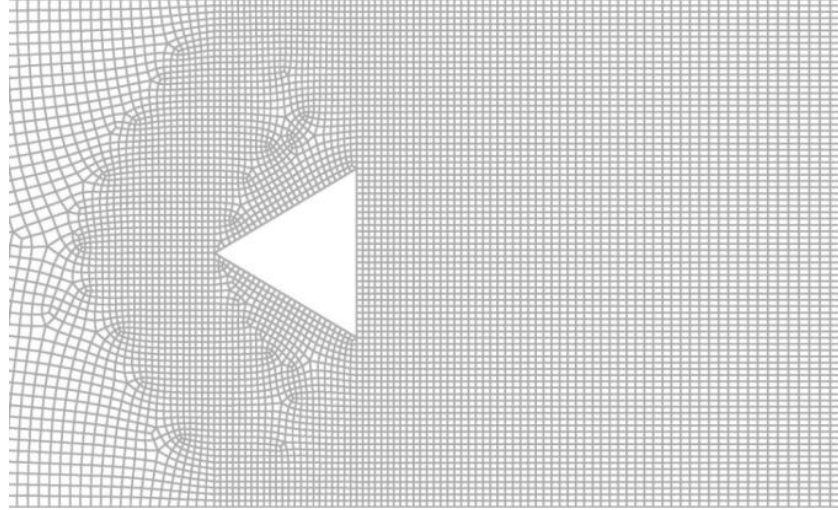


**Figure 12:** Grid around cylinder in crossflow

Figure 13 shows a visual representation of the flow using the DDES-SST and the SAS-SST models with the Q-criterion (see 7.1). Both simulations have been carried out using the BCD scheme. Both models generate resolved turbulence structures in agreement with the expectation for the grid provided. Figure 14 show a comparison with the experimental data (Sjunnesson et al., 1992) for the wake velocity profiles as well as for turbulence characteristics.

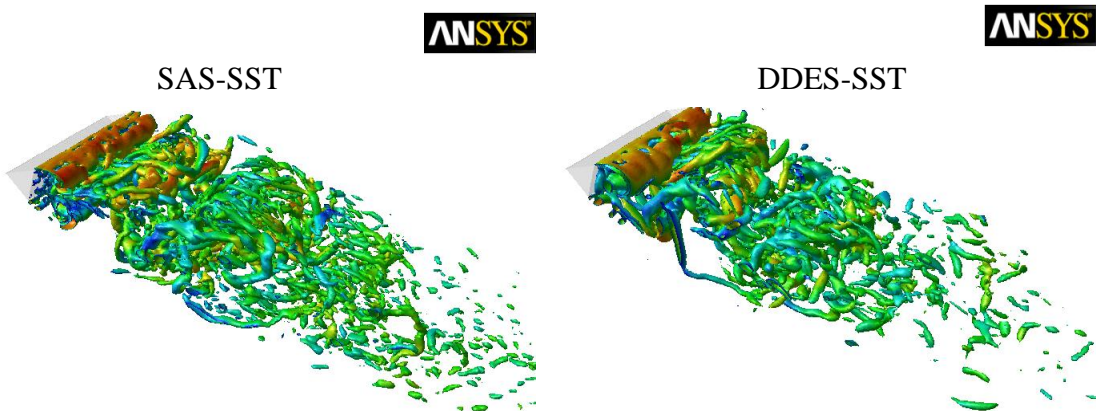


**Figure 13:** Turbulence structures for flow around a cylinder in crossflow.

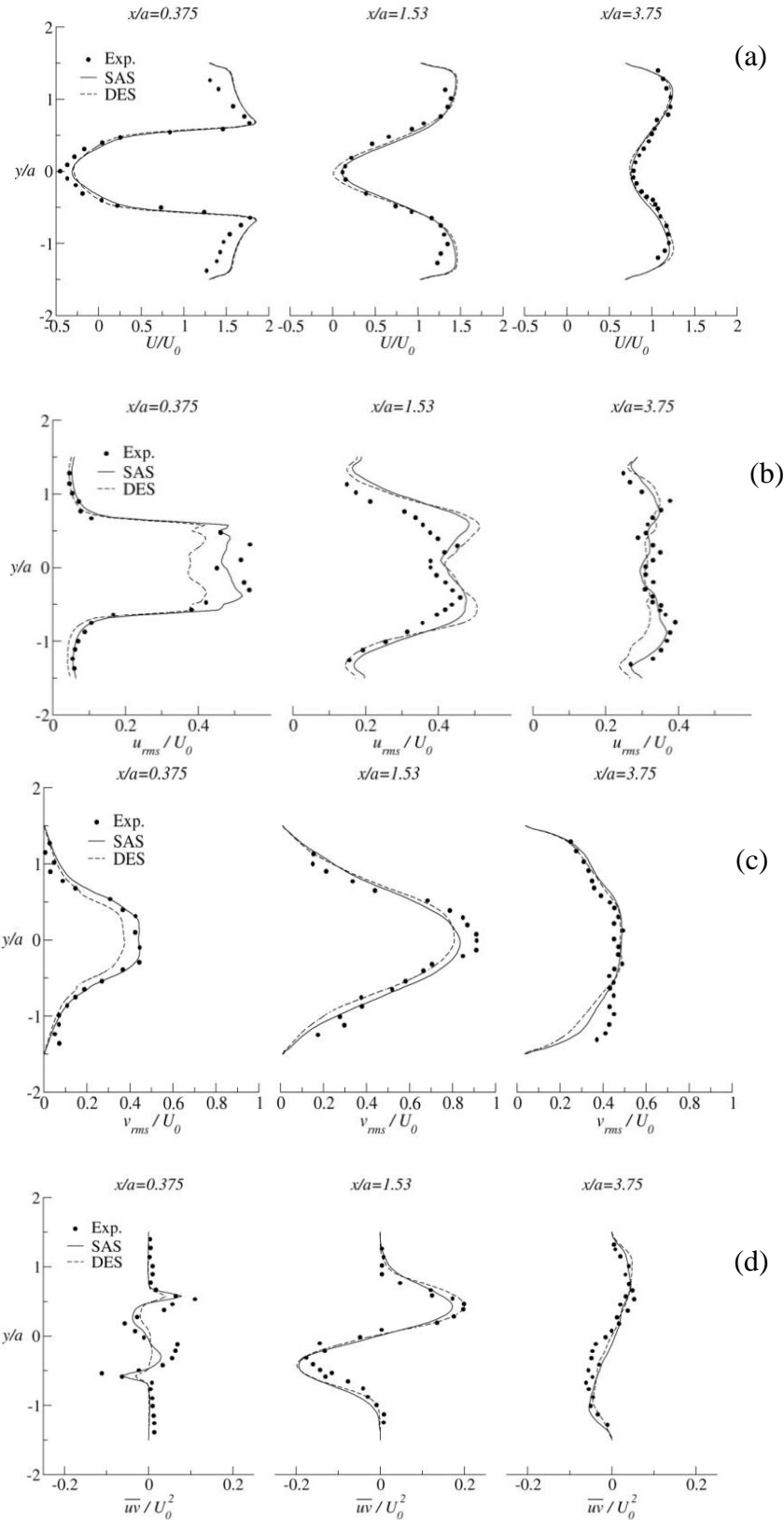


**Figure 14: Velocity profiles and turbulence RMS profiles for three different stations downstream of the triangular cylinder ( $x/a=0.375$ ,  $x/a=1.53$ ,  $x/a=3.75$ ). Comparison of SAS-SST, DES-SST models, and experiment. (a)  $U$ -velocity, (b)  $u_{rms}$ , (c)  $v_{rms}$ , (d)  $u'v'$**

Figure 15 shows a comparison of the CD and the BCD scheme for the triangular cylinder using the SAS-SST model. The turbulence content is almost identical, except that some smaller scales are present in the CD simulation downstream of the body. A comparison with experimental data showed results that are almost identical to the ones shown in Figure 14 and independent of whether the CD or the BCD scheme was used.

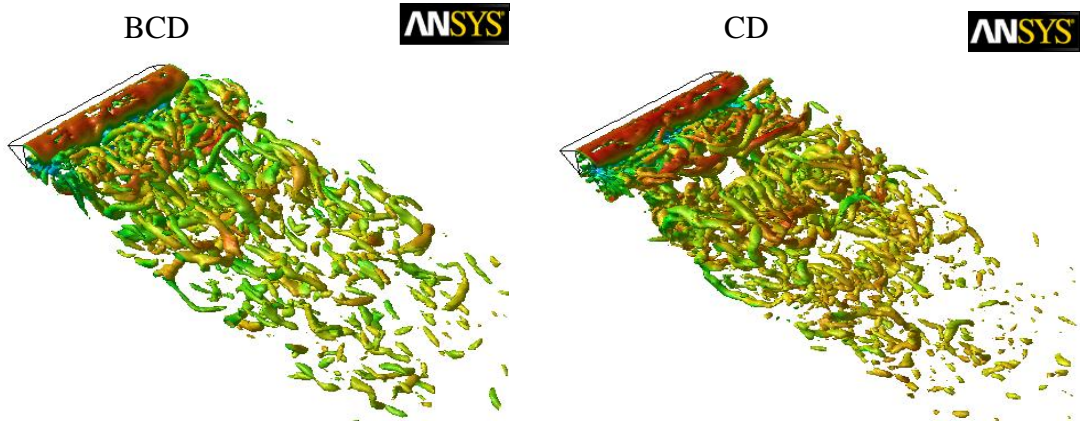


**Figure 15: SAS-SST simulation for flow around a triangular cylinder using the BCD and the CD scheme for the convective fluxes**

#### *ITS Combustion Chamber*

The SAS-SST model is applied to the flow in a single swirl burner investigated experimentally by Schildmacher et al. (2000) at ITS (Institut für Thermische Strömungsmaschinen) of the University of Karlsruhe. The ITS burner is a simplified industrial gas turbine combustor. It concentrates on the swirl flow in the combustion region. Similar to the triangular cylinder test case, the wall boundary layers are not important – meaning that this test case is also accessible to pure LES simulations. However, in many industrial combustion chambers wall boundary layers and auxiliary pipe flows have to be considered, thus making them unsuitable for pure LES.

There are two co-axial inlet streams and both are swirling in the same direction. The swirl is generated by means of the two circumferential arrays of blades, which are not included in the current computational domain. The axisymmetric velocity profiles with the circumferential component corresponding to the given swirl number are used as the inlet boundary conditions. The swirl gives the flow a strong global instability, which can be captured well by global SRS models.

Figure 16 shows the geometry. The grid, shown in Figure 17 consists of  $3.6 \cdot 10^6$  tetrahedral elements. As stated the wall boundary layers are not important and are therefore not resolved on this tetrahedral mesh. The simulation was run with ANSYS CFX, which internally converts the grid to a polyhedral grid with  $6 \cdot 10^5$  control volumes around the grid points for the node-based solver. This means that the polyhedral grid cells are larger than the visual impression from Figure 17 with ~20-30 cells covering the relevant length scale L shown in Figure 17. The grid does not feature any near-wall boundary layer resolution. It is recommended to provide such a boundary layer grid for industrial flows (typically more than 10 structured cells across the boundary layer), as in some geometries the separation characteristics near the burner entrance can depend on such details. The convection scheme selected was the default hybrid scheme; however, BCD should also work well.

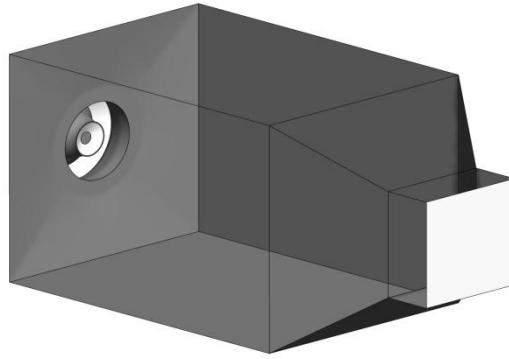


**Figure 16:** Computational domain for the ITS swirl burner

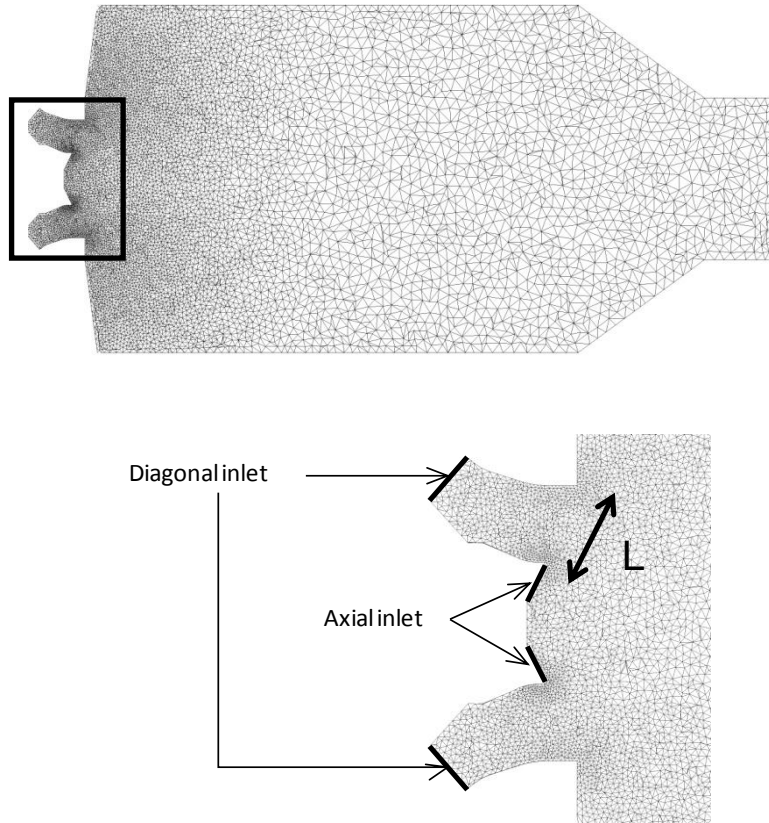
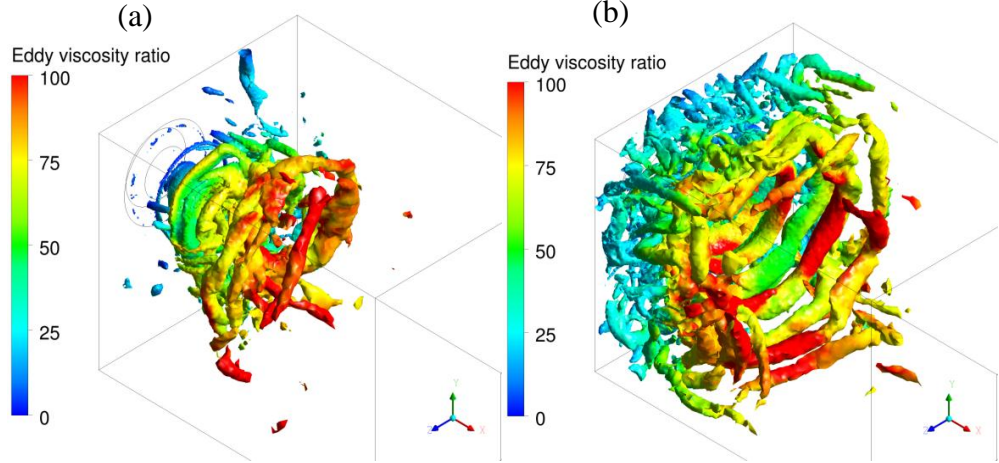


**Figure 17:** Unstructured grid on the symmetry plane and boundary locations for the ITS swirl burner and relevant length scale,  $L$

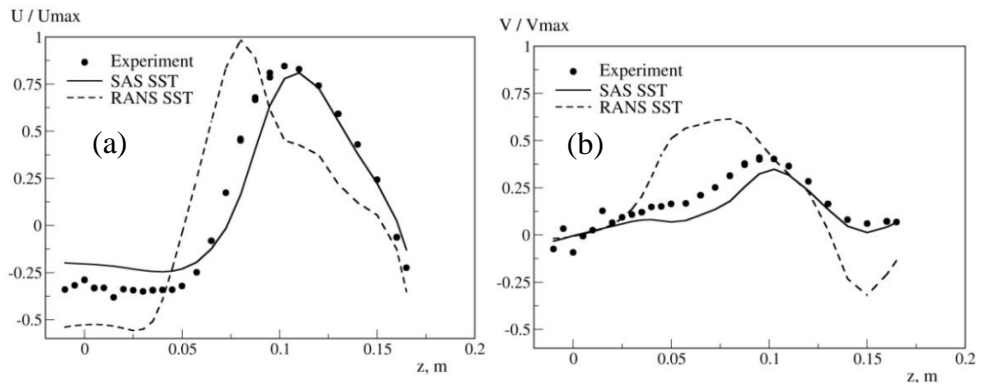
The flow structures from the SAS-SST computations of the non-reacting and the reacting flow at a given instance in time are shown in Figure 18 using the  $Q$ -criterion ( $Q=2\times 10^7 \text{ } 1/\text{s}^2$ , see 7.1). The main turbulence structures seem to be captured well in the simulations. Clearly, small-scale turbulence cannot be resolved on such a grid. The grid resolution used here should not be considered as a recommendation for combustion chambers, but as the lowest limit for which such SRS models can be applied.

Figure 19 shows a comparison of the standard  $k-\varepsilon$  RANS and SAS results at a given distance from the burner entrance. It is just to show the level of improvement which results from the application of SRS methods. Many more details of this simulation can be found in Egorov et al.

(2010) or in a more detailed analysis of a more complex combustion chamber in Widenhorn et al. (2009).



**Figure 18:** SAS solution for ITS combustion chamber, iso-surface  $Q=1/2(S^2-\Omega^2)=2\times 10^7 \text{ s}^{-2}$  (a) non-reacting, (b) reacting flow



**Figure 19:** Reacting flow velocity profiles at the axial distance from the inlet  $x=103 \text{ mm}$  (a) Axial velocity. (b) Tangential velocity

## 4.2. Locally Unstable Flows

### 4.2.1. Flow Physics

The expression ‘locally unstable flows’ is not easily definable as every turbulent flow is by nature unstable. It is meant to characterize flows which also produce ‘new’ turbulence, typically downstream of a geometry change, but where the flow instability producing this turbulence is significantly weaker than for globally unstable flows.

Consider the computation of a mixing layer starting from two wall boundary layers in RANS mode (see Figure 20). As the flat plate ends, the two boundary layers form a turbulent mixing layer, which becomes relatively quickly independent of the turbulence of the two boundary layers on the flat plate (yellow circles). The mixing layer instability (red) provides for a de-coupling of the boundary layer and the mixing layer turbulence. For this reason, one can neglect the boundary layer turbulence downstream of the trailing edge (the dashed yellow boundary layer turbulence

sketched in Figure 20) and concentrate on using SRS mode to resolve the mixing layer turbulence, which will quickly dominate the flow.

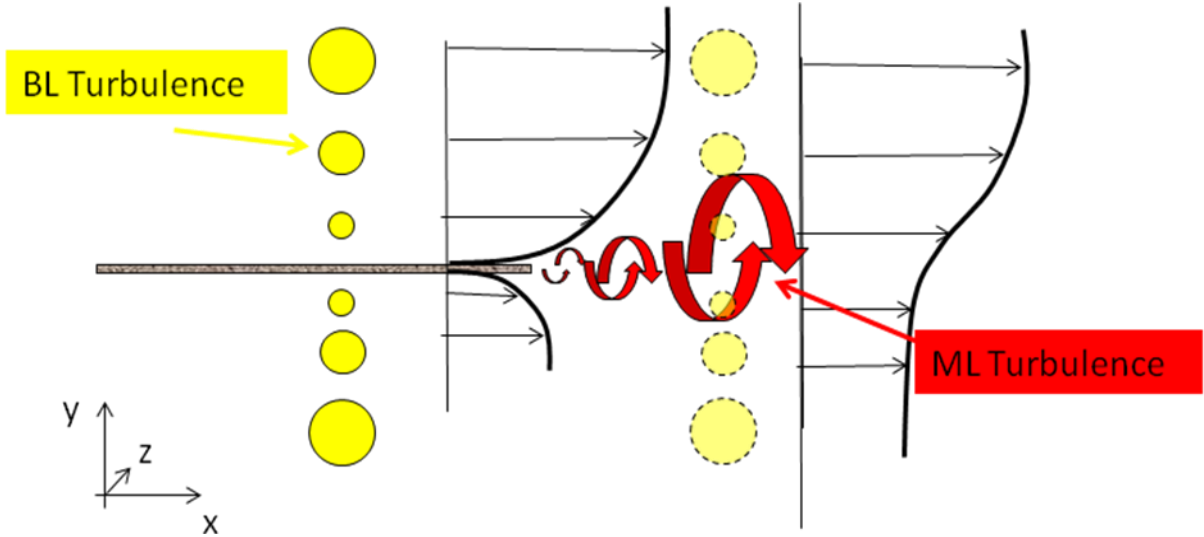


**Figure 20: Schematic of locally unstable flow: Mixing layer originating from a flat plate with two boundary layers of different freestream velocity. Full yellow circles – boundary layer turbulence. Dashed yellow circles - remains of the boundary layer turbulence. Red arrows – new mixing layer turbulence.**

Examples of locally unstable flows:

- Generic Flows
  - All equilibrium free-shear flows emanating from walls (jets, wakes, mixing layers).
  - Backward-facing step flow
  - Weakly interacting equilibrium flows
  - Flows with weak swirl

#### 4.2.2. Modeling

The goal in SRS is to cover the boundary layer turbulence (solid yellow circles in Figure 20) in RANS and the mixing layer turbulence (red) in resolved mode. This can only be achieved if the impact of the RANS turbulence model is significantly reduced downstream of the trailing edge; otherwise the formation of unsteady structures would be suppressed.

The SAS model will typically not switch to SRS mode in such situations, independent of the mesh provided, as the eddy-viscosity produced in the mixing layer will be too large for the flow instability at hand. From a pure turbulence modeling standpoint, this is often acceptable, as such flows are typically covered with reasonable accuracy by using RANS models (mixing layers, wakes, back step, etc.). However, in cases where unsteady information is required for other reasons (e.g. acoustics), the SAS model will likely not be suitable, unless an interface is used that converts modeled turbulence energy into resolved energy (see 3.5).

DDES allows SRS behavior, as the shielding function is turned off past the trailing edge of the plate, and the eddy-viscosity is reduced, assuming a fine (LES) grid is provided downstream of the plate. The DDES model then switches to LES mode in the wake, and the mixing-layer

instability is strong enough to generate resolved turbulence relative quickly (within a few boundary layer thicknesses). It is important to point out that the ability of the DDES model to generate unsteady structures in the mixing layer depends on the grid provided in that area. Assuming an overly coarse grid (for example, in the spanwise direction), the DES limiter would not engage and the model would stay in RANS mode, which will not allow the formation of resolved structures. Remember that the DES length scale is defined as:

$$L_{DES} = \min(L_t, C_{DES} \Delta_{\max})$$

with  $\Delta_{\max}$  being the largest edge length for each cell. For this case, assume that the grid in the x-y plane shown in Figure 20 is very fine (of LES quality), and  $\Delta_{\max}=\Delta z$  is the grid resolution in the spanwise (z) direction. Conversely, if  $\Delta z$  is very coarse, the DES limiter would always select the RANS length scale  $L_t$  and the model would remain in RANS mode in the wake region. No unsteady structures would develop as the RANS model will damp them out. As the grid in the z-direction is refined, the DES limiter will be activated at some location downstream of the trailing edge where  $\Delta z=L_{t,\max}$  (note that  $L_t$  grows as the mixing layer becomes thicker). With further grid refinement, the location of the implicit RANS-LES interface would move closer to the trailing edge. Eventually, the entire mixing layer would be covered by LES. This behavior of (D)DES is both a disadvantage and an advantage. The disadvantage and the danger lie in the strong grid sensitivity introduced explicitly into the turbulence model. As a result, the user of DDES must be very careful to provide a suitable grid for a given application. The advantage is that the model can be applied to locally unstable flows without the definition of an explicit RANS-LES interface. However, the grid sensitivity can be reduced by employing an interface which converts modeled turbulence to resolved turbulence using the DDES model upstream and downstream of the interface (see 3.5).

The most general approach to the flows discussed here is the use of the embedded or zonal RANS-LES methods, where the boundary layers are covered by a RANS model and the mixing layer by a LES model. The models are explicitly switched from RANS to LES at a pre-defined interface upstream or at the trailing edge. In order to obtain a proper LES solution, a grid with LES resolution is required in the mixing layer. Frequently a non-conformal interface between the RANS and the LES part is used to reduce the grid resolution in the upstream RANS region. For a fully consistent simulation, one must introduce synthetic turbulence at the RANS-LES interface. By such ‘injection’ of synthetic turbulence, the balance between RANS and LES turbulence across the interface is preserved (e.g. the yellow dashed circles in Figure 20 are accounted for).

The recommendation for flows with local instabilities is to use ELES/ZLES models if the geometry and the application allow the definition of well-defined interfaces (e.g. internal flows, like pipe flows etc.). Synthetic turbulence should be introduced at these interfaces in order to preserve the balance between the RANS and LES turbulence content. Should the geometry/application be complex such that the definition of explicit RANS and LES zones is not easily possible (e.g. turbomachinery flows, external flows), apply the DDES model. However, ensure careful tailoring of the grid with sufficient resolution on the LES region to avoid undefined model behavior somewhere between RANS and LES mode. It is advisable to refrain from using conventional DES in flows with extensive boundary layers, as the danger of affecting the boundary layers is too high.

It is very important to understand that for locally unstable flows, failure to capture the instability of the Separating Shear Layer (SSL) can have a pronounced effect on the solution downstream. The turbulence field is a result of this initial instability and missing it can severely limit the resolved content of the simulation and contaminate a rather expensive SRS solution. This danger is much reduced with ELES/ZLES models, (relative to DDES) because the flow enters the SSL with a prescribed synthetic turbulent content from the RANS-LES interface.

### 4.2.3. Meshing Requirements

In order to generalize the concepts discussed for the mixing layer example (Figure 20), we introduce the terminology of a Separating Shear Layer (SSL). It refers to the shear layer that starts at the point of separation from the body and moves into a free shear flow (we are not considering small separation bubbles embedded within the boundary layer). In Figure 20 this would be the mixing layer forming downstream of the plate. In other flows it can be a separating boundary layer from a corner. In the case of locally unstable flows, the  $\Delta_{\max}$  spacing should be sufficiently small to allow resolution of the initial flow instability of the SSL. The main quantity of relevance is the ratio of RANS to grid length scale:

$$R_L = \frac{\Delta_{\max}}{L_t^{\text{RANS}}} ; \quad L_t^{\text{RANS}} = \left( \frac{k^{3/2}}{\varepsilon} \right)^{\text{RANS}} = \left( \frac{k^{1/2}}{C_\mu \omega} \right)^{\text{RANS}}$$

It is important to emphasize that this quantity must be evaluated based on a precursor RANS solution. This implies that such a solution exists and is meaningful. If the precursor solution is not available, then one can estimate the ratio based on the thickness of SSL. For equilibrium mixing layers, the following ratio is approximately correct:

$$L_t^{\text{RANS}} = 0.7 \cdot \delta^{\text{mixing}}$$

where  $\delta^{\text{mixing}}$  is the thickness of the mixing layer. The value of  $R_L$  should be:

$$R_L \leq 0.2 - 0.1$$

where 0.2 should be considered an extreme lower limit of resolution and 0.1 the desirable lower limit. Again, higher grid resolution should be used if computing power permits. The value of  $R_L=0.1$  corresponds to a resolution of  $\sim 15$  cells across the mixing layer. This is not a very fine grid resolution, but equal resolution should ideally be provided in all 3 space dimensions. In addition, the SSL can be thin relative to the body dimensions, resulting in very high computational costs. The initial SSL instability is akin to a Helmholtz instability and is initially two-dimensional. Two times the coarser grid spacing in the spanwise direction is therefore acceptable.

It is not always possible to achieve such resolution directly from the onset of the separating shear layer, especially if this layer is very thin relative to the body dimensions. This is not necessarily a problem as, typically, the thickness of the SSL increases strongly downstream of the separation point/line. Therefore  $R_L$  is decreasing relatively quickly and reaches sufficiently low values to provide the required resolution. It is, however, important to note that for cases where the small scales play a significant role, such as in acoustics simulations, the delay of the initial instability can result in a loss of spectral information at high wave numbers (small scales). It is advisable to visually inspect the displayed results for the presence of the unsteady turbulent structures at the intended locations.

Of special concern are geometries with high aspect ratios, meaning a large domain size in the direction perpendicular to the SSL (long cylinders in crossflow, stalled wings of high aspect ratios, and so on). In such situations, it is not always possible to sufficiently resolve the third direction. It might then be necessary to solve only a portion of the real flow domain in SRS mode, either by using suitable boundary conditions (e.g., periodicity in the spanwise direction) or by restricting the SRS to a limited portion of the domain.

#### 4.2.4. Numerical Settings

The general numerical settings described in Section 5 should be applied. In addition, locally unstable flows can be very sensitive with respect to numerics. For the application of the DDES model, the recommended choice for the advection terms is the Bounded Central Difference (BCD) in the entire domain. The PRESTO pressure interpolation should be avoided in such simulations, as it has been observed that this option can suppress the initial formation of resolved turbulence.

Experience suggests that the BCD scheme is also the most suitable choice when using ELES/ZLES methods. In some applications with high demands on accuracy and where a high quality isotropic mesh can be provided in the LES region, the application of the CD scheme in the LES zone might be advantageous.

#### 4.2.5. Examples

##### *Backward-Facing Step I*

The backward-facing step flow experimentally investigated by Vogel and Eaton (1985) was computed. In this flow, the height of the channel upstream of the step is equal to four step heights ( $4H$ ). A summary of the physical parameters is given in Shur et al. (2008):

$Re_H [-]$	28 000
$\Delta t [s]$	0.02
$\mu [\text{Pa}\cdot\text{s}]$	$3.5714 \times 10^{-5}$
$\rho [\text{kg}\cdot\text{m}^{-3}]$	1.0

**Table 3: Parameters for simulation of a backward-facing step**

The computational domain for the test case is shown in Figure 21. The characteristic length is the step height,  $H$ , which is equal to 1 [m] in the current study. The domain dimension in  $z$ -direction is equal to  $4H$ . The domain upstream of the step has dimensions in the  $x$ - and  $y$ -directions of  $3.8 \cdot H$  and  $4 \cdot H$  respectively. The downstream domain has dimensions in the  $x$ - and  $y$ -direction, of  $20 \cdot H$  and  $5 \cdot H$  respectively.

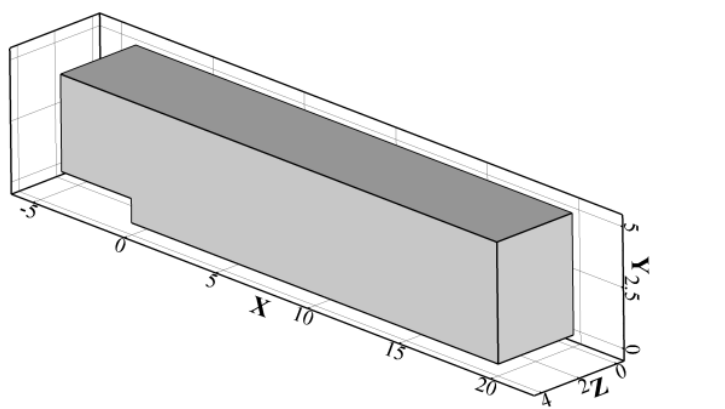


**Figure 21: The computational domain for the Backward-Facing Step test case**

An example of the computational grid used for the test case is shown in Figure 22(a-c). The grid has 2.25 million hexahedral cells (2.3 million nodes) providing a near-wall resolution in wall units to be less than one. A non-dimensional time step (based on step height and inlet velocity) of  $\Delta t=0.02$  ensures that the CFL number is less than unity in the unsteady mixing zone downstream of the step. The number of cells in the spanwise direction is 80. The solution was averaged over 5000 time steps.

In Figure 22(b) all boundary conditions are shown. In the spanwise direction (cyan colored boundary), a periodic boundary condition; on the red-colored boundaries, no-slip wall conditions; on the blue-colored boundary, an outlet condition; and on the green-colored boundary, an inlet condition was applied. The latter was provided in the form of steady state RANS profiles. Therefore, unsteadiness resulted solely from the local flow instability past the step.

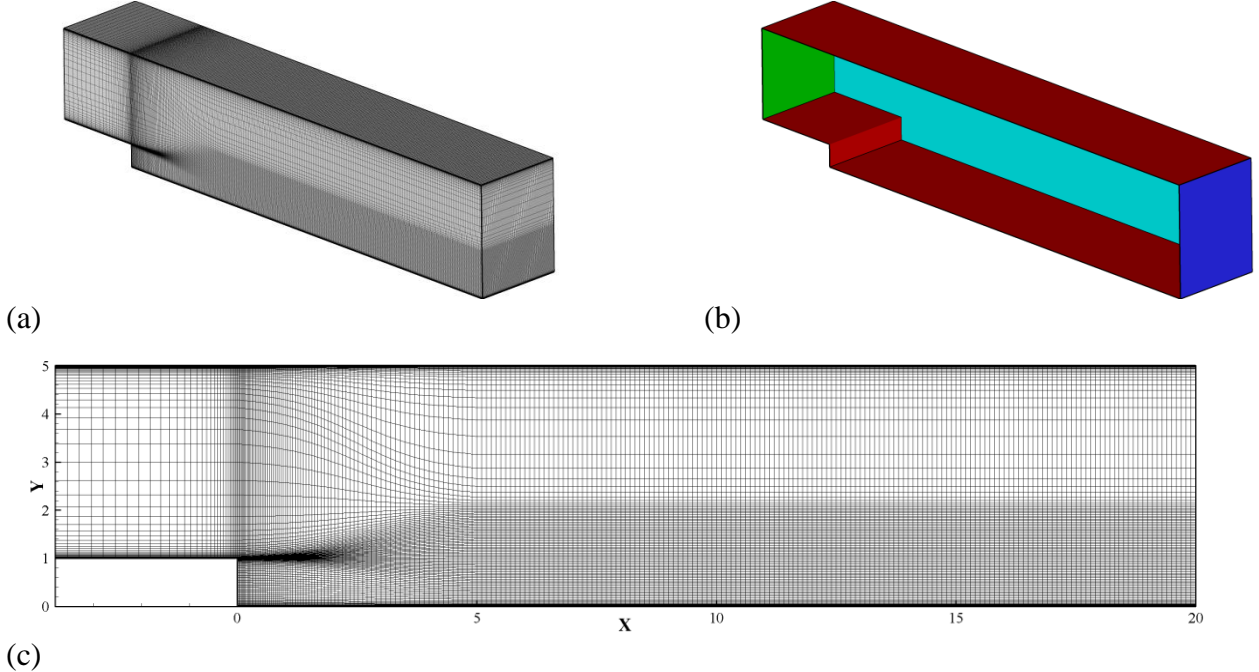


**Figure 22: Computational grid (a), (c) and applied boundary conditions (b) for Backward-Facing Step test case**

Figure 23 shows turbulent structures visualized by an iso-surface of the Q-criterion colored with the streamwise velocity. It can be seen that these structures develop quickly downstream of the step due to the local flow instability.

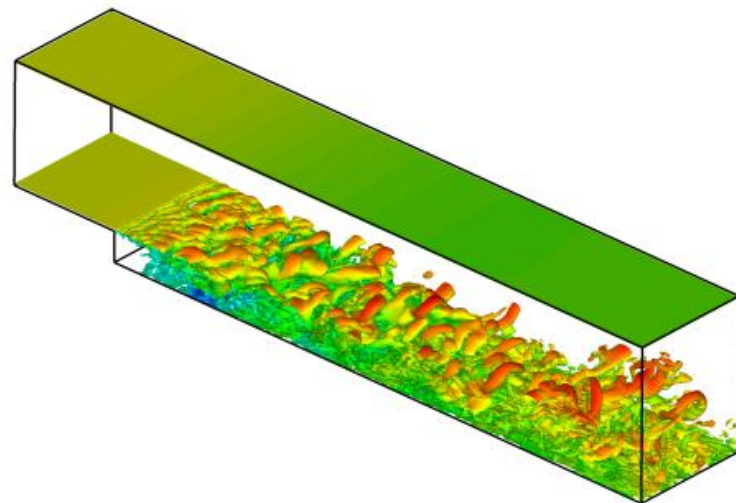


**Figure 23: Isosurface of Q-criterion equal to  $Q=1$  [non-dimensional with  $U_{\text{inlet}}$  and  $H$ ] colored by velocity using the DDES-SST model**

While test cases of the type discussed in Section 4.1 with strong global instabilities are relatively insensitive to modeling and numerical details, cases with only local instabilities are much more fragile. Figure 24 - Figure 26 show a comparison of the time-averaged skin-friction coefficient distribution for different model variants and solver settings. In particular, Figure 24 shows that the details of the formulation of the DDES shielding function can have a strong effect on such flows. The use of the conservative function  $F_2$  of the SST model delays the formation of resolved turbulence structures and thereby delays flow reattachment. For this reason, the shielding functions of the DDES-SST model have recently been optimized and the new DDES-SST shielding function proposed in Gritskevich et al. (2011) is recommended (and used in the current simulation).

The selection of the Central Difference (CD) scheme vs. the Bounded Central Difference (BCD) scheme did not show any significant impact on the solution as is seen in Figure 25.

However, the selection of the pressure interpolation scheme proved to be quite influential as shown in Figure 26. Figure 27 shows the consequences of missing or delaying the flow instability of the SSL. The model does not really operate in LES mode through a significant part of the recirculating region as shown in Figure 27(b). Similar behavior can be observed on under-resolved grids. It is worth re-iterating that this is less likely to be a problem in globally unstable flows. The effect can largely be avoided by using the ELES formulation, where unsteady structures are introduced at the RANS-LES interface. The solution does not depend as critically on the resolution of the first few shear layer thicknesses downstream of the step and on the numerical settings as critically as it does with DDES.

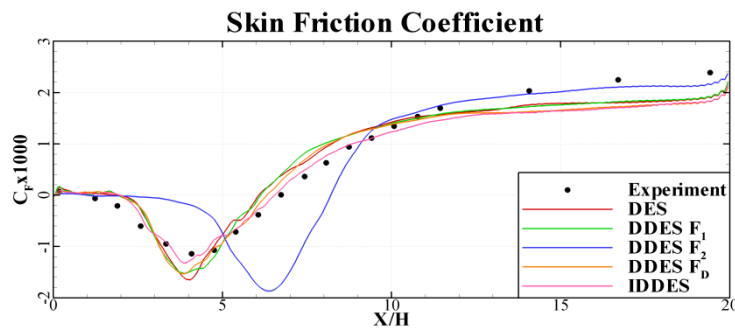


**Figure 24:** Skin friction coefficient for different turbulence models ( $F_1$  - 1<sup>st</sup> SST model blending function,  $F_2$  - 2<sup>nd</sup> SST model blending function,  $F_d$ -new DDES shielding function)

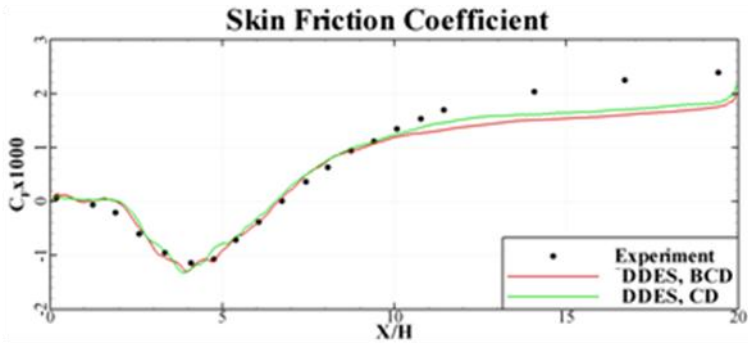


**Figure 25:** Skin friction coefficient for DDES with different advection schemes

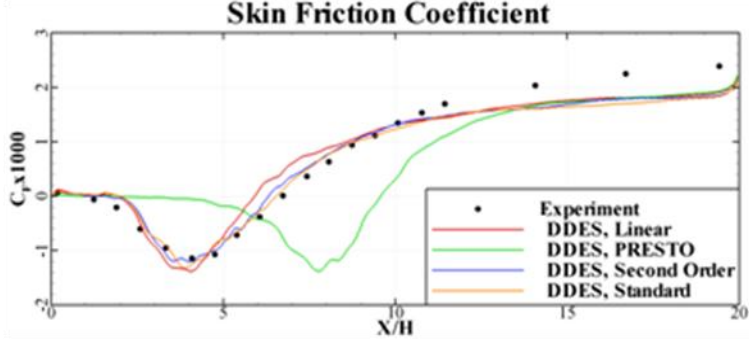


Figure 26: Skin friction coefficient for DDES with different pressure interpolation schemes

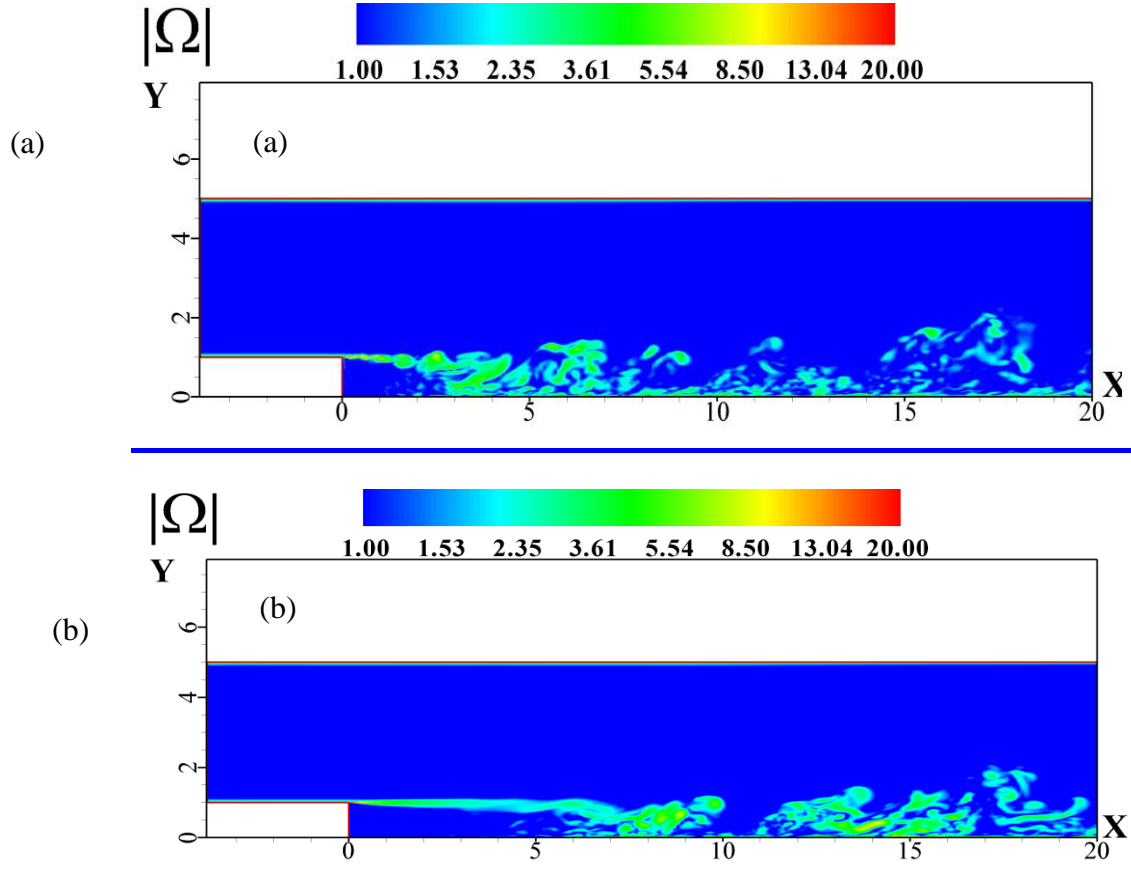


Figure 27: Strongly delayed shear layer instability due to numerics settings (a) standard pressure interpolation (b) PRESTO scheme

### 4.3. Stable Flows and Wall Boundary Layers

#### 4.3.1. Flow Physics

Stable flows in this context are characterized by a continuous development of the turbulence field. For such flows, the turbulence at a certain location depends strongly/entirely on the turbulence upstream of it. There is no mechanism for quickly generating ‘new’ turbulence and over-riding the upstream turbulence field. Stable flows in the context of this discussion are essentially wall-bounded flows - either attached or with small separation bubbles.

- Generic Flows
  - Channel and pipe flows (attached and mildly separated)
  - Boundary layers (attached and mildly separated)

### 4.3.2. Modeling

For stable flows, the use of embedded or zonal RANS-LES methods with a well-defined interface between the RANS and the LES zone is essential. Synthetic turbulence must be introduced at the RANS-LES interface to ensure a proper balance between the modeled and the resolved content of turbulence. The introduction of resolved turbulence allows the balance between RANS and LES turbulence across the interface to be preserved (assuming the synthetic turbulence is of sufficient quality). Neither DDLES nor SAS-type models are able to switch from RANS to SRS mode in such stable situations. Even in cases where resolved turbulence is specified at the inlet (or an interface) these models will typically switch back to their underlying RANS mode after some boundary layer thicknesses (e.g. Davidson 2006).

Even an explicit switch from a RANS to a LES model (and the corresponding grid refinement in the LES zone) at the interface without an introduction of synthetic turbulence would not work well. If sufficient resolution is provided in the LES zone, the flow would eventually go through a transitional process and recover the fully turbulent state. However, such a process would require many boundary layer thicknesses, with an entirely unbalanced model formulation in-between. This is not acceptable in most technical flows and must be avoided.

In such stable flows, the most suitable selection of hybrid RANS-LES models are Embedded- or Zonal models, where the RANS and the LES zones are defined by the user and synthetic turbulence is injected at the RANS-LES interface. As mentioned previously, the RANS-LES interface should be placed in a non-critical region of the flow (equilibrium flow), since existing synthetic turbulence generators do not provide realistic turbulent fluctuations for strongly non-equilibrium flows. As a result, placing the interface in such regions results in a too-slow relaxation from synthetic to “real” turbulence (typically, several boundary layer thicknesses).

As an alternative, the RANS and LES simulations can be carried out separately. The RANS domain would include the full geometry whereas the LES solution can be carried out on a smaller portion of the original domain. This separate LES domain would be identical to the LES zone in the equivalent ELES setup. The information from the ‘larger’ RANS solution can then be mapped onto the boundaries of the LES domain. Synthetic turbulence should be introduced at the inlet of the LES domain. This approach can be used if one is confident that the physical decoupling has very little or no effect onto the overall flow topology. The advantage of the decoupled method over the ELES approach is that the RANS solution does not have to carry the burden of the excessive temporal resolution that the LES domain would have otherwise required. However, one should be aware that some scripting is required for mapping the results from RANS to LES in the decoupled approach.

The models selected in the RANS and LES zone depend on the flow physics. In the RANS zone, a suitable model for the flow should be selected. In the LES zone, the use of a WMLES formulation is typically recommended for wall boundary layers in order to avoid the unfavorable Reynolds number scaling of classical LES models. For free shear flows, the WALE model should provide optimal performance.

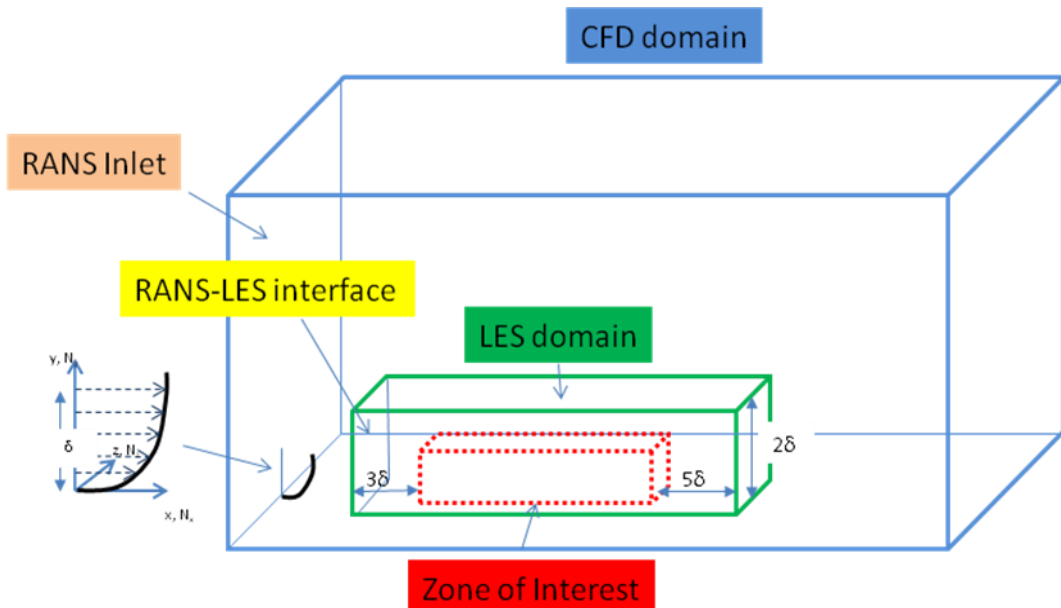
### 4.3.3. Meshing Requirements

Figure 28 shows the schematic of an ELES setup. There is a central area (red) which is the domain of interest (for example, a boundary layer with a separation bubble). This area is not specifically defined in the ELES setup, but is just used to demonstrate how such a zone would be handled. Clearly, one would not place the LES zone (green) directly at the start of the zone of interest, but extend it upstream and downstream of that region by several boundary layer thicknesses as indicated in Figure 28. For fully developed pipe/channel flow, the boundary layer

thickness should be estimated as  $\frac{1}{2}$  of the pipe diameter/channel height. The LES zone is then embedded into a larger RANS zone (blue).

The meshing requirements are those of the underlying turbulence models. In the RANS zone typical RANS resolution requirements should be satisfied (20-30 cells across the wall boundary layer with possibly a  $y+ \sim 1$  and 15-20 cells across free shear flows).

In the LES zone, the resolution requirements depend on the details of the LES model formulation and the flow type. For free shear flows, cubic grid cells with a minimum of  $\sim 15-20$  cells per shear layer thickness should be used. For wall-bounded flows, the resolution requirements are those described in Section 3.3 for classical LES and in Section 3.4 for WMLES.



**Figure 28: Sketch of embedded LES (ELES) domain**

For wall-bounded flows, it is clear that large domains cannot be covered in SRS mode, even when using WMLES. In most cases one would limit the domain size of the LES zone by one or more of the following concepts:

- Use only a limited spanwise domain size.
  - apply periodic boundary conditions where appropriate – however, the domain size has to cover a minimum of 3-5 boundary layer thicknesses in the spanwise direction to avoid inaccuracies caused by the spanwise periodicity condition. Care must be taken that this requirement is satisfied for the entire LES domain. In case the boundary layer grows in the streamwise direction, the most downstream location is relevant for the estimate.
  - in cases where no periodicity can be applied, place the spanwise interfaces into a region of limited interest.
- Place the upstream RANS-LES interface economically to reduce the size of the LES domain. However, the interface should be located in a zone of ‘undisturbed’ equilibrium flow. Place the RANS-LES interface at a minimum of  $\sim 3$  boundary layer thicknesses upstream of the zone of interest (e.g. a separation region). Limit the size of the RANS-LES interface to the shear layer you want to capture; that is, do not extend the interface far into the freestream, as the code will then generate resolved turbulence

in freestream regions where no LES is required. The Vortex Method (VM) would also generate a large number of vortices if the RANS-LES interface were too large.

- Place the downstream LES-RANS interface economically to reduce the size of LES domain. However, do not place the interface immediately downstream of the zone of interest but several boundary layer thicknesses farther downstream to avoid any negative influence of the downstream RANS model (e.g. let the boundary layer recover several boundary layer thicknesses downstream of a separation before switching back to RANS).
- Limit the height of the LES zone. However, allow for some space above the boundary layer. Typically the LES zone should be about twice as thick as the boundary layer.

In order to check the quality of the simulation, sensitive quantities like time-averaged wall shear stress should be plotted across the RANS-LES zones. There should be no large jump in those quantities and the unavoidable disturbance caused by the interface should be recovered before entering the zone of interest.

#### 4.3.4. Numerical Settings

Zonal methods typically allow a separate selection of numerical settings in the RANS and LES zones. For very sensitive simulations, one can therefore select a pure central difference (CD) in the LES domain, while using an appropriate numerical scheme in the RANS parts. However, one can also select a global scheme, in which case the bounded central difference (BCD) scheme is recommended.

#### 4.3.5. Examples

##### *Periodic Channel*

The periodic channel flow is not an ELES, but a WMLES application. It is however shown in this section of the report as WMLES is typically used in the LES portion of ELES/ZLES applications. The entire domain is WMLES and there are no RANS-LES interfaces. Simulations of this flow have been carried out assuming incompressible fluid at several Reynolds numbers based on friction velocity  $u_\tau$  and channel height  $h=H/2$ ,  $Re=395, 760, 1100, 2400, \text{ and } 18000$ . The flow is driven by a constant pressure gradient  $dp/dx=-2\cdot\rho\cdot u_\tau u_\tau/H$ , where  $p$  is the pressure and  $\rho$  is the density. This pressure gradient is taken into account in the governing equations via a source term in the momentum equations, which allows imposing periodic boundary conditions not only in the spanwise direction  $z$ , but also in the streamwise direction  $x$ . Note that within such an approach, the bulk velocity of the flow is not specified and should be obtained as a part of the solution, which means that it could be different with different turbulence models. Alternatively, one can specify the mass flow and the solver will adjust the imposed pressure gradient accordingly.

The size of the computational domain shown in Figure 29 is equal to  $4H$  in the streamwise direction and  $1.5H$  in the spanwise direction. For all considered Reynolds numbers, the computational grid is unchanged in the streamwise and spanwise directions with a uniform grid-spacing of  $0.05H$  and  $0.025H$  respectively. This gives 10 cells per channel half width,  $h=H/2$ , ( $h$  being the relevant boundary layer thickness) in the streamwise and 20 cells per  $h$  in the spanwise direction. Different grids have been used in the wall-normal direction. This arrangement provides a sufficient resolution ( $\Delta y_w^+ < 1$  near the wall) at different Reynolds numbers. Note, however, that all simulations could have been performed on the finest grid. The non-dimensional time step is  $U\Delta t/H=0.02$  which ensures that the CFL number is  $CFL<0.5$  in the entire domain. The solution was averaged in time over 5000 time steps. Table 4 gives the details of the grids used in the simulations and the resulting non-dimensional grid spacing. Note that classical wall-resolved LES would require values of  $\Delta x+<40$ ,  $\Delta z+<20$ , demonstrating the substantial savings that can be

achieved with WMLES for higher  $Re$  numbers. The  $y^+$  range in Table 4 covers the range of  $y^+$  values in the wall normal direction, with the largest values located at the center of the channel.

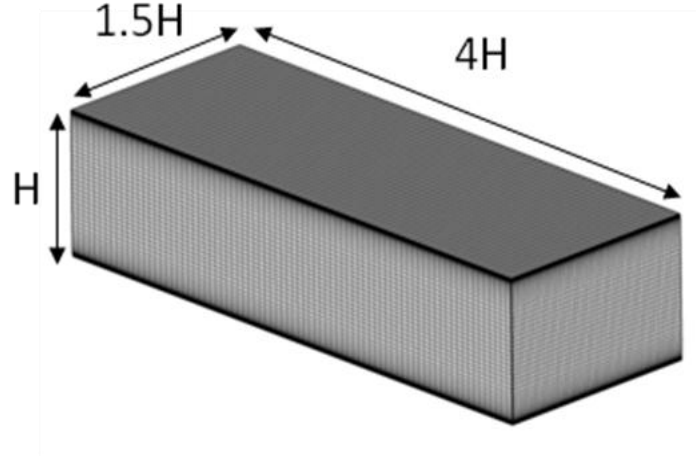


**Figure 29: Computational domain and grid for WMLES of channel flow**

$Re_\tau$	Cells Number	Nodes Number	$\Delta x^+$	$\Delta y^+$	$\Delta z^+$
395	384 000	$81 \times 81 \times 61$	40.0	$0.2 \div 30$	20.0
760	480 000	$81 \times 101 \times 61$	76.9	$0.2 \div 30$	38.5
1100	480 000	$81 \times 101 \times 61$	111.4	$0.2 \div 30$	55.7
2400	528 000	$81 \times 111 \times 61$	243.0	$0.2 \div 30$	121.5
18000	624 000	$81 \times 131 \times 61$	1822.7	$0.2 \div 30$	911.4

**Table 4: Grid resolution for WMLES channel flow simulations**

Figure 30 shows the turbulence structures using the Q-criterion ( $Q=350 [s^{-2}]$ ). The color of the iso-surface is the streamwise velocity.

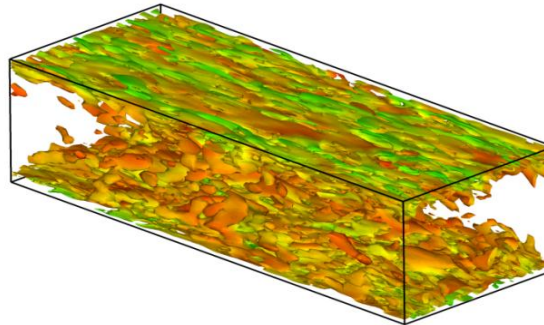


**Figure 30: Turbulence structures for WMLES of channel flow at lowest Reynolds number ( $Q=350 [s^{-2}]$ )**

Figure 31 shows the flow in a horizontal cut through the domain for the lowest and the highest Reynolds numbers. The thin region of RANS modeling near the wall for the high Reynolds

number is indicated by the high eddy-viscosity (note the different scales in the plot for the eddy-viscosity ratio for the different Reynolds numbers). RANS modeling in this context is as described in Section 3.4, based on the near-wall mixing length formulation.

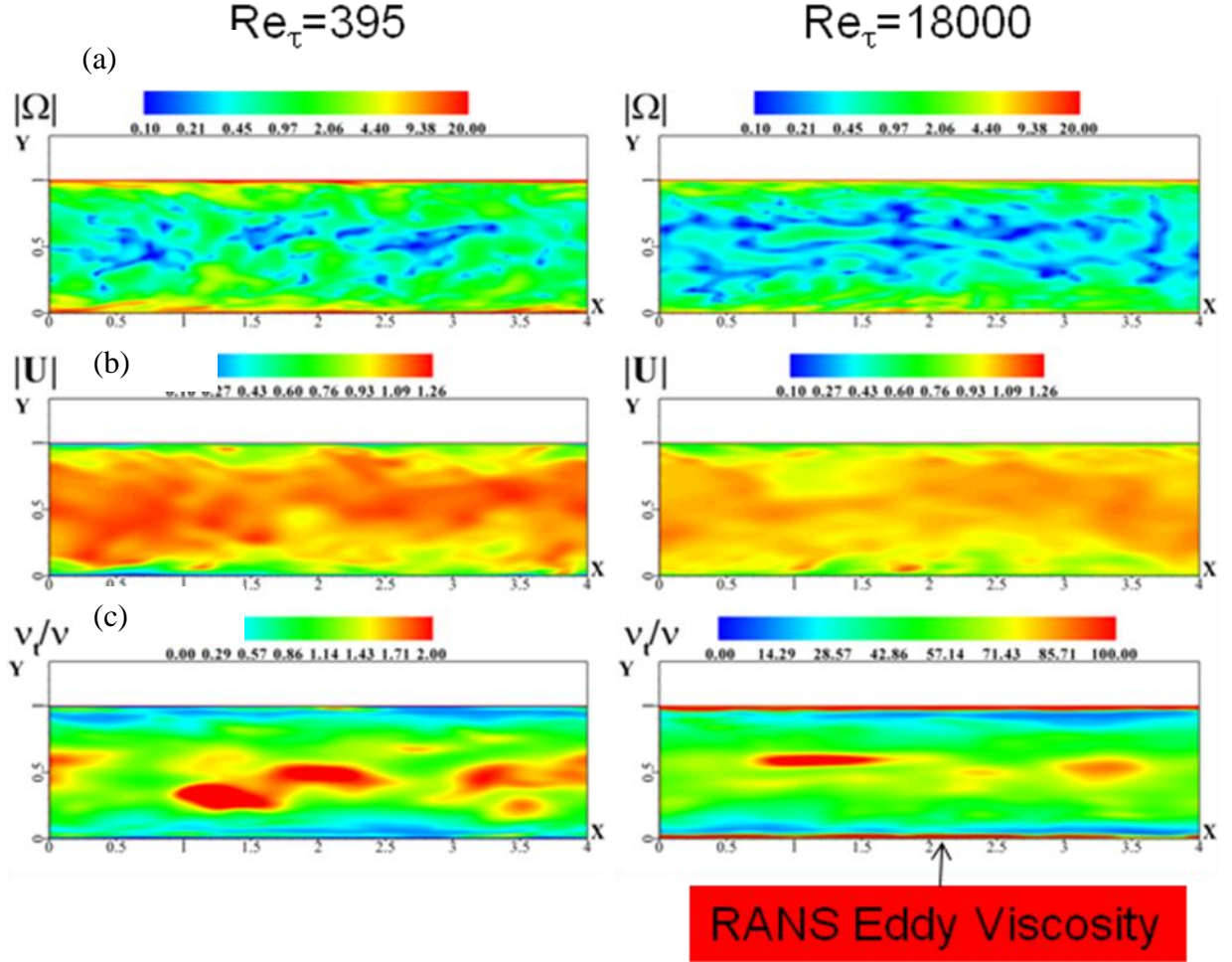


**Figure 31:** Flow visualization for WMLES of channel flow (a) Vorticity rate  $\Omega$ . (b) absolute value of velocity  $U$  (c) Ratio of eddy-viscosity to molecular viscosity

Results of the WMLES formulation and their comparison with the empirical correlation of Rechart (1951) are shown in Figure 32. It can be seen that the WMLES solutions reproduce the logarithmic layer with good accuracy. There is a slight kink at the switch from the RANS to the LES formulation, but it is moderate and does not affect global properties such as the wall shear stress.

The above simulations have been carried out with ANSYS Fluent. Similar results can be obtained with ANSYS CFX where WMLES is the default formulation inside the LES zone of the ZFLES method.

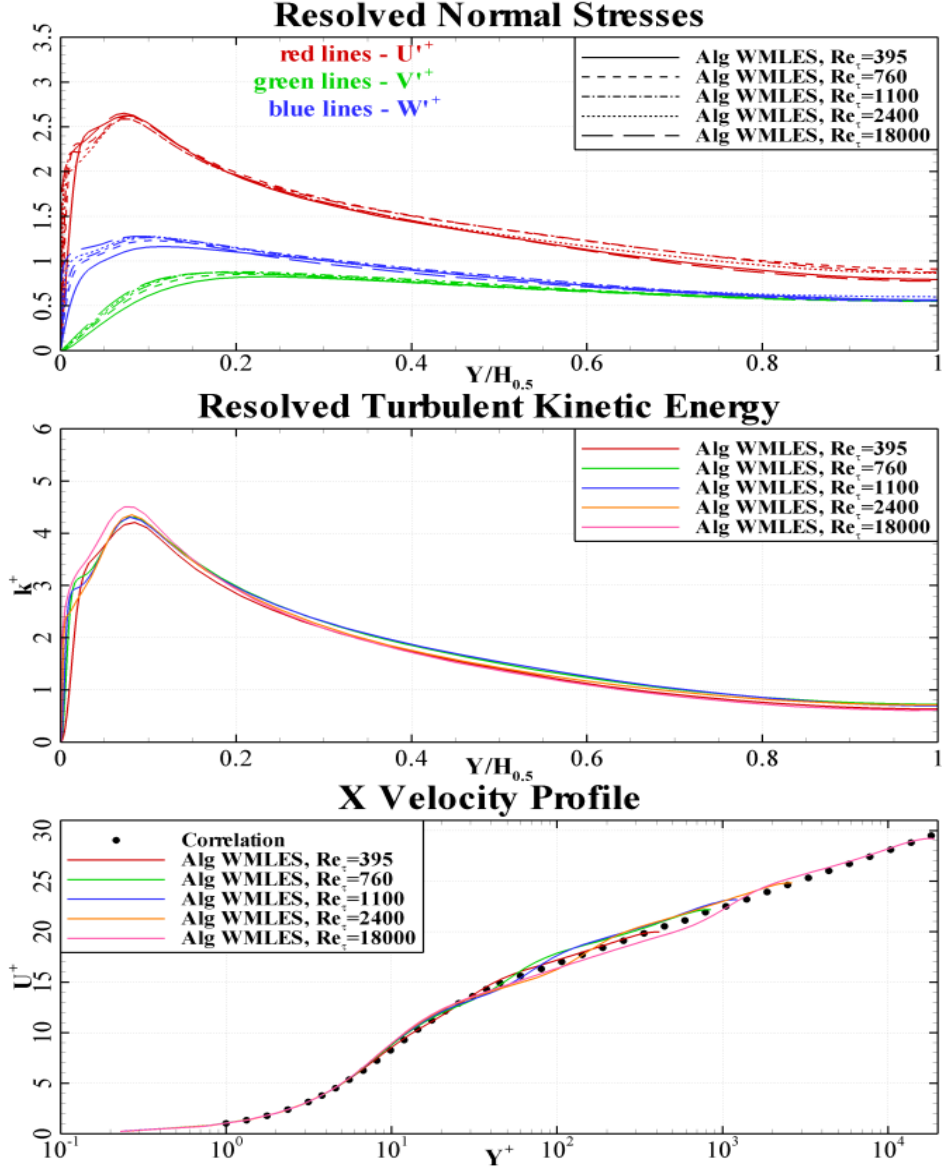


**Figure 32:** Resolved normal stresses, turbulent kinetic energy, and mean velocity profiles for WMLES at different Reynolds numbers

#### Wall Boundary Layer

The zero pressure gradient wall boundary layer is a benchmark test case which is commonly used for turbulence model investigation due to its geometric and physical simplicity. Unlike the periodic channel test case, the wall boundary layer needs unsteady boundary conditions because there is no periodicity in the streamwise direction. In the current simulations, the Vortex Method (VM) was used for these purposes (Mathey et al., 2003).

A computational domain for this test case is shown in Figure 33. The characteristic length, which determines the geometry, is the plate length,  $L$ , of 1 [m] in the current study. Dimensions of the computational domain in  $x$ ,  $y$ , and  $z$  directions are equal to  $L$ ,  $0.4 \cdot L$ , and  $0.1 \cdot L$  respectively.

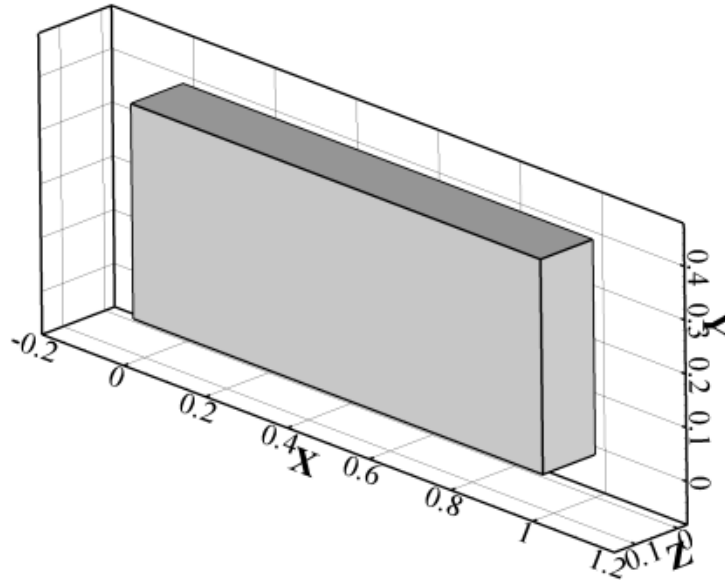


**Figure 33: Computational domain for a Wall Boundary Layer test case**

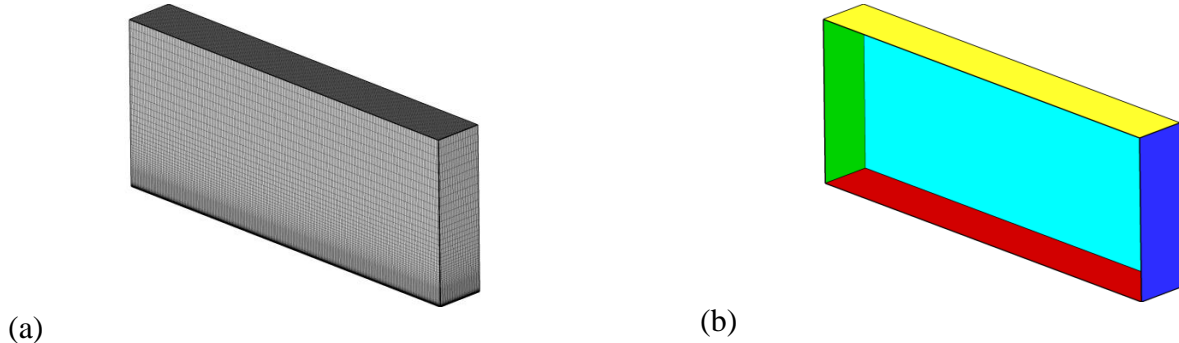
The simulations have been performed for an incompressible fluid. A summary of physical parameters is presented in Table 5.

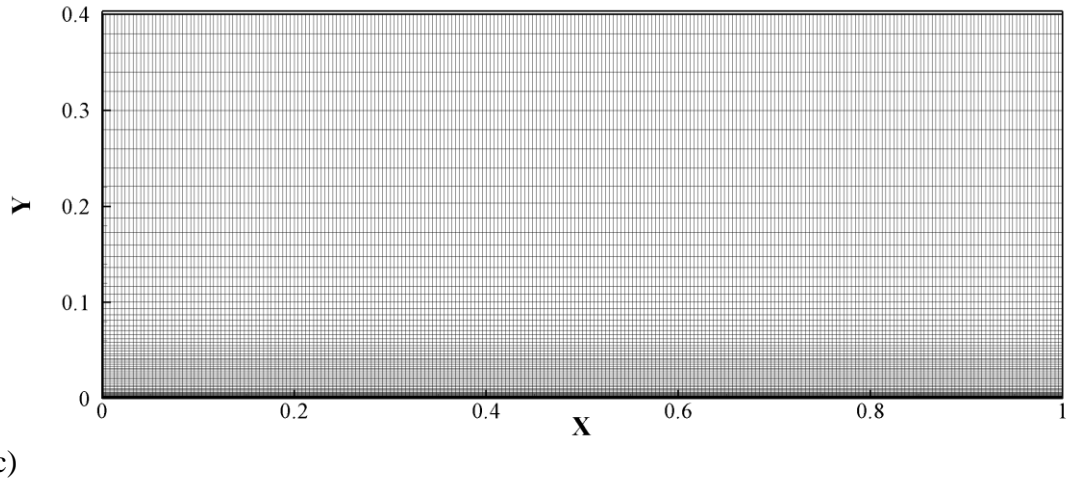
$Re_\theta [-]$	1000	10000
Inlet boundary layer thickness $\delta^+ [m]$	0.032	0.032
$\Delta t [s]$	0.001	0.001
$\mu [\text{Pa}\cdot\text{s}]$	$4.4483 \times 10^{-6}$	$4.4483 \times 10^{-7}$
$\rho [\text{kg}\cdot\text{m}^{-3}]$	1.0	1.0

**Table 5: Properties for flat plate boundary layer simulations**

The geometry and the computational grid used for the test case are shown in Figure 34. The base grid is uniform in the  $x$ - and  $z$ -directions with steps  $0.004 [m]$  and  $0.002 [m]$  respectively. In the wall normal direction the grid was expanded by a factor of 1.15. For all computations the value of  $\Delta y^+$  is less than 1, which means that the governing equations are integrated to the wall. A complete summary of all used grids is presented in Table 6.

Figure 34b presents all the boundary condition types used in the simulations. The cyan color shows one of the periodic planes, the red color the no-slip wall boundary, the blue color the outlet boundary, the green color the inlet boundary, and the yellow color the symmetry boundary.





(c)

**Figure 34: Computational grid (a), (c) and applied boundary conditions (b)**

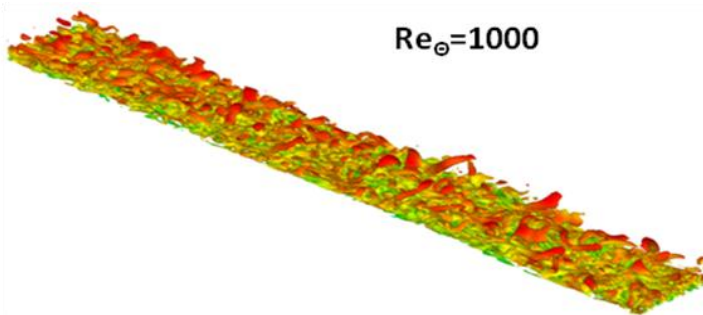
$Re_\theta$	Cells Number	Nodes Number	$\Delta x^+$	$\Delta y^+$	$\Delta z^+$
1000	1 085 000	251×71×63	68.0	0.30 ÷ 0.80	34.0
10000	1 333 000	251×87×63	680.0	0.25 ÷ 0.60	340.0

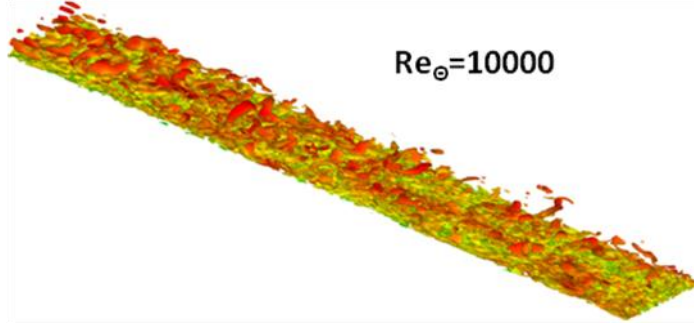
**Table 6: Information on grids for flat plate test case**

Two cases have been computed using the numerical grids with the parameters shown in Table 6. They have different inlet Reynolds numbers which are based on the boundary layer momentum thickness ( $Re_\theta$ ).

The Non-Iterative Time Advancement (NITA) algorithm based on Fractional Time Step method was applied with the second order scheme for the approximation of time derivatives. The convective terms in the momentum equations have been approximated with the second order central difference scheme and the Green-Gauss cell-based method was used for interpolation of variables on cell faces. The Standard option was selected for the pressure interpolation scheme.

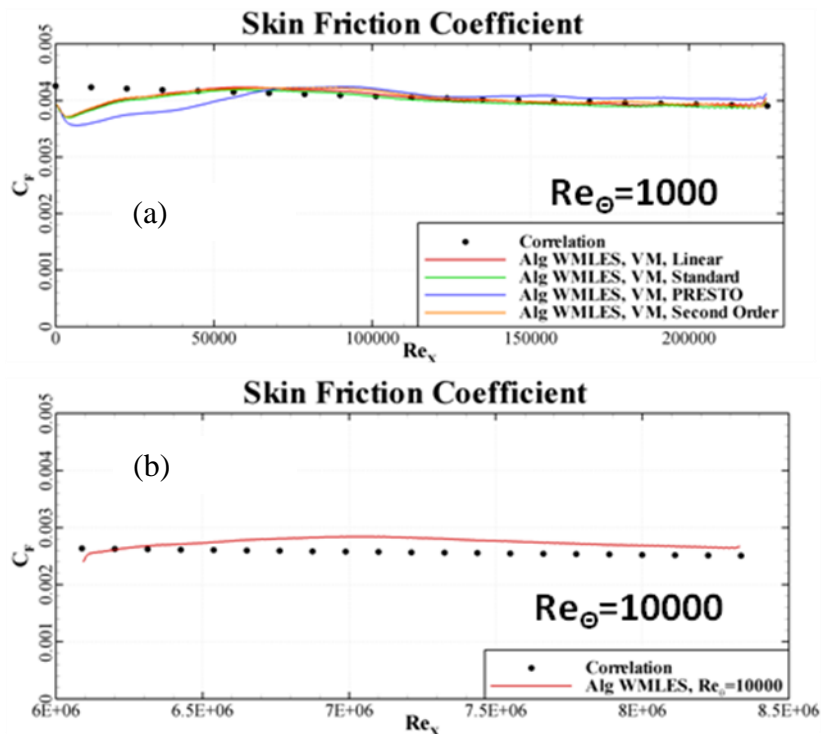
Visualizations of the flow at two values of  $Re_\theta$  are shown in Figure 35. Iso-surfaces of the  $Q$ -criterion that are equal to  $200 \text{ [s}^{-2}\text{]}$  and colored with the velocity magnitude are depicted. It can be seen that the turbulence structures are well-developed and do not show any visual decay or disruption downstream of the inlet. This indicates that the Vortex Method provides sufficiently realistic turbulent content at the inlet boundary.





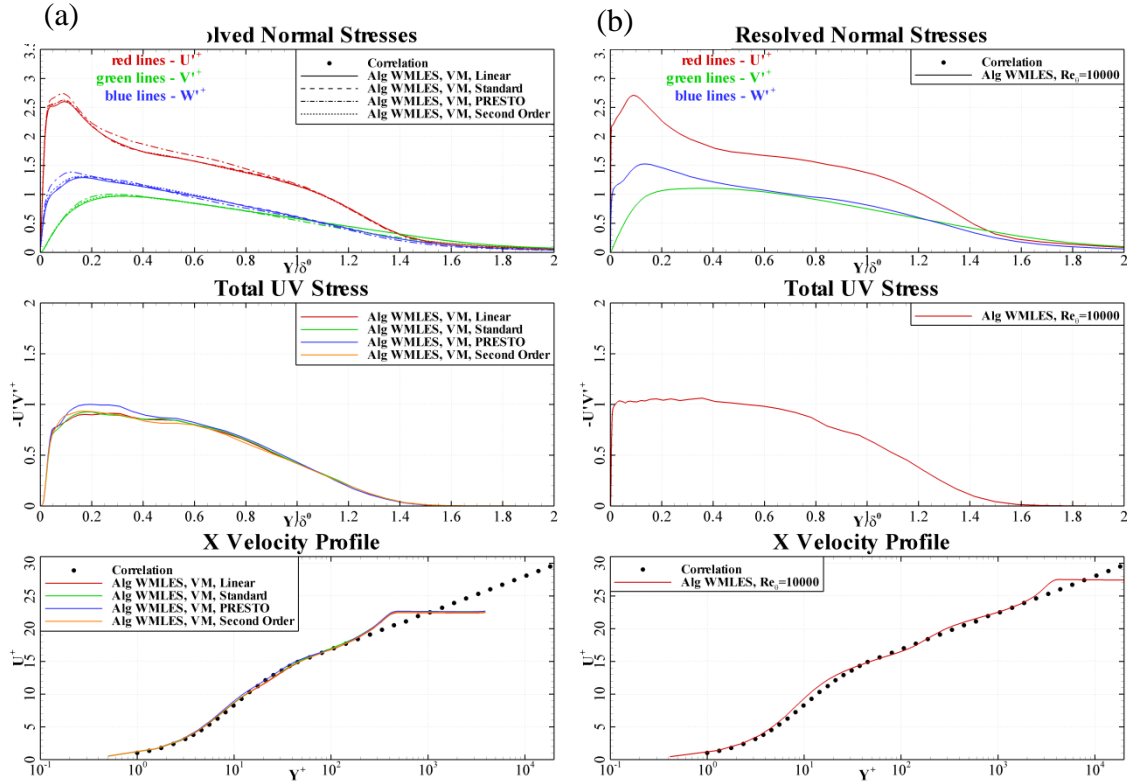
**Figure 35:** Iso-surfaces of Q-criterion ( $Q=200 \text{ [s}^{-2}\text{]}$ ) colored with velocity for a flat plate at two different Reynolds numbers

Figure 36 shows the skin-friction coefficient for the two Reynolds numbers. The results demonstrate that the inlet wall friction provided by the RANS inlet velocity profiles is maintained without any major disruption. This indicates again that the vortex method produces sensible synthetic inlet turbulence. In addition, the models react properly to the Reynolds number variation, suggesting that the WMLES can maintain a boundary layer accurately even at high Reynolds numbers, where standard LES models would fail due to a lack of resolution. Figure 36(a) shows the impact of the pressure interpolation scheme, which has proven to be critical for locally stable flows. As seen in Figure 36, the effect of the PRESTO scheme turns out to be not as pronounced in the fully developed turbulent boundary layers as it has been in the backward-facing step example shown in Figure 26. It is worth re-iterating that the PRESTO scheme requires slightly more ‘running length’ to recover the correct levels of turbulence and wall shear stress.



**Figure 36:** Skin friction distributions along a flat plate predicted by WMLES at two Reynolds numbers (a)  $Re_\theta=1000$  with different numerical settings (b)  $Re_\theta=10000$

Figure 37 shows Reynolds stresses and velocity profiles from the simulations. The figure suggests that, just as for the channel flow, the quality of the simulations is fairly high in terms of both the mean flow prediction (the logarithmic profile is reproduced faithfully) and Reynolds stresses (they are well within the range expected from known DNS studies of the flat plate boundary layer).



**Figure 37: Profiles of resolved normal and shear Reynolds stresses and mean velocity in the flat plate boundary layer predicted by WMLES at two Reynolds numbers (a)  $Re_\theta=1000$  with different numerical settings (b)  $Re_\theta=10000$  with the second order pressure interpolation**

The above simulations have been carried out with ANSYS Fluent. Similar results can be obtained with ANSYS CFX where WMLES is the default formulation inside the LES zone of the ZFLES method.

#### NASA Hump Flow

A challenging test case for ELES in combination with WMLES was computed within the EU project ATAAC. The case models the flow over a hump with a relatively large separation zone on the leeward side. Figure 38 shows the experimental setup (Greenblatt et al., 2005). Due to the limited separation zone, this flow would be categorized as a stable flow in the present context.

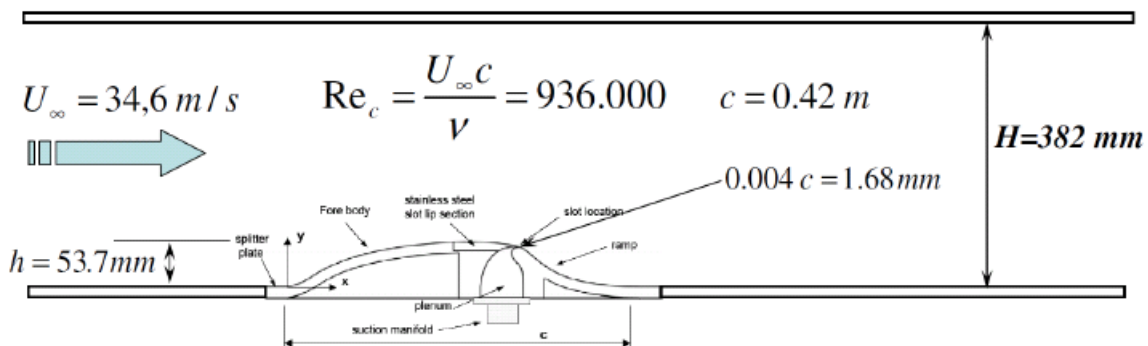


**Figure 38: Experimental setup up for NASA hump flow experiment**

The flow was computed with ANSYS-Fluent 13.0 using the SST model in the RANS zone, the vortex method at the RANS-LES interface and the algebraic WMLES option in the LES zone. The Reynolds number, based on the free-stream velocity,  $U_\infty$ , and hump chord,  $C$ , is equal to  $9.36 \cdot 10^5$ . The simulation was carried out in the full domain, which extends from  $-2.14C$  to  $4C$  ( $0$  corresponds to the hump beginning). In the spanwise direction, the extent of the domain is  $0.2C$ . The inflow boundary conditions for RANS have been set based on the preliminary flat plate boundary layer computations up to the flow section  $x/C = 2.14$  ( $Re_\theta = 7200$ ), where the parameters of the incoming boundary layer have been measured in the experiment. At the upper wall of the channel, free-slip wall conditions have been specified.

The grid in the LES zone (see Figure 39) consists of  $200 \times 100 \times 100$  cells and was designed to provide  $10 \times 40 \times 20$  cells per boundary layer volume in the streamwise, wall normal, and spanwise directions. The RANS grid is much coarser, especially in the spanwise direction. Figure 39 also presents a visualization of the turbulent structures in the LES zone that suggests a high resolution provided by the simulation (note that the momentum thickness Reynolds number at the inlet to the LES domain is relatively high ( $Re_\theta = 7000$ )). In retrospect, the setup might not be fully optimal, as the RANS-LES interface is placed relatively close to the non-equilibrium/separation zone of the boundary layer. There are only about 2 boundary layer thicknesses between the interface and the bend of the geometry. A more optimal grid should cover more of the upstream boundary layer and allow the synthetic turbulence to develop over a longer running length.

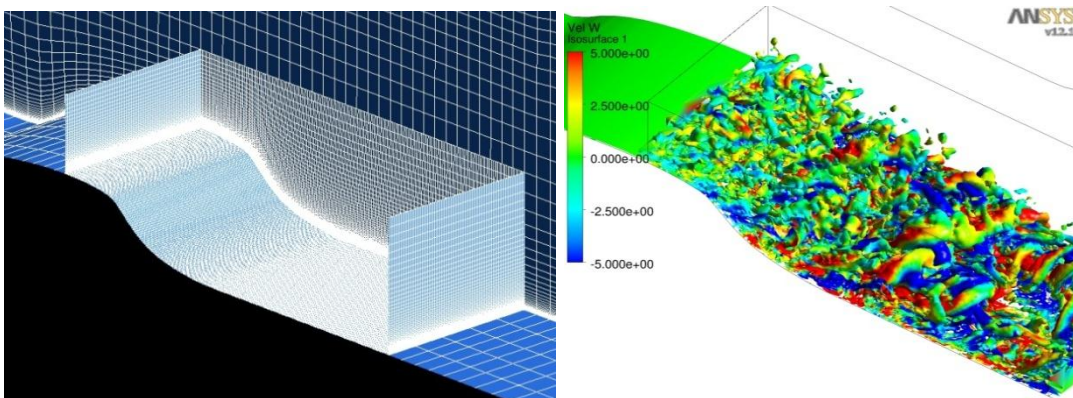


**Figure 39:** (a) Grid used for the NASA hump simulation (b) Turbulent structures in the LES domain (Q-criterion colored with spanwise velocity component)

Figure 40 shows the skin-friction and wall-pressure coefficient distributions from the simulations. It can be seen that the use of ELES combined with the WMLES model in the LES zone results in very close agreement with the data, even though the skin-friction is known to be very sensitive to simulation details. A comparison of the results obtained using WMLES with those obtained using the standard WALE model in the LES zone is shown in Figure 40. The results suggest that the latter performs considerably worse than the former. In particular, in the simulations using the WALE model, the wall shear stress drops immediately after the RANS-LES interface to unrealistically small values due to the lack of resolution. The results with this model further downstream are therefore no longer reliable as the wall shear stress has a strong influence on the overall boundary layer development. Further investigations of this flow are on-going – so the results should not be considered final, but are provided only to demonstrate the basic concepts.

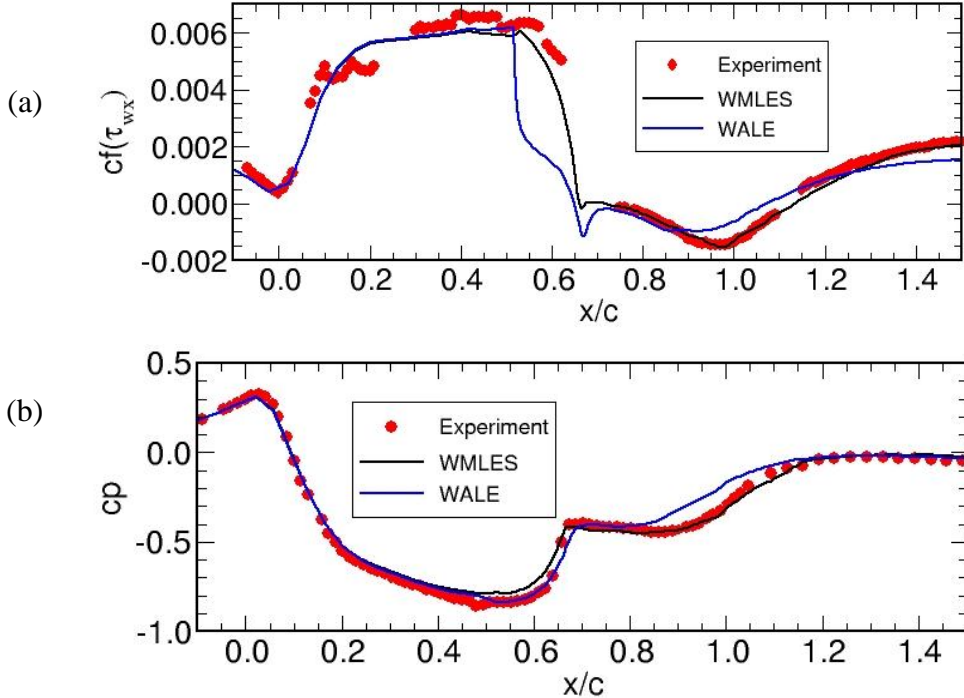


**Figure 40:** (a) Skin-friction,  $c_f$ , and (b) wall pressure coefficients,  $c_p$ , from NASA hump flow simulations. Comparison of WMLES and WALE LES methods in the LES domain.

### T-Junction with Thermal Mixing

The following example is a flow through a pipe T-junction with two streams at different temperatures Westin et al. (2006). This test case was used as a benchmark of the OECD to evaluate CFD capabilities for reactor safety applications. This flow is not easily categorized in the current framework. It can be placed somewhere between a globally and a locally unstable flow. As shown below, this flow can be modeled with SAS and DDES, but special care must be taken in choosing the numerical settings.

The setup consists of a horizontal pipe for the cold water flow, and a vertically oriented pipe for the hot water flow. The hot water pipe is attached to the upper side of the horizontal cold water pipe. In the experiments, the length of the straight pipes upstream of the T-junction is more than 80 diameters for the cold water inlet, and approximately 20 diameters for the hot water inlet. The flow conditions are listed in Table 7.

	Diameter	Bulk velocity	Mass flow	Temperature	Re number
Hot Pipe	100 [mm]	$1.53 [\text{m}\cdot\text{s}^{-1}]$	$12 [\text{l}/\text{s}]$	$30^\circ[\text{C}]$	$Re=1.9\cdot10^5$
Cold Pipe	140 [mm]	$1.56 [\text{m}\cdot\text{s}^{-1}]$	$24 [\text{l}/\text{s}]$	$15^\circ[\text{C}]$	$Re=1.9\cdot10^5$

**Table 7:** Flow conditions for T-Junction test case

A sketch of the domain is depicted in Figure 41. The domain dimensions are as follows. The hot leg inlet is located at the  $z/D=22$  section, the cold leg inlet is located at the  $x/D=-27$  section, and the outlet is located at  $x/D=142$ , with  $D$  being the diameter of the cold leg of the pipe. When ELES was used, two additional interfaces have been introduced in the domain, where the synthetic fluctuations generated with the use of the Vortex Method have been specified. These sections have been placed at  $z/D=0.7$  in the hot leg and at  $x/D=-1.0$  in the cold leg.

The computational grid for this flow comprises about 4.9 million hexahedral cells (see Figure 41). The wall normal grid spacing was set to 0.0001 [m] which yields  $\Delta y^+=0.2\text{-}9.0$  in the entire

domain. The grid spacing in the axial and circumferential directions was set as follows. For the cold water pipe where the inlet boundary layer thickness  $\delta_{cold}$  is equal to 0.07 [m], the grid spacing was chosen  $\Delta_{axial}=0.0035$  [m] and  $\Delta_{circumferential}=0.0021$  [m], which yields  $\delta_{hot}/\Delta_{axial}\approx 20$  and  $\delta_{hot}/\Delta_{circumferential}\approx 33$ . For the hot water pipe the inlet boundary layer thickness  $\delta_{hot}$  was set to 0.022 [m] and the grid spacing was chosen  $\Delta_{axial}=0.0035$  [m] and  $\Delta_{circumferential}=0.0014$  [m], which yields  $\delta_{hot}/\Delta_{axial}\approx 6$  and  $\delta_{hot}/\Delta_{circumferential}\approx 15$ . In wall units, the grid spacing is  $(\Delta_{axial}^+, \Delta_{circumferential}^+) \approx (7500, 3000)$  for the hot water pipe and  $(\Delta_{axial}^+, \Delta_{circumferential}^+) \approx (7500, 4500)$  for the cold water pipe, which means that the flow requires near-wall turbulence modeling. The time step was set to 0.001 [s], which leads to  $CFL\sim 1$  in the central mixing zone.

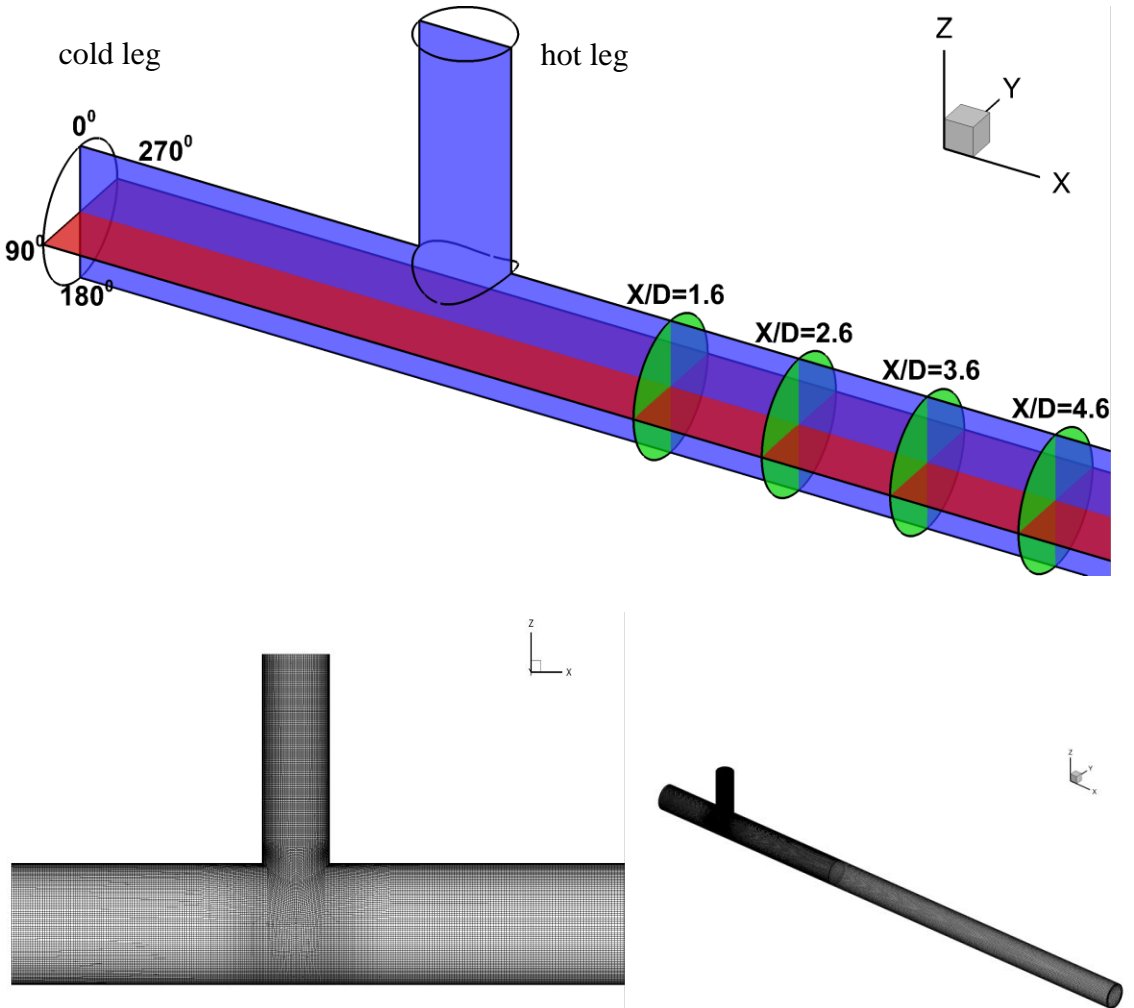


**Figure 41: Geometry and grid of T-Junction test case with measurement planes**

The boundary conditions for this case have been specified as follows. For the inlet boundaries, the precursor simulations of the pipe flow have been performed using the SST model. For the cold water pipe, a fully developed pipe flow was calculated using the SST model and the profiles of velocity and turbulence quantities have been specified at the inlet boundary. For the hot leg and the pipe, the profiles in the experiments were not fully developed. For this reason, a separate pipe flow simulation was conducted using constant inlet values for velocity and turbulence. The inlet profiles for the hot leg have then been extracted from this precursor simulation at the location where they matched the experimental profiles most closely.

It bears repeating that this flow is not easily categorized into one of the three groups described above, but might be described as between globally unstable and locally unstable. It was originally computed with the global SAS and DDES models. Although both simulations turn into a proper SRS mode in the interaction zone of the two streams, the results turned out to be very sensitive to numerical details and solver settings, especially for the SAS model. As an illustration, in Figure 42, the turbulence structures are shown as predicted by the SAS-SST model with the use of the CD and BCD numerical schemes: the effect of the scheme on the resolved flow is striking. This is an indication that the underlying flow instability is not very strong and can only be represented by the SAS model with the use of a low dissipative numerical scheme such as CD in this particular case. Under such conditions, it is not advisable to apply global methods like SAS (and to a lesser extent, DDES), as will be seen from the temperature distributions later. It is important to emphasize that in more unstable flows, the difference between CD and BCD is not nearly as strong and often barely noticeable.

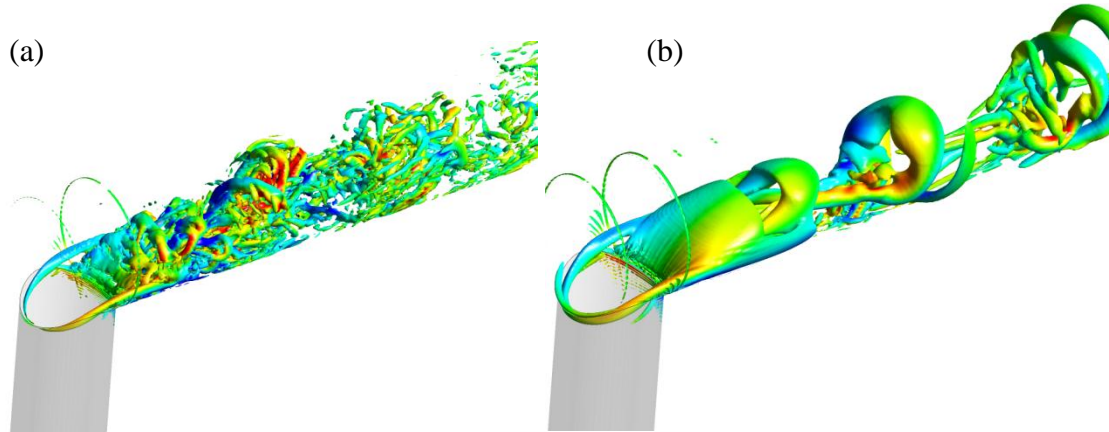


**Figure 42: Turbulence structures for SAS-SST model (a) Central Difference (CD) scheme. (b) Bounded Central Difference (BCD) scheme**

It is therefore recommended to apply the ELES model with synthetic turbulence specified at predefined RANS-LES interfaces located in both pipes upstream of the interaction zone. Switch from the RANS to LES at these interfaces using the vortex method. In this case, the SST model was employed in the RANS zone and the WMLES approach was used in the LES part of the domain. As seen in Figure 43, with this approach resolved turbulence is generated well-upstream of the interaction zone and is then maintained through the interaction zone independent of the numerical scheme (CD or BCD).

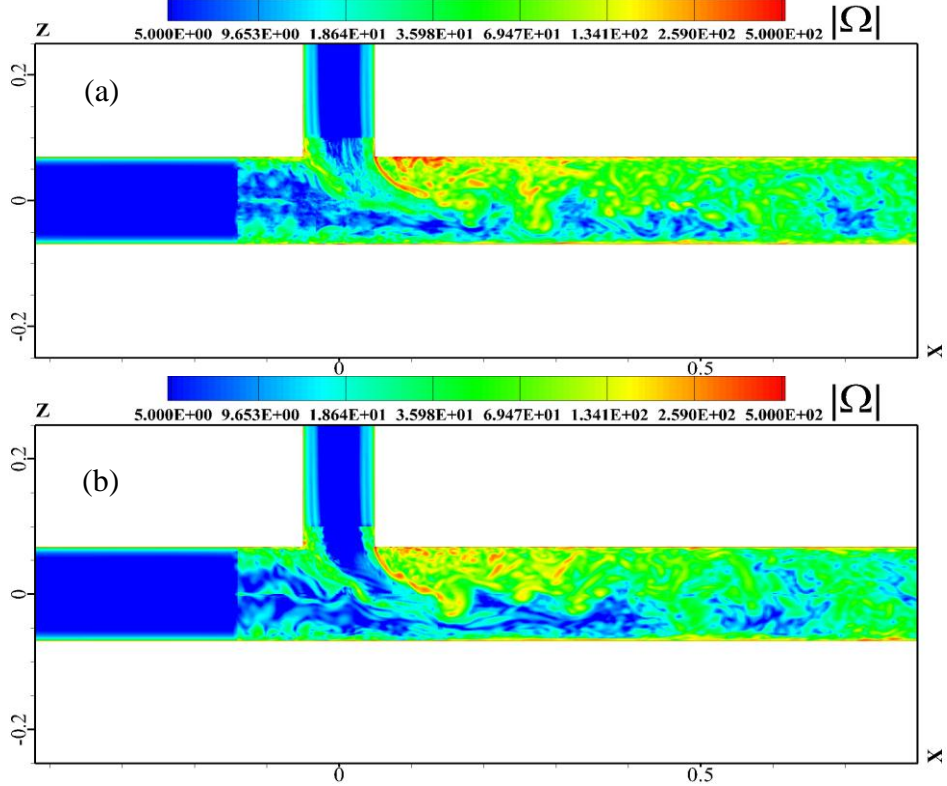


**Figure 43: Vorticity contours for ELES/WMLES simulation (a) CD scheme (b) BCD scheme**

Figure 44(a) and (b) show velocity profiles of different velocity components at different measurement locations (see Figure 41). Figure 44(a) shows results for the DDES, ELES/WMLES, and SAS simulations using the CD scheme. All simulations agree well with each other and with the experimental data. Figure 44(b) shows the same models, but computed using the BCD scheme. As discussed, the SAS/BCD model shows marked differences compared to the experimental data, as already expected from Figure 42. It stays in URANS mode, which for this case turns out to be inadequate. The other models are less sensitive to the numerical setup and provide almost identical results when using the BCD and the CD scheme.

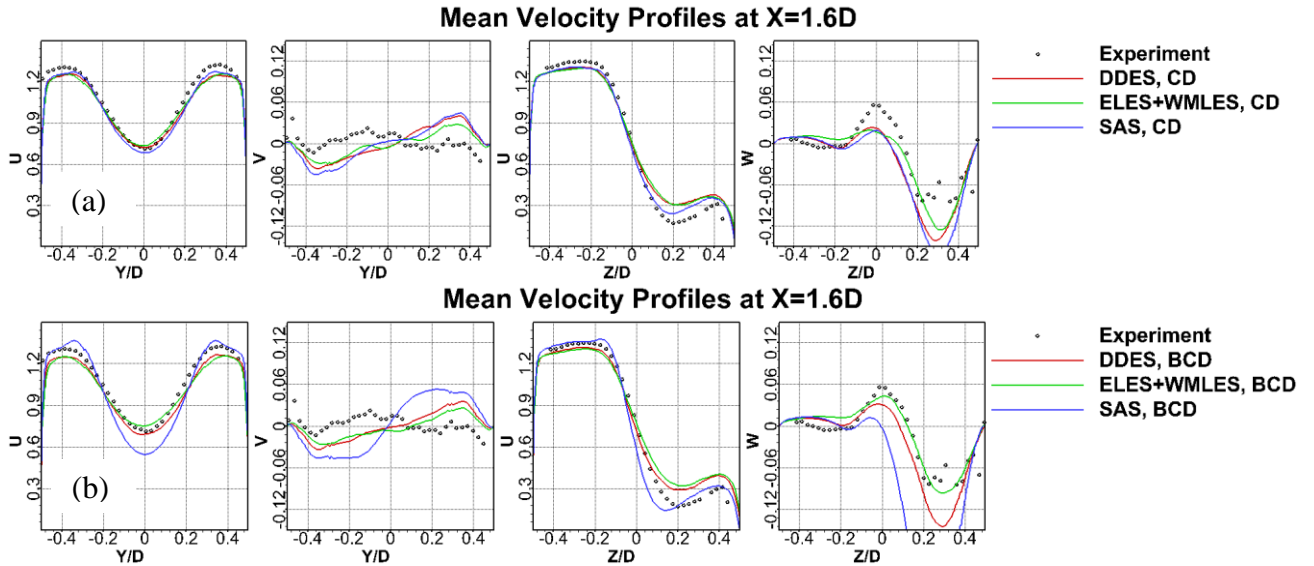


**Figure 44: Comparison of the experimental and computational velocity profiles for T-Junction flow for different turbulence models (a) CD scheme (b) BCD scheme (note that scales of coordinate axes change by large factors between curves)**

From an application-oriented standpoint, the most important outcome of these simulations is the thermal mixing and the resulting wall temperature distributions. Results for the different simulations are shown in Figure 45-Figure 48. The comparison is depicted for four lines located on the wall of the main pipe downstream of the intersection at the Top ( $0^\circ$ ), Front ( $90^\circ$ ), Bottom ( $180^\circ$ ), and Rear ( $270^\circ$ ) (see Figure 41). One can find significant differences between the global and the ELES formulations, especially on the top wall. The temperature mixing is more accurately predicted with the ELES model because the transitional process between RANS and LES is not well-defined in global models. While the solution of global hybrid models is much better than URANS (not shown here), the details can still be missed in the initial mixing zone. The ELES method is more consistent, as it provides a clear interface where modeled and resolved turbulence are exchanged (RANS-LES interface with synthetic turbulence). Because of that, well-defined resolved turbulence is already present upstream of the junction, thereby avoiding the ambiguities of the formation of resolved turbulence in the interaction zone.

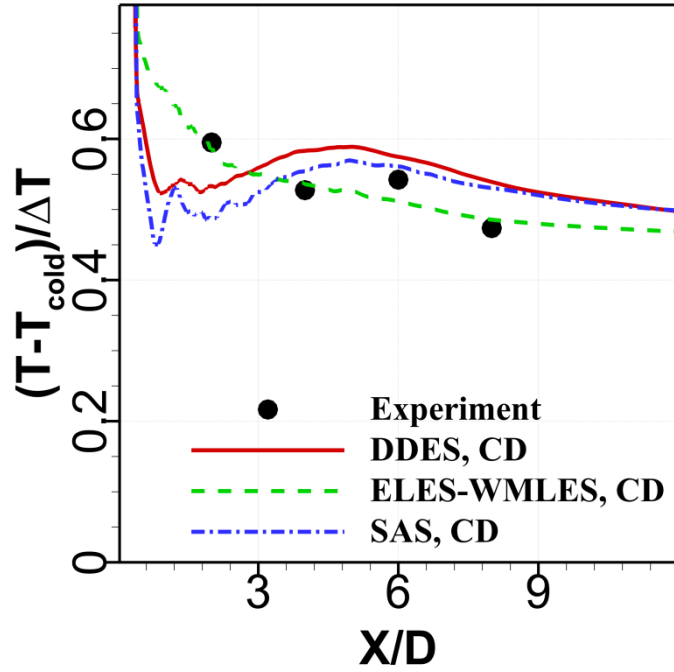


Figure 45: Comparison of the experimental and computational wall temperature distributions for T-Junction flow at the Top wall ( $0^\circ$  - Figure 41) of the main pipe

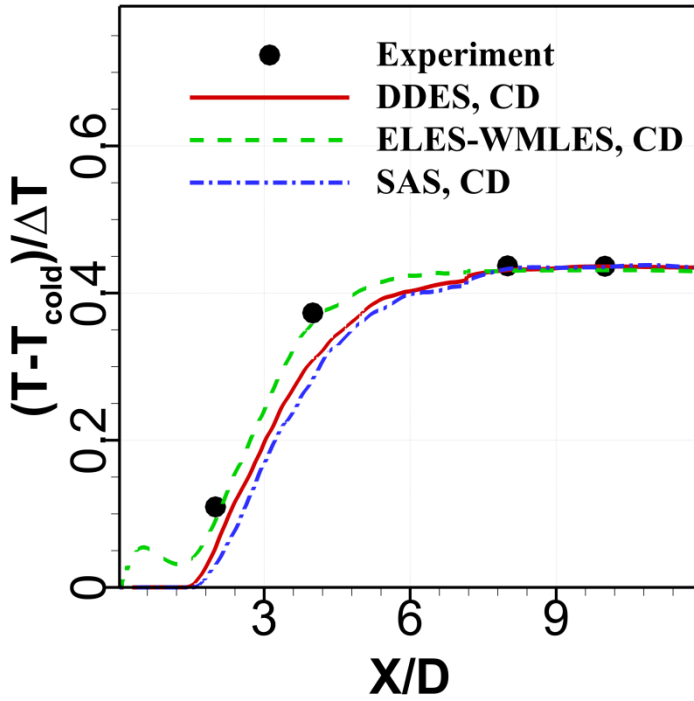


Figure 46: Comparison of the experimental and computational wall temperature distributions for T-Junction flow at the Front wall ( $90^\circ$  - Figure 41) of the main pipe

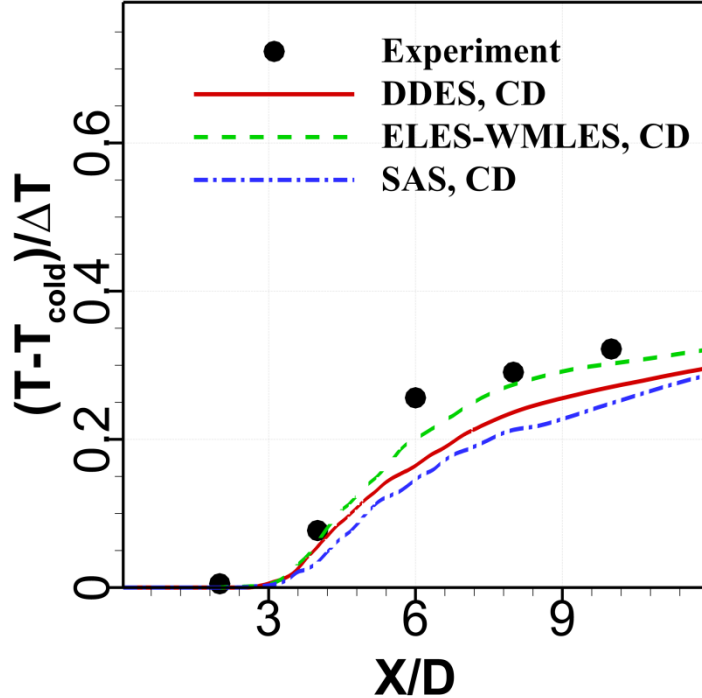


Figure 47: Comparison of the experimental and computational wall temperature distributions for T-Junction flow at the Bottom wall ( $180^\circ$  - Figure 41) of the main pipe

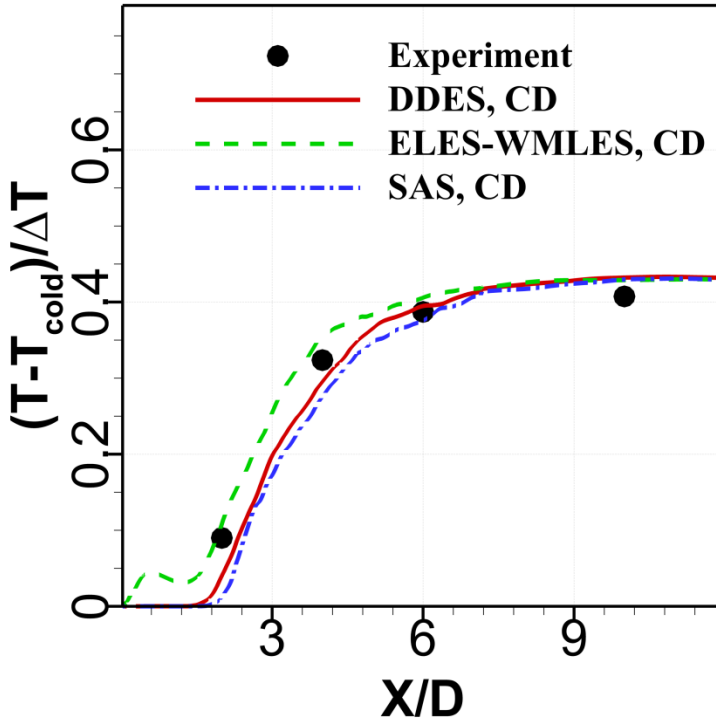
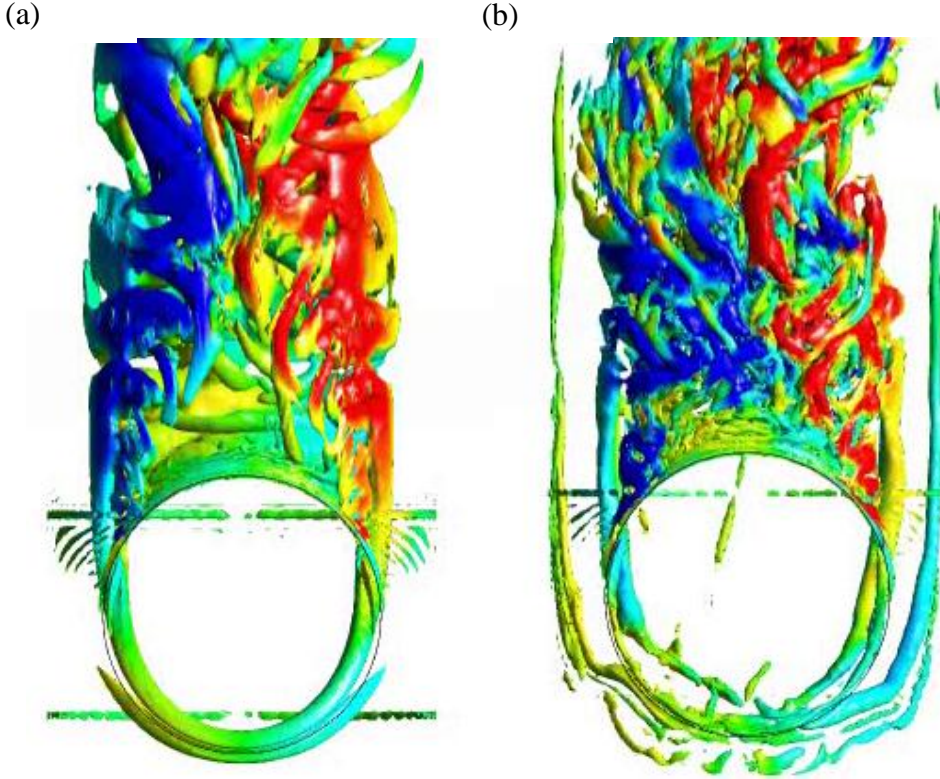


Figure 48: Comparison of the experimental and computational wall temperature distributions for T-Junction flow at the Rear wall ( $270^\circ$  - Figure 41) of the main pipe

Details of the resolved turbulence can be seen in Figure 49 which shows the region just downstream of the pipe intersection on the Top wall ( $0^\circ$  - Figure 41) where the temperature predictions between ELES and DDES differ the most (Figure 45). ELES shows significantly stronger resolved turbulence activity than DDES, confirming the arguments above.



**Figure 49: Comparison of turbulence structures on the Top wall downstream of the pipe intersection (a) DDES model (b) ELES model**

## 5. Numerical Settings for SRS

### 5.1. Spatial Discretization

#### 5.1.1. Momentum

SRS models, as described in the previous section, serve the main purpose of dissipating the energy out of the turbulence spectrum at the limit of the grid resolution. The eddy viscosity is defined to provide the correct dissipation at the larger LES scales. This assumes that the numerical scheme is non-dissipative and that all dissipation results from the LES model. For this reason, one is required to select a numerical scheme in the LES region with low dissipation, relative to the dissipation provided by a subgrid LES model. Another strategy is to avoid the introduction of the LES (subgrid) eddy viscosity and provide all damping through the numerical scheme. This approach is called MILES (Monotone Integrated Large Eddy Simulation) (Boris et al. (1992)). In ANSYS-CFD, the standard LES methodology is followed, whereby the dissipation is introduced by an LES eddy viscosity model and the numerical dissipation is kept at a low value.

In order to achieve low numerical dissipation, one cannot use the standard numerical schemes for convection that were developed for the RANS equations (e.g. Second Order Upwind Schemes – SOU), which are dissipative by nature. In contrast, LES is carried out using Central Difference (CD) schemes. In industrial simulations, 2<sup>nd</sup> order schemes are typically employed, however, in complex geometries with non-ideal grids, CD methods are frequently unstable and produce unphysical wiggles (see Figure 50), which can eventually destroy the solution. To overcome this problem, variations of CD schemes have been developed with more dissipative character, but still

much less dissipative than Upwind Schemes. An example is the Bounded Central Difference (BCD) scheme of Jasak et al. (1999).

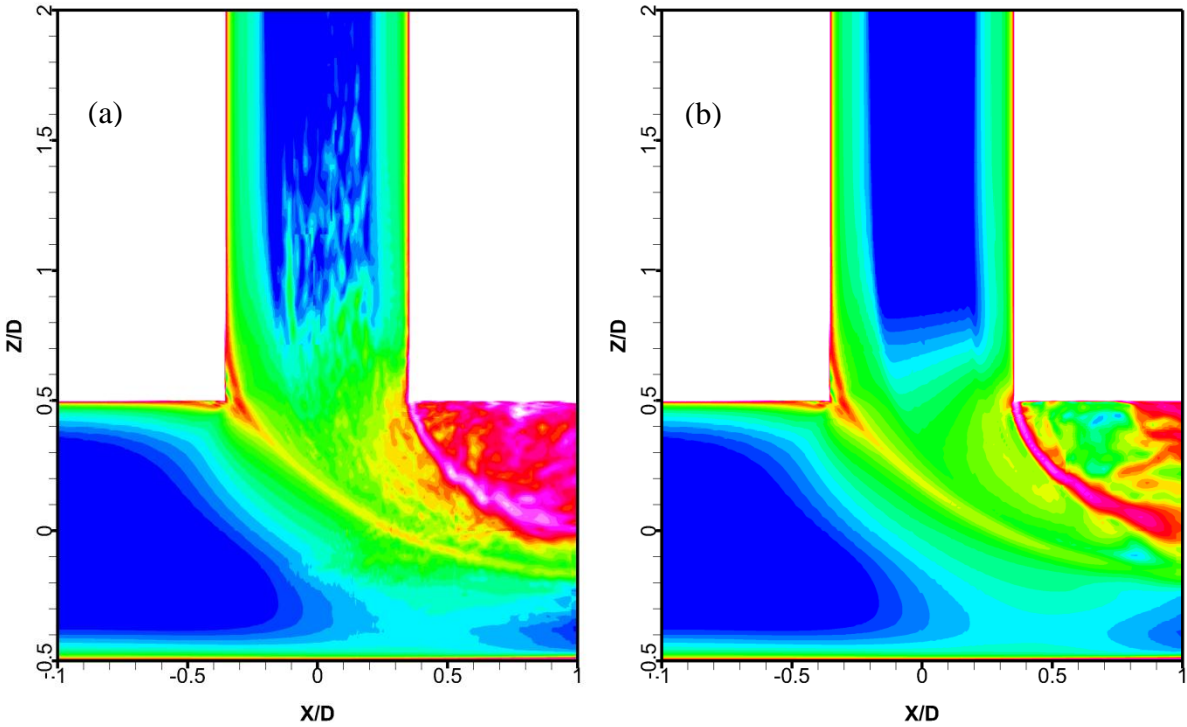


**Figure 50: Example of scheme oscillations in T-Junction flow shown by vorticity: (a) CD, (b) BCD**

The CD scheme can be used successfully for (WM)LES of simple flows on optimal grids (typically hexahedral grids with low skew) such as channel or pipe flows etc. For more complex geometries, ELES allows the reduction of the LES domain to a limited region with high quality grids. Under such conditions, CD can be employed inside the LES portion of the grid, while using a standard upwind biased scheme for the RANS part of the domain.

For global models, like SAS or DDES, involving RANS and LES portions without a well-defined interface between them, most cases require the use of the BCD scheme, which can also handle both the RANS and LES domains with acceptable accuracy.

When using ELES in ANSYS Fluent, one can also switch the numerical scheme between the RANS and the LES regions (e.g. Cokljat et al., 2009) by hand.

In ANSYS CFX, the default for the SAS and DDES models is a numerical scheme that switches explicitly between a second order upwind and the CD scheme, based on the state of the flow, using a switch proposed by Strelets (2001). This switching scheme is relatively complex and it is advisable to apply the less complex BCD scheme that is also available in the code. In ANSYS CFX there is an additional parameter for the BCD scheme that allows a continuous variation of the scheme from BCD to CD. The parameter is called “CDS Bound”. *CDS Bound=1* applies only BCD and *CDS Bound=0* applies only CD.

### 5.1.2. Turbulence Equations

The spatial discretization of the convection terms of the turbulence model is not critical in SRS, as the models are dominated by their source terms. The first order upwind scheme is therefore sufficient for these equations, but second order is also suitable.

### 5.1.3. Gradients (ANSYS Fluent)

The selection of a specific gradient method is not of much relevance to SRSs on high quality hexahedral meshes. For skewed or polyhedral meshes, the Least Square Method (LSM) is recommended. For the SAS model one should always use the LSM.

### 5.1.4. Pressure (ANSYS Fluent)

SRS can be relatively sensitive to the pressure interpolation. Validation studies have shown that the PRESTO scheme is more dissipative than the other options and should be avoided unless required for other reasons. For the validation studies, the standard pressure interpolation was typically used.

## 5.2. Time Discretization

### 5.2.1. Time Integration

Time integration should be carried out with the second order backward Euler scheme. This has proven of sufficient accuracy for a wide range of applications. For turbulence (and other positive) variables, use the Bounded Second Order Implicit Euler scheme (this must be selected in ANSYS Fluent and is the default in ANSYS CFX).

The time steps should be selected to achieve a Courant number of  $CFL \approx 1$  in the LES part of the domain. For complex geometries and grids with high stretching factors, the definition of the CFL number is not always very reliable (e.g. if the flow passes through a region of highly stretched cells). In such situations, estimates can be built upon the physical dimensions of the shear layer to be resolved. If  $N$  cubic cells would be required for resolving a shear layer (say  $N=15-20$  across a mixing layer of thickness  $\delta$ ) and a certain CFL number is to be achieved, then a time step of

$$\Delta t = \frac{CFL \cdot \delta}{N \cdot U}$$

is required. Considering that  $\delta$  is proportional to the RANS turbulent length scale  $L_t$  (with a constant of order 1), this estimate may be further simplified to:

$$\Delta t = \frac{CFL \cdot L_t}{N \cdot U}; \quad L_t = \frac{k^{3/2}}{\varepsilon} = \frac{k^{1/2}}{C_\mu \omega}$$

$C_\mu=0.09$ . This means that the time step  $\Delta t$  can be estimated on a pre-cursor RANS simulation.

One could also apply a more global estimate by assessing the through flow time. This is the time required by a fluid element to pass through the LES domain of length  $L$  with velocity  $U$ :  $T_{tf}=L/U$ . With an estimate of how many cells,  $N$ , will be passed along this trajectory, one obtains  $\Delta t=T_{tf}/N \cdot CFL$ .

### 5.2.2. Time Advancement and Under-Relaxation (ANSYS Fluent)

There are several different settings for time advancement in ANSYS Fluent. The first choice is between the Iterative (ITA) and the Non-Iterative Time Advancement (NITA). NITA works well on high quality grids and for flows with limited additional physical coupling between the equations. This is just a general guideline; NITA should be checked for any new application as it can result in significant CPU savings. Within NITA, the fractional step scheme is recommended; however, one must be very cautious and conservative with the assessment of the time step size.

An attempt to perform a simulation with  $CFL>1$  can lead to an incorrect solution. In addition, one should reduce residual tolerance for all equations to 0.0001.

For the ITA schemes (everything except NITA), the segregated solvers are typically faster than the coupled solver. The optimal choice is in most cases the SIMPLEC scheme. The default under-relaxation parameters for this scheme are set for steady-state simulations. For SRS model simulations, they should be changed to values as close as possible to 1 to improve iterative convergence. Typically, the number of inner iteration loops ( $N_{inner} \sim 10-20$ ) required with SIMPLEC, depends on the complexity of the flow problem. The most critical quantity is the mass conservation. Mass residuals should decrease by at least one order of magnitude every time step.

The coupled solver is slower per iteration, but can lead to more robust convergence and for complex cases can be advantageous. For the coupled solver, one would typically also specify under-relaxation values of (or close to) 1. The number of inner loops is typically  $N_{inner} \sim 5-10$ . In ANSYS CFX, the coupled solver is used in all simulations.

For flows with additional physics (multiphase, combustion, and so on), the number of inner iterations per time step can increase significantly for all solvers.

It is important to emphasize that the optimal under-relaxation factors and the optimal number of inner iterations is case-dependent. Some optimization might be required for achieving the most efficient results.

## 6. Initial and Boundary Conditions

### 6.1. Initialization of SRS

In most cases it is best to initialize the SRS model using a RANS model solution. This is especially true for global hybrid RANS-LES models (SAS, DDES) which are based on an underlying RANS model.

For pure LES or WMLES, ANSYS Fluent offers an option for initializing the flow by converting turbulence from RANS to LES mode (*solve/initialize/init-instantaneous-vel*) using a synthetic turbulence generation routine. This option should be used with caution as it can, at times, have a detrimental effect on the robustness of the simulation. It should be executed mainly for cases where no synthetic turbulence is generated at an inlet/interface and where the inherent flow instability is not strong enough to generate resolved turbulence on its own. A typical example would be the LES of a channel flow with periodic boundary conditions in the streamwise direction. For such flows, the solver could return a laminar solution even at super-critical (turbulent) Reynolds numbers if no initial disturbance is provided.

In ANSYS CFX, synthetic turbulence is generated automatically in the first time step inside the LES region of a ZLES setup.

### 6.2. Boundary conditions for SRS

#### 6.2.1. Inlet Conditions

Inlet conditions should be selected based on the physics of the flow and applied in a similar manner as RANS computations.

For global models (SAS, DDES), use standard (typically steady-state) RANS inlet conditions.

For LES or WMLES, provide synthetic turbulence at the inlet.

#### 6.2.2. Outlet Conditions

If possible, outflow or average pressure is better than constant pressure outlets as vortices carry non-constant pressure distributions across the boundary. For certain acoustics calculations, like jet noise, use non-reflecting boundary conditions.

### 6.2.3. Wall Conditions

For all models except LES, use low  $y^+$  values of around  $y^+=1$ . The models are, however, formulated in a  $y^+$ -insensitive fashion, so larger values of  $y^+$  can be tolerated as long as the overall boundary layer resolution is sufficient.

For LES, one would typically have to apply wall functions in order to avoid the large resolution requirements near the wall. The wall resolution in streamwise ( $x$ ), normal ( $y$ ) and spanwise ( $z$ ) directions are coupled.

$$\begin{aligned}\Delta x^+ < 40, \quad \Delta z^+ < 20 \quad & \text{for} \quad \Delta y^+ < 10 \\ \Delta x^+ < 4\Delta y^+, \quad \Delta z^+ < 2\Delta y^+ \quad & \text{for} \quad \Delta y^+ \geq 10\end{aligned}$$

### 6.2.4. Symmetry vs. Periodicity

In most cases, periodicity or slip conditions cannot be employed in regions that border on zones of resolved turbulence, even if the geometry and the time-averaged flow are symmetric with respect to a given plane. The reason is that unsteady turbulence does not obey symmetry instantaneously. The application of symmetry boundaries would therefore impose an unphysical constraint onto the resolved scales. It is therefore essential to either compute the full domain, or to apply periodicity at such planes if possible (e.g. if there is a matching plane at the other end of the domain).

Symmetry and slip wall conditions can be used if the resolved turbulence is confined to regions not touching these boundaries.

Periodicity conditions can lead to problems for axi-symmetric situations. As the radius approaches zero, the circumferential size of the domain goes to zero, and periodicity conditions would not allow turbulence structures of finite size to exist. An example is the flow in an axi-symmetric pipe. If one were to compute that flow in a pipe segment with periodicity conditions in the circumferential direction, one would restrict the size of the resolved eddies to zero near the axis. This is not correct and would substantially alter the solution. Such a simulation would therefore have to be carried out in full  $360^\circ$  mode. Note that the situation would be different in the case of the flow through a ring segment, where the axis is excluded from the SRS domain. Periodicity could be applied in the case of  $(R_2-R_1)/R_1 < C$  with  $R_2$  being the outer radius,  $R_1$  the inner radius of the segment and  $C$  being a constant of the order 1 or larger.

## 7. Post-Processing and Averaging

### 7.1. Visual Inspection

The first and most important step in any SRS is the visual inspection of the turbulence structures. This is typically done using an iso-surface of the  $Q$ -criterion. The definition of  $Q$  is:

$$Q_{Dim} = C_Q (\Omega^2 - S^2); \quad Dim = [s^{-2}]$$

where in different definitions the constant might be different (for historic reasons,  $C_Q=0.5$  in ANSYS Fluent and  $C_Q=0.25$  in ANSYS CFD-Post). The value of the constant  $C_Q$  is typically unimportant as we are only interested in visual impressions when using this quantity. In this definition,  $S$  is the absolute value of the Strain Rate and  $\Omega$  the absolute value of Vorticity.

$$S = \sqrt{2S_{ij}S_{ij}}; \quad \Omega = \sqrt{2\omega_{ij}\omega_{ij}}; \quad S_{ij} = \frac{1}{2} \left( \frac{\partial U_i}{\partial x_j} + \frac{\partial U_j}{\partial x_i} \right); \quad \omega_{ij} = \frac{1}{2} \left( \frac{\partial U_i}{\partial x_j} - \frac{\partial U_j}{\partial x_i} \right)$$

The rationale behind this definition is that one wants to visualize vorticity, which characterizes turbulence vortices, but also to subtract the mean shear rate in order to avoid displaying steady shear layers (where  $S = \Omega = 1/2|dU/dy|$ ).

There are different definitions of  $Q$ , some of them non-dimensional. Avoid using non-dimensional  $Q$  values as they can be mainly used for visualization of free vortices and their dynamics (e.g. tip vortex of an airplane wing). In turbulent flows, they can elevate very weak turbulence structures to the same level as the strong ones and thereby produce an incorrect picture.

In ANSYS Fluent, the variable  $Q$  is called “Q criterion” (under ‘Turbulence’) and in ANSYS CFD-Post “Velocity.Invariant Q” in the variable list. Both codes also have a non-dimensional version of  $Q$  (ANSYS Fluent: “Normalized q criterion”, ANSYS CFD-Post: “Location / Vortex Core Region , Method = Q-Criterion”), which are not suitable for turbulence vortex fields.

The dimensional  $Q$ -values can be very large and can vary greatly in the domain. Frequently, values up to  $Q_{max} \sim 10^8$  can be found in high Re number flows. In such cases, iso-surfaces in the range of  $Q \sim 10^4 - 10^5$  are typically sensible. One must experiment with some values for the iso-surface before obtaining a suitable picture. It might be helpful to first plot  $Q$  on a fixed surface as a contour plot and select the correct scaling from that contour plot. Use positive values for the iso-surface. Do not use  $Q=0$  for visualization, as it will show very weak structures not relevant to turbulence visualizations.

It is also advisable to color the iso-surface of  $Q$  with some other variable. Interesting quantities are the eddy-viscosity ratio ( $\mu_e/\mu$ ), or a velocity component which is small or zero in RANS (e.g. spanwise velocity), or the CFL number etc. The visual inspection should be done continuously during the entire start-up and run-time of the simulations (e.g. once per day or after every 1000 time steps). It serves the following purposes (see for example Figure 12 and Figure 13):

- Check if unsteady turbulence develops at all and at the expected locations.
- Check large scale symmetries/asymmetries of the flow.
- Check the solution for numerical wiggles (odd-even decoupling)
- Check the size of the resolved eddies and see if they are as one would expect from the grid resolution.
- Check the CFL number on these eddies. It should be smaller than  $CFL \approx 1$ . Check the eddy-viscosity ratio. It should be much smaller than RANS.
- Check for global SRS turbulence models (SAS/DDES) if the turbulence structures develop early in the separating shear layer or if a noticeable delay is observed (see Figure 27 (b)).
- Check for ELES/Unsteady inlet conditions, if synthetic turbulence is reasonable and does not decay (e.g. Figure 35).
- Check the progress of the simulation towards a statistically converged solution. This means that the resolved turbulence requires some time until it has developed and has been transported through the domain. Time-averaging has to wait until that stage has been achieved. These next 3 tips do not match the ones above. Perhaps they should go under a different category, like ‘Other Tips on Post-Processing’
- Include pictures of turbulence structures in any reports of the test case (slides, reports, publications, service requests).
- If possible make animations. This helps to understand the flow physics and is also helpful for others to understand the flow.
- Add monitoring points at interesting locations and plot their development in time to demonstrate statistical convergence.

For all examples in this report, visual impressions of the flows are included. These serve as a guideline on how to process the results.

## 7.2. Averaging

Unsteady simulations with scale resolution require special care in post-processing and averaging. Engineers are usually interested only in time-averaged results and not in the details of the unsteady flowfield. It is therefore important to follow a systematic approach when computing such quantities.

The typical process is to start from a RANS solution (or reasonable initial condition). When switching to any SRS model, the flow will require some time to statistically settle into a new state for the following reasons:

- The resolved turbulence requires some time to develop and be transported through the domain.
- The global flow topology might change from the initial (RANS) solution.
- Other physical effects might require longer start-up times (e.g. multi-phase).

The general strategy is therefore to run the simulation for some start-up time  $\Delta T_s$ , before activating the averaging process (or initiating the acquisition of, for e.g., acoustics information). When should this process be started and how long does it take until the flow is statistically steady? This is the stage where any increase in  $\Delta T_s$  would not change the averaged solutions. Unfortunately  $\Delta T_s$  depends strongly on the flowfield and no general guidelines can be given. For some flows, the flow develops quickly (in a few thousand time steps). For others it takes tens of thousands of steps to reach that point. However, a first estimate can be obtained by estimating ‘throughflow time’  $T_{TF}$ . This is the time that the mean flow requires to pass one time through the domain  $T_{TF} = L_{CFD}/U_\infty$  where  $L_{CFD}$  is the length of the domain and  $U_\infty$  is the mean flow velocity. The turbulence statistics typically require several (3-5) throughflow times to establish themselves. Again, this is just a rough estimate and can depend on the particular flow.

In order to determine  $\Delta T_s$  more systematically, one must monitor the simulation. It is advisable to monitor some local and some global quantities.

- Continuously inspect the solution visually with the aid of regular images and updated animations.
- Inspect solution variables at monitor points in the critical zone of simulation (pressure, velocity, temperature etc.) as a function of time. The amplitude and frequency of local oscillations should become regular before the averaged statistics can be gathered.
- Monitor global quantities (forces on body, massflow, integrated swirl, ...). Interesting quantities are often those which would be zero for RANS (spanwise forces, etc.) as they are sensitive to the SRS characteristics. They also help to evaluate the overall symmetry of the solution (they should fluctuate around zero) and to determine slow transients (quantities that fluctuate around zero but with low overlaid frequencies).

Only when all indicators show that the flow is no longer changing statistically (meaning only the details of the turbulence structures are a function of time) should the averaging be activated. It is important to document the number of steps that have already occurred when averaging was started and how many steps have been averaged. With respect to averaged quantities:

- Monitor time-averaged quantities and ensure that they are not ‘drifting’ They will drift initially, but should then settle to an asymptotic value.
- Ensure that they satisfy the symmetry conditions of the flow. Any asymmetry is an indicator of non-convergence (exceptionally, there are flows which develop physical asymmetries despite a symmetric setup. Example: some symmetric diffusers separate from one side and stay attached on the other).

- Ensure that the averaged quantities are smooth.
- In zonal/embedded simulations, check if averaged quantities are reasonably smooth across RANS-LES interfaces (they will never be perfectly smooth, but should also not change drastically).

## 8. Summary

An overview of hybrid Scale-Resolving Simulation (SRS) technologies was given. Due to the nature of the subject, only a rough outline of the models could be provided. The rational and the advantages-disadvantages of each model family have been discussed. Based on the description of the models, an attempt has been made to categorize flows into sub-classes, and to map the modeling strategies onto these classes. It should be emphasized again, that the proposed categories are not easily and clearly defined and have significant overlap. Still it is considered necessary to explain that no single SRS model is suitable for all applications and it is not possible to generalize about which model should be used for which type of flow.

In principle, ELES and ZFLES, in combination with WMLES are suitable for all flows, but require a substantial amount of pre-processing work to define the corresponding zones and provide suitable grids for all of them. For complex applications, this is not always feasible/practical and the global models (SAS, DDES) are favored. However, as detailed, they work only if a sufficient level of instability is present in the flow. If in doubt, it is better to select the safer option, over the more convenient one.

Details on many aspects of SRS have been provided, ranging from numerics, to grid resolution all the way to post-processing. Numerous examples have been shown to allow the reader to properly place the intended application into this framework. It is anticipated that the document will evolve over time, as new questions are posed by users and as the SRS models themselves will evolve.

A brief summary of the more important points is provided in the Appendices.

## Acknowledgment

The material in this report was prepared with the help of members of the turbulence team at ANSYS – Jochen Schütze, Yuri Egorov, Richard Lechner, as well as with the help of the colleagues at NTS in St. Petersburg – Mikhail Gritskevich and Andrey Garbaruk. Aleksey Gerasimov at ANSYS has provided a very thorough review, which has resulted in the removal of numerous inconsistencies and has significantly improved the quality and readability of the document. Some of the test cases have been run in the framework of the EU projects DESIDER and ATAAC.

## References

1. Boris, J. P., Grinstein, F. F., Oran, E. S., Kolbe, R. S., (1992), “New insights into Large Eddy Simulation”, Fluid Dynamic Research, 10 :199-228.
2. Cokljat D., Caradi D., Link G., Lechner R. and Menter F.R., (2009), “Embedded LES Methodology for General-Purpose CFD Solvers”. Proc. Turbulent Shear Flow Phenomena, Proc. 6th Int. Symp. Turbulence and Shear Flow Phenomena, Seoul, Korea, 22-24 June 2009, 1191-1196.
3. Comte-Bellot, G. and Corrsin, S., (1971), “Simple Eulerian time correlation of full- and narrow-band velocity signals in grid-generated, ‘isotropic’ turbulence”, J. Fluid Mech., Vol. 48, Part 2, pp. 273-337.
4. Davidson, L. (2006), “Evaluation of the SAS-SST Model “Channel Flow, Asymmetric Diffuser and Axi-Symmetric Hill”, Proceedings European Conference on Comp. Fluid Dyn. ECCOMAS CFD.
5. Durbin, P., and Pettersson Reif, B.A., (2003), *Statistical theory of turbulent flows*, John Wiley and Sons, Ltd, UK.

6. Egorov Y., Menter F.R. and Cokljat D., (2010), “Scale-Adaptive Simulation Method for Unsteady Flow Predictions. Part 2: Application to Aerodynamic Flows”, Journal Flow Turbulence and Combustion, Vol. 85, No. 1, pp. 139-165.
7. Fröhlich J., Mellen C.P., Rodi W., Temmerman L., Leschziner M., (2005), Highly resolved large-eddy simulation of separated flow in a channel with streamwise periodic constrictions, J. of Fluid Mech., vol. 526, pp. 19-66.
8. Fröhlich J. and von Terzi, D., (2008), Hybrid LES/RANS methods for simulation of turbulent flows, Progress in Aerospace Sciences, Vol. 44, Issue 5, pp 349-377.
9. Girimaji, S. S., (2004), “Partially-Averaged Navier-Stokes Method: A RANS to DNS Bridging Method,”
10. Girimaji, S. and Abdul-Hamid, K.S. (2005), Partially-averaged Navier-Stokes model for turbulence: implementation and validation, AIAA paper 2005-0502
11. Gritskevich, M.S. Garbaruk, A.V. and Menter F.R. (2012), “Sensitization of DDES and IDDES Formulations to the  $k-\omega$  Shear-Stress Transport Model. To be published: Journal Flow Turbulence and Combustion.
12. Guerts, J. B., (2004), *Elements of direct and large-eddy simulation*, Edwards Inc. Philadelphia, USA.
13. Hanjalic, K. and Launder, B., (2011), *Modelling Turbulence in Engineering and the Environment*, Cambridge University Press, Cambridge, UK.
14. Jasak H, Weller H.G. and Gosman A.D., (1999), “High Resolution Differencing Scheme for Arbitrarily Unstructured Meshes”, Int. J. Numer. Meth. Fluids, v31, pp 431-449.
15. Mathey, F., Cokljat, D., Bertoglio, J.P. and Sergent, E., (2003), “Specification of LES Inlet Boundary Condition Using Vortex Method”, 4th International Symposium on Turbulence, Heat and Mass Transfer, Antalya.
16. Menter, F.R., (1994): “Two-equation eddy-viscosity turbulence models for engineering applications”, AIAA Journal, Vol. 32, No. 8, pp. 1598-1605.
17. Menter F.R., Garbaruk A. and Smirnov P., (2009) “Scale adaptive simulation with artificial forcing”, Proc. 3rd Symposium on Hybrid RANS-LES Methods.
18. Menter, F.R. and Egorov, Y., (2010), “Scale-Adaptive Simulation Method for Unsteady Flow Predictions. Part 1: Theory and Model Description”, Journal Flow Turbulence and Combustion, Vol. 85, No. 1, pp 113-138.
19. Menter, F.R., Kuntz, M., (2003), Adaptation of Eddy-Viscosity Turbulence Models to Unsteady Separated Flow Behind Vehicles. Proc. Conf. The Aerodynamics of Heavy Vehicles: Trucks, Busses and Trains, Asilomar, Ca, Springer.
20. Michelassi V., Wissink, J. G. and Rodi W., (2003), “Direct numerical simulation, large eddy simulation and unsteady Reynolds-averaged Navier-Stokes simulations of periodic unsteady flow in a low-pressure turbine cascade: A comparison”, Journal of Power and Engineering. Vol 217, Number 4, pp. 403-411.
21. Nicoud, F. and Ducros, F. , (1999), “Subgrid-scale stress modelling based on the square of the velocity gradient tensor”. Flow, Turb. Combust. 62, 183-200.
22. Reichardt, H., (1951), Vollständige Darstellung der turbulenten Geschwindigkeitsverteilung in glatten Leitungen“, Zeitschrift fur Angewandte Mathematik und Mechanik 31, p. 208–219.
23. Rotta J. C., (1972), *Turbulente Strömungen*. BG Teubner Stuttgart.
24. Sagaut, P., Deck, S. And Terracol, M., (2006), *Multiscale and multiresolution approaches in turbulence*, Imperial College Press, London.
25. Schildmacher, K.-U., Koch, R., Wittig, S., Krebs, W. and Hoffmann, S., (2000), “Experimental investigations of the temporal air-fuel mixing fluctuations and cold flow instabilities of a premixing gas turbine burner”, ASME Paper 2000-GT-0084.

26. Shur, M.L., Spalart, P.R., Strelets, M.K. and Travin, A.K., (2008), “A hybrid RANS-LES approach with delayed-DES and wall-modeled LES capabilities”, International Journal of Heat and Fluid Flow 29, pp. 1638-1649.
27. Sjunnesson, A., Henriksson, R. and Lofstrom C., (1992), CARS measurements and Visualization of Reacting Flows in Bluff Body Stabilized Flame. AIAA Paper 92 – 3650.
28. Smagorinsky, J., (1963), “General Circulation Experiments with the Primitive Equations”, Monthly Weather Review 91, p. 99–165.
29. Spalart, P.R., Jou, W., Strelets, M., Allmaras, S., (1997). “Comments on the feasibility of LES for wings, and on a hybrid RANS/LES approach”. In: Advances in DNS/LES, 1st AFOSR Int. Conf. on DNS/LES.
30. Spalart P. R., (2000), “Strategies for turbulence modelling and simulations”, Int. J. Heat Fluid Flow, 21, pp. 2.
31. Spalart, P., Deck, S., Shur, M., Squires, K., Strelets, M., Travin, A. (2006), “A New Version of Detached Eddy Simulation, Resistant to Ambiguous Grid Densities”, Journal of Theoretical and Computational Fluid Dynamics 20, pp. 181–195.
32. Strelets, M., (2001), “Detached Eddy Simulation of massively separated flows”. AIAA Paper 2001-879.
33. Travin, A., Sur M., Strelets, M., Spalart P., (2000), “ Physical and numerical upgrades in the detached eddy simulation of complex turbulent flows”, In Advances in LES of complex flows”, eds. R. Friedrich, W. Rodi , p. 239-254, New York, Kluwer Acad.
34. Vogel, J.C. and Eaton, J.K., (1985), “Combined heat transfer and fluid dynamic measurements downstream of a backward-facing step,” Journal of Heat and Mass Transfer, vol. 107, p. 922–929.
35. Wagner, C., Hüttl, T. and Sagaut, P., (2007), *Large-eddy simulation for acoustics*, Cambridge University Press.
36. Westin, J., Alavyoon F., Andersson, L. Veber, P., Henriksson, M. and Andersson, C., (2006), “Experiments and Unsteady CFD-Calculations of Thermal Mixing in a T-Junction,” OECD/NEA/IAEA Workshop on the Benchmarking of CFD Codes for Application to Nuclear Reactor Safety (CFD4NRS), Munich Germany, pp. 1-15.
37. Widenhorn, A., Noll, B, and Aigner, M., (2009), “Numerical Study of a Non-Reacting Turbulent Flow in a Turbine Model Combustor”, AIAA Paper 2009-647, Orlando Florida.
38. Wilcox, D. C., (2006), *Turbulence Modeling for CFD*, DCW Industries Inc., 3. Edition.

## Appendix 1: Summary of Numerics Settings with ANSYS Fluent

	Unsteady Simulation	Comment
Convection Terms	CD / BCD	CD on simple geometries (also inside LES regions). In case of wiggles in solution use BCD (most industrial cases)
Pressure Discretization	Any except PRESTO	Use PRESTO only if required for other reasons. Note that the initial formation of turbulence structures can be delayed (inhibited) with PRESTO.
Velocity Gradients	Least Squares Cell based	No significant impact on SRS, typically Least Square Cell Based. <u>With SAS ‘Least Square Cell Based’ is essential.</u>
Iterative Method	SIMPLEC	NITA/Fractional step only for simple flows Monitor convergence: at least 1 order in mass conservation. SIMPLEC with 5-10 inner loops. For cases which are difficult to converge try the coupled solver. More expensive, but potentially lower inner iterations required. Increase Under-Relaxation Factors to values ~1
Under-relaxation	URF≈1	Start with all URF≈1 (typically 0.8.-0.95). Reduce in case of convergence problems. Lower values for additional physics (combustion, multi phase, ...)
Time Discretization	Second order backward Euler	Use CFL<1 in LES zones if possible. This condition can also be relaxed depending on the flow and CFL~5 was used for the T-junction test case successfully. <u>Bounded for 2<sup>nd</sup> order turbulence quantities (<math>k</math>, <math>\omega</math>, <math>\epsilon</math>) and other positive quantities (volume fraction, ...)</u>

## Appendix 2: Summary of Numerics Settings With ANSYS CFX

	Unsteady Simulation	Comment
Convection Terms	CD / BCD	<p>CD on simple geometries (also inside LES regions). In case of wiggles in solution use BCD</p> <p>The default scheme for DDES and SAS is a hybrid scheme which switches automatically between High Res and CD. Recent experience indicates that BCD is generally easier to apply and often yield the same accuracy.</p> <p>From Release 14 on, there is also a parameter in the GUI (CDS Bound) which allows shifting between the classical BCD scheme and the central difference scheme.</p>
Time discretization	Second order backward Euler	<p>Use CFL&lt;1 in LES zones if possible. This condition can also be relaxed depending on the flow.</p> <p><u>Bounded for 2<sup>nd</sup> order turbulence quantities is default (k, ω, ε) and other positive quantities (volume fraction, ...)</u></p>

## Appendix 3: Models

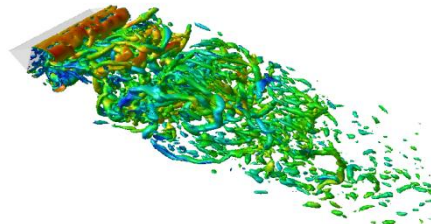
	Applications	Comments
Scale-Adaptive Simulation (SAS)	<ul style="list-style-type: none"> <li>• Use for globally unstable flows</li> <li>• Use CFL~1 for best results (higher CFL possible but less resolution)</li> <li>• Avoid PRESTO scheme</li> <li>• With SAS ‘Least Square Cell Based’ is essential</li> <li>• Check Q-criterion carefully during run time to ensure SRS structures</li> </ul>	<ul style="list-style-type: none"> <li>• ‘Safest’ SRS model, as it has URANS fallback position on coarse grids/time steps</li> <li>• Danger of falling into URANS mode if flow instability is not strong</li> </ul>
Detached Eddy Simulation (DES)	<ul style="list-style-type: none"> <li>• Use for globally unstable flows and with care also for locally unstable flows</li> <li>• Always use DDES to avoid impact of DES limiter on attached boundary layers – use DDES shielding function</li> <li>• Grid in SRS region must be of LES quality – no RANS fallback position</li> <li>• Use CFL~1</li> <li>• Avoid PRESTO scheme</li> <li>• Check Q-criterion carefully during run time to ensure SRS structures</li> </ul>	<ul style="list-style-type: none"> <li>• More aggressive than SAS in terms of unsteadiness</li> <li>• Careful grid generation important – otherwise danger of grey zones or grid-induced separation</li> </ul>
Large Eddy Simulation (LES)	<ul style="list-style-type: none"> <li>• Use for free shear flows</li> <li>• Use if boundary layers are laminar</li> <li>• Use for turbulent boundary layers only with high grid resolution at low Reynolds numbers</li> <li>• Use CFL~1</li> <li>• Apply synthetic turbulence at inlets</li> <li>• Check Q-criterion carefully during run time to ensure SRS structures</li> </ul>	<ul style="list-style-type: none"> <li>• Typically too expensive for wall-bounded flows</li> </ul>
Wall Modeled LES (WMLES)	<ul style="list-style-type: none"> <li>• Use for wall boundary layers at moderate and high Reynolds numbers</li> <li>• Resolve boundary layer volume (<math>\delta x \delta x \delta</math>) by 10x40x20 cells</li> <li>• Use CFL~1</li> <li>• Apply synthetic turbulence at inlets</li> <li>• Check Q-criterion carefully during run time to ensure SRS structures</li> </ul>	<ul style="list-style-type: none"> <li>• Scales much more favorably with Reynolds number than standard LES but still very expensive</li> <li>• Limit wall region to a small portion of flow domain (ELES)</li> </ul>

Embedded LES (ELES) Zonal Forced LES (ZFLES)	<ul style="list-style-type: none"> <li>• Use for wall boundary layers at moderate and high Reynolds numbers</li> <li>• Resolve boundary layer volume (<math>\delta \times \delta \times \delta</math>) by 10x40x20 cells</li> <li>• Use CFL~1</li> <li>• Apply synthetic turbulence at RANS-LES interface</li> <li>• Check Q-criterion carefully during run time to ensure SRS structures</li> </ul>	<ul style="list-style-type: none"> <li>• Allows flexible combination of models in different parts of the domain.</li> <li>• If wall boundary layers in LES domain – consider using WMLES (default in CFX)</li> </ul>
Vortex Method (VM) - Fluent	<ul style="list-style-type: none"> <li>• Use to generate synthetic turbulence at RANS-LES interface or LES (WMLES) inlet</li> <li>• Restrict interface zone to minimal section where turbulence needs to be converted (do not extend LES zone far into the freestream)</li> <li>• If large RANS-LES interface cannot be avoided increase (and check) the number of vortices specified. Can be as high as <math>10^4</math>.</li> <li>• Use CFL~1</li> <li>• Check Q-criterion carefully during run time to ensure SRS structures</li> </ul>	<ul style="list-style-type: none"> <li>• Grid in LES region of interface must be of LES quality</li> </ul>
Harmonic Turbulence Generator (HTG) - CFX	<ul style="list-style-type: none"> <li>• Restrict inlet zone to LES minimal section where turbulence needs to be converted (do not extend LES zone far into the freestream)</li> </ul>	<ul style="list-style-type: none"> <li>• Grid in LES region of interface must be of LES quality</li> </ul>

## Appendix 4: Generic Flow Types and Modeling

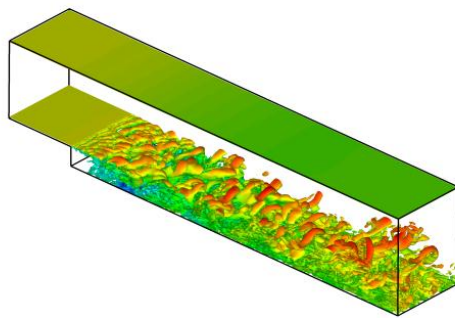
### Globally Unstable Flows:

ANSYS



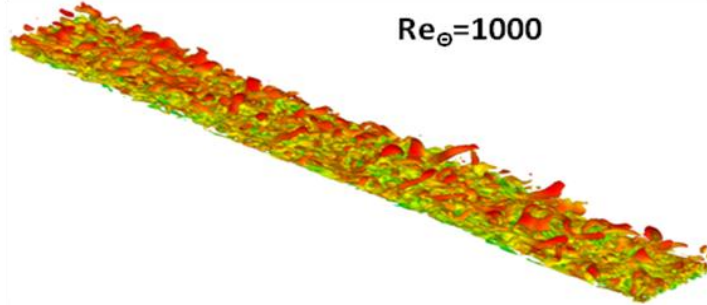
Examples	<ul style="list-style-type: none"><li>• <b>Flows past bluff bodies</b><ul style="list-style-type: none"><li>◦ Flow past buildings</li><li>◦ Landing gears of airplanes</li><li>◦ Baffles in mixers etc.</li><li>◦ Side mirrors of cars</li><li>◦ Stalled wings/sails</li><li>◦ Trains/trucks/cars in crossflow</li><li>◦ Tip gap of turbomachinery blades</li><li>◦ Flows past orifices, sharp nozzles etc.</li></ul></li><li>• <b>Flows with strong swirl instabilities</b><ul style="list-style-type: none"><li>◦ Flow in combustion chambers of gas turbines etc.</li><li>◦ Some tip vortex flows in adverse pressure gradients</li><li>◦ Flows past vortex generators</li><li>◦ and so on</li></ul></li><li>• <b>Flows with strong flow interaction</b><ul style="list-style-type: none"><li>◦ Impinging/colliding jets</li><li>◦ and so on</li></ul></li></ul>
Modeling	<ul style="list-style-type: none"><li>• SAS model is safest option as it has RANS fall-back position</li><li>• DDES in case SAS does not show sufficient content of resolved turbulence. Provide suitable LES grid in ‘LES’ region</li><li>• Often SAS and DDES give very similar solutions.</li><li>• ELES typically not required</li></ul>
Critical	<ul style="list-style-type: none"><li>• Visually check turbulent structures</li><li>• Run flow until statistically converged</li></ul>

# Locally Unstable Flows:



Examples	<ul style="list-style-type: none"><li>• Flows with large separation zones (&lt; boundary layer thickness)<ul style="list-style-type: none"><li>◦ Backward-facing step type flows</li><li>◦ Bump flows with large separation</li><li>◦ Cavity flows</li><li>◦ Mixing layer leaving plate/trailing edge</li></ul></li><li>• Flows with weak swirl instabilities<ul style="list-style-type: none"><li>◦ Flames with low or zero swirl</li></ul></li><li>• Flows with weak flow interaction<ul style="list-style-type: none"><li>◦ Jet in crossflow with low momentum ratio</li></ul></li></ul>
Modeling	<ul style="list-style-type: none"><li>• Use ELES where geometry permits</li><li>• DDES on high quality grids and low dissipation numerics (CD/BCD)</li></ul>
Critical	<ul style="list-style-type: none"><li>• Instability of Separating Shear Layer (SSL) must be resolved with DDES quickly. ELES is safer as it provides unsteady inlet to separation zone but generally much more expensive</li><li>• Visually check turbulent structures in SSL</li></ul>

# Stable Flows:



Examples	<ul style="list-style-type: none"> <li>Attached and mildly separated wall bounded flows             <ul style="list-style-type: none"> <li>Boundary layers</li> <li>Channel/pipe flows</li> </ul> </li> </ul>
Modeling	<ul style="list-style-type: none"> <li>LES in separate domain if possible             <ul style="list-style-type: none"> <li>WMLES for higher Re numbers</li> <li>Maybe interpolate larger domain RANS solution onto LES zone boundaries</li> <li>Use unsteady (synthetic) turbulence at inlet – preferred Vortex Method</li> </ul> </li> <li>ELES in combined RANS-LES simulation             <ul style="list-style-type: none"> <li>Define LES zone as detailed in Section 4.3. Extend LES zone to leave space around critical area.</li> <li>Place RANS-LES interface into region of uncritical flows (equilibrium boundary layers etc.)</li> </ul> </li> </ul>
Critical	<ul style="list-style-type: none"> <li>Visually check turbulent structures</li> <li>Provide sufficient grid resolution in (WM)LES zones especially for wall-bounded flows (Chapter 4.3.3).</li> <li>CFL number &lt; 1</li> </ul>